

การสังเคราะห์คอลลอยด์อนุภาคนาโนของเงินความเข้มข้นสูง

นายภัทวัฒน์ มณีวัฒนิกัญญา

วิทยานิพนธ์นี้เป็นส่วนหนึ่งของการศึกษาตามหลักสูตรปริญญาวิทยาศาสตรดุษฎีบัณฑิต

สาขาวิชาเคมี ภาควิชาเคมี

คณะวิทยาศาสตร์ จุฬาลงกรณ์มหาวิทยาลัย

ปีการศึกษา 2552

ลิขสิทธิ์ของจุฬาลงกรณ์มหาวิทยาลัย

SYNTHESIS OF HIGH CONCENTRATION SILVER NANOPARTICLES COLLOID

Mr. Pattwat Maneewattanapinyo

A Dissertation Submitted in Partial Fulfillment of the Requirements
for the Degree of Doctor of Philosophy Program in Chemistry

Department of Chemistry

Faculty of Science

Chulalongkorn University

Academic Year 2009

Copyright of Chulalongkorn University

Thesis Title SYNTHESIS OF HIGH CONCENTRATION SILVER
 NANOPARTICLES COLLOID
By Mr.Pattwat Maneewattanapinyo
Field of Study Chemistry
Thesis Advisor Associate Professor Sanong Ekgasit, Ph.D.
Thesis Co-Advisor Nuttaporn Pimpha, Ph.D.

Accepted by the Faculty of Science, Chulalongkorn University in Partial
Fulfillment of the Requirements for Doctoral Degree

..... Dean of the Faculty of Science
(Professor Supot Hannongbua, Dr.rar.net)

THESIS COMMITTEE

..... Chairman
(Associate Professor Sirirat Kokpol, Ph.D.)

..... Thesis Advisor
(Associate Professor Sanong Ekgasit, Ph.D.)

..... Thesis Co-Advisor
(Nuttaporn Pimpha, Ph.D.)

..... Examiner
(Rojrit Rojanathanes, Ph.D.)

..... Examiner
(Associate Professor Chuchaat Thammacharoen)

..... External Examiner
(Boonsong Sutapun, Ph.D.)

ภัททวัฒน์ มณีวัฒนภิญโญ: การสังเคราะห์คอลลอยด์อนุภาคนาโนของเงินความเข้มข้นสูง (SYNTHESIS OF HIGH CONCENTRATION SILVER NANOPARTICLES COLLOID) อ.ที่ปรึกษาวิทยานิพนธ์หลัก: รศ. ดร.สนอง เอกสิทธิ์, อ.ที่ปรึกษาวิทยานิพนธ์ร่วม: ดร.ณัฐพร พิมพะ, 100 หน้า.

งานวิจัยชิ้นนี้มีจุดมุ่งหมายที่จะสังเคราะห์อนุภาคระดับนาโนเมตรของเงินความเข้มข้นสูงและพัฒนาเครื่องปฏิกรณ์ไหลแบบท่อสำหรับผลิตอนุภาคระดับนาโนเมตรของเงินปริมาณมากอย่างต่อเนื่อง อนุภาคระดับนาโนเมตรของเงินความเข้มข้นสูงผลิตโดยกระบวนการรีดักชันด้วยวิธีทางเคมี ระหว่างสารละลายเกลือของโลหะเงินและสารละลายตัวรีดิวซ์ในเครื่องปฏิกรณ์ไหลแบบท่อ จากการทดลองพบว่าเครื่องปฏิกรณ์ไหลแบบท่อสามารถผลิตอนุภาคระดับนาโนเมตรของเงินความเข้มข้น 1,000-10,000 ส่วนในล้านส่วน ในอัตรา 240 ลิตรต่อชั่วโมง อนุภาคระดับนาโนเมตรของเงินความเข้มข้นสูงที่สังเคราะห์ด้วยเครื่องปฏิกรณ์ไหลแบบท่อมีความอยู่ตัวสูง อนุภาคระดับนาโนเมตรของเงินความเข้มข้นสูงที่สังเคราะห์โดยเครื่องปฏิกรณ์ไหลแบบท่อมีขนาดเล็กและมีค่าการกระจายตัวที่แคบ ภาพถ่ายกล้องจุลทรรศน์อิเล็กตรอนแบบส่องผ่านแสดงให้เห็นว่าอนุภาคระดับนาโนเมตรของเงินมีขนาดประมาณ 10 นาโนเมตร ต้นทุนการผลิตอนุภาคระดับนาโนเมตรของเงินมีราคาต่ำกว่าอนุภาคระดับนาโนเมตรของเงินที่มีจำหน่ายในเชิงพาณิชย์มาก อนุภาคระดับนาโนเมตรของเงินความเข้มข้นสูงแสดงสมบัติยับยั้งแบคทีเรียและไม่เป็นพิษต่อเซลล์

ภาควิชา.....	เคมี.....	ลายมือชื่อนิสิต.....
สาขาวิชา.....	เคมี.....	ลายมือชื่อ อ.ที่ปรึกษาวิทยานิพนธ์หลัก.....
ปีการศึกษา.....	2552.....	ลายมือชื่อ อ.ที่ปรึกษาวิทยานิพนธ์ร่วม.....

4873837923 : MAJOR CHEMISTRY

KEYWORDS : SILVER NANOPARTICLES / TUBULAR FLOW REACTOR
CONTINUOUS PROCESS

PATTWAT MANEEWATTANAPINYO: SYNTHESIS OF HIGH
CONCENTRATION SILVER NANOPARTICLES COLLOID. THESIS
ADVISOR: ASSOC. PROF. SANONG EKGASIT, Ph.D., THESIS CO-
ADVISOR: NUTTAPORN PIMPHA, Ph.D., 100 pp.

This research aims to study the synthesis of high concentration silver nanoparticles and to develop the tubular flow reactor for continuous production of large amount of silver nanoparticles. The highly concentrated silver nanoparticles were synthesized by chemical reduction of silver salt with a reducing agent in a tubular flow reactor. The tubular flow reactor was continuously produced silver nanoparticles at 240 liters per hour at the silver nanoparticles concentration of 1,000-10,000 ppm. The synthesized silver nanoparticles were very stable. These highly concentrated silver nanoparticles had small size and narrow size distribution. The transmission electron microscopy images of synthesized silver nanoparticles reveal an average diameter of 10 nm. Moreover, the production cost of these highly concentrated silver nanoparticles was significantly lower than that of the imported commercial products. In addition, high concentration silver nanoparticles show antibacterial activity without any toxicological effects.

Department : Chemistry Student's Signature

Field of Study : Chemistry Advisor's Signature

Academic Year : 2009 Co-Advisor's Signature

ACKNOWLEDGEMENTS

I would like to express my sincere gratitude to my thesis advisor, Associate Professor Dr. Sanong Ekgasit and my thesis co-advisor Dr. Nuttaporn Pimpha for wholeheartedly provide the useful guidance, understanding, training and teaching the theoretical background and technical skills during my research.

I would like to thank Associate Professor Dr. Sirirat Kokpol, Dr. Rojrit Rojanathanes, Associate Professor Chuchaat Thammacharoen and Dr. Boonsong Sutapun for usefully substantial suggestions as the thesis committee.

I also thank Associate Professor Dr. Wijit Banlunara and Dr. Theerayuth Kaewamatawong of Department of Pathology, Faculty of Veterinary Science for safety testing in laboratory animals, and Associate Professor Dr. Sirirat Rengpipat, Assistant Professor Dr. Tanapat Palaga and Mr. Kamol Rodyou of Department of Microbiology, Faculty of Science, Chulalongkorn University for antibacterial activity testing.

Warmest thanks to my friends, and my colleagues at the Sensor Research Unit, Department of Chemistry, Faculty of Science, Chulalongkorn University.

This research was partial supported by the Center for Petroleum, Petrochemicals, and Advanced Materials.

Above all, I am profoundly grateful to my parents and endearing family for all their loves, understanding, support, and encouragement during the whole period of my study.

CONTENTS

	Page
ABSTRACT IN THAI.....	iv
ABSTRACT IN ENGLISH.....	v
ACKNOWLEDGEMENTS.....	vi
CONTENTS.....	vii
LIST OF TABLES.....	xii
LIST OF FIGURES.....	xiii
LIST OF ABBREVIATIONS.....	xviii
LIST OF SYMBOLS.....	xix
CHAPTER I INTRODUCTION.....	1
1.1 The objectives.....	2
1.2 Scopes of research	2
1.3 Benefits of the Research.....	3
CHAPTER II THEORETICAL BACKGROUND.....	4
2.1 Silver nanoparticles and synthesis of silver nanoparticles.....	4
2.2 Colloids.....	6
2.2.1 Lyophobic colloid	6
2.2.2 Lyophilic colloid	7
2.2.3 Amphiphilic colloid.....	7
2.3 Colloid stability	8
2.4 Stabilizers.....	9
2.5 Characterization of synthesized silver nanoparticles	13
2.6 Tubular flow reactor.....	15

CHAPTER III EXPERIMENT.....	16
3.1 Materials and Instruments.....	16
3.1.1 Materials.....	16
3.1.2 Instruments.....	16
3.2 Novel reactor for preparation of highly concentrated colloid of silver nanoparticles	16
3.2.1 The Design, develop and invent reactor for the continuous system.....	16
3.2.1.1 Batch reactor.....	17
3.2.1.2 Jet Semi-Continuous Flow Reactor.....	18
3.2.1.3 Tubular flow reactor (The pulse flow processes).....	19
3.2.1.4 Tubular flow reactor (The continuous flow processes).....	20
3.3 Synthesis of our homemade silver nitrate.....	21
3.4 Factors affecting the synthesis of high concentration silver nanoparticles.....	21
3.4.1 Influence of reducing agent.....	22
3.4.2 Influence of stabilizer.....	22
3.4.3 Influence of order of addition of reactant solution	22
3.4.4 Influence of the concentration of reducing agent and stabilizer.....	23
3.5 The factors affecting the production of large amount and high concentration silver nanoparticles.....	23
3.5.1 Comparison of synthesized silver nanoparticles from batch reactor with the reactor volume of 1 liter and 40 liters.....	23
3.5.2 Synthesis of large amount and high concentration silver nanoparticles by novel reactor.....	23
3.5.2.1 Jet Semi-continuous flow reactor.....	23
3.5.2.2 Tubular flow reactor (the pulse flow processes).....	24

3.5.2.3 Tubular flow reactor (the continuous flow processes)	24
3.5.3 Influence of flow rates on the synthesis of silver nanoparticles.....	24
3.5.4 Influence of reactor diameter	25
3.5.5 Comparison of the synthesized silver nanoparticles from batch reactor with that of tubular flow reactor.....	25
3.6 Comparison of silver nanoparticles from our synthesis by tubular flow reactor with the available commercial product.....	25
3.7 The stability of synthesized silver nanoparticles.....	25
3.8 Economical point of view.....	25
3.9 Characterization of synthesized high concentration silver nanoparticles.....	26
3.9.1 UV-Visible spectroscopy.....	26
3.9.2 Transmission electron microscope (TEM).....	27
3.10 Antibacterial activity testing and safety testing in laboratory animals with our synthesized silver nanoparticles.....	27
3.10.1 Antibacterial activity testing with our synthesized silver nanoparticles.....	27
3.10.2 Safety testing in laboratory animals with our synthesized silver nanoparticles.....	28
3.11 Industrial applications of our synthesized silver nanoparticles.....	28
CHAPTER IV RESULTS AND DISCUSSION.....	29
4.1 Various factors affecting the synthesis of high concentration silver nanoparticles.....	29
4.1.1 The influence of reducing agents	29
4.1.2 The effect of various stabilizers	33
4.1.3 Influence of the order of addition of reactant solution.....	35

	Page
4.1.4 The effect of the concentration of reducing agent & stabilizer.....	37
4.2 The various factors affecting the production of large amount and high concentration silver nanoparticles.....	40
4.2.1 Comparison of the synthesized silver nanoparticles from batch reactor with the reactor volume of 1 liter and 40 liters.	40
4.2.2 Synthesis of large amount and high concentration silver nanoparticles by novel reactor.....	43
4.2.2.1 Jet semi-continuous flow reactor.....	43
4.2.2.2 Tubular flow reactor (the pulse flow processes).....	46
4.2.2.3 Tubular flow reactor (the continuous flow processes).....	49
4.2.3 Influence of flow rates on the synthesis of silver nanoparticles.....	51
4.2.4 Influence of reactor diameter.....	54
4.2.5 Comparison of synthesized silver nanoparticles from batch reactor and tubular flow reactor.....	56
4.3 Comparison of silver nanoparticles from our synthesis by tubular flow reactor with the available commercial product.....	58
4.4 The stability of synthesized silver nanoparticles.....	60
4.5 Antibacterial activity testing and safety testing in laboratory animals with our synthesized silver nanoparticles.....	62
4.5.1 Antibacterial activity testing.....	62
4.5.2 Safety testing in laboratory animals with our synthesized silver nanoparticles.....	64
4.6 Industrial applications of our synthesized silver nanoparticles.....	65
CHAPTER V CONCLUSIONS.....	67
REFERENCES.....	69

APPENDICES.....	74
APPENDIX A.....	75
APPENDIX B.....	78
APPENDIX C.....	83
APPENDIX D.....	88
VITAE.....	100

LIST OF TABLES

Table	Page
3.1 Comparison of silver nitrate properties and cost with our homemade and commercially available analytical grade.....	21
3.2 Comparison cost of high concentration silver nanoparticles with our synthesis and the available commercial product.....	26
4.1 Extinction maxima and FWHH of extinction spectra of synthesized silver nanoparticles obtained from various reducing agents.....	32
4.2 Extinction maxima and FWHH of extinction spectra of synthesized silver nanoparticles obtained from various stabilizers.....	35
4.3 Reynolds numbers, Re, at various flow rates.....	53
4.4 Reynolds numbers, Re, at various reactor tube diameter.....	56
4.5 The antibacterial test	64
4.6 The toxicity test in laboratory animals	65
4.7 The applications of synthesized silver nanoparticles in some commercial products.....	66
A 1 Estimated cost of our homemade silver nitrate.....	76
A 2 Estimated cost of our synthesis of high concentration silver nanoparticles (10,000 pm/1 liter).....	77

LIST OF FIGURES

Figure		Page
2.1	The proposed mechanism for stepwise formation of nanoparticles...	5
2.2	Schematic illustrations of aggregation, steric stabilization and electrostatic stabilization.....	10
2.3	Structure of gelatin.....	11
2.4	Structure of methyl cellulose.	12
2.5	Structure of starch.	12
2.6	Localized Surface Plasmon Resonance (LSPR) phenomenon.....	13
2.7	The extinction spectrum of silver nanoparticles.....	14
2.8	Illustration of the flow patterns of the fluid in a tube.....	15
3.1	The batch reactor for the synthesis of high concentration silver nanoparticles.....	17
3.2	Jet semi-continuous flow reactor for the synthesis of high concentration silver nanoparticles.....	18
3.3	Tubular flow reactor (the pulse flow processes) for the synthesis of high concentration silver nanoparticles.....	19
3.4	The tubular flow reactor for continuous synthesis of high concentration silver nanoparticles.....	20
3.5	Ocean Optics Portable UV-Visible spectrometer.....	26
3.6	JEOL JEM-2010 analytical transmission electron microscope.....	27
4.1	The normalized extinction spectra of highly concentrated silver nanoparticles (5,000 ppm) synthesized from batch reactor with various reducing agents.....	30
4.2	The transmission electron microscopy (TEM) images of the silver nanoparticles synthesized by various reducing agents: (A) glucose (B) sodium borohydride.....	31

Figure	Page
4.3 The proposed growth pathways of silver nanoparticles when (A) weak reducing agents and (B) strong reducing agents were employed as reducing agents.....	32
4.4 The normalized extinction spectra of 5,000 ppm silver nanoparticles synthesized from batch reactor with various stabilizers.....	34
4.5 The normalized extinction spectra of synthesized silver nanoparticles when using different the order of reactant addition.....	35
4.6 The illustration of order of addition for synthesizing high concentration silver nanoparticles.....	36
4.7 The normalized extinction spectra of highly concentrated silver nanoparticles (5,000 ppm) synthesized from batch reactor with various concentration of soluble starch (0.5, 2.0 and 4.0 %) and various concentration of sodium borohydride (A) 23 mM, (B) 35 mM, (C) 46 mM and (D) 70 mM.....	38
4.8 The normalized extinction spectra of 5,000 ppm silver nanoparticles synthesized from batch reactor with 1 liter and 40 liters reactor volume.....	40
4.9 The TEM images representing silver nanoparticles synthesized from batch reactor with (A) 1 liter and (B) 40 liters reactor volume..	41
4.10 The illustrations of the high concentration silver nanoparticles synthesized from batch reactor.....	42
4.11 The normalized extinction spectrum of 5,000 ppm silver nanoparticles synthesized from (A) the jet semi-continuous flow reactor by using primary mixing chamber as three-ways connection tube, (B) the jet semi-continuous flow reactor by using primary mixing chamber as three-ways connection tube with external mixing chamber, (C) batch reactor with 1 liter and (D) the comparison of the normalized extinction spectra of silver nanoparticles synthesized form the jet semi-continuous flow reactor	

Figure	Page
by using primary mixing chamber as three-ways connection tube and as three-ways connection tube with external mixing chamber, and batch reactor with 1 liter.....	45
4.12 The normalized extinction spectra of 5,000 ppm silver nanoparticles synthesized from the batch reactor with 1 liter, the jet semi-continuous flow reactor by using primary mixing chamber as three-ways connection tube with external mixing chamber and the batch reactor with 40 liters.....	46
4.13 The normalized extinction spectrum of 5,000 ppm silver nanoparticles synthesized from the tubular flow reactor (the pulse flow processes) by using (A) primary mixing chamber as three-ways connection tube with external mixing chamber, (B) primary mixing chamber as modified from hypodermic syringe, (C) primary mixing chamber as custom-made modified from hypodermic syringe and (D) the comparison of the normalized extinction spectra of silver nanoparticles synthesized from the tubular flow reactor (the pulse flow processes) with various mixing chamber.....	48
4.14 The normalized extinction spectra of silver nanoparticles synthesized from batch reactor with 1 liter batch reactor, the tubular flow reactor (the pulse flow processes) by using primary mixing chamber as custom-made modified from hypodermic syringe and batch reactor with 40 liters.....	50
4.15 The normalized extinction spectra of silver nanoparticles synthesized from batch reactor with 1 liter, tubular flow reactor (the continuous flow processes) by using primary mixing chamber as custom-made modified from syringe and batch reactor with 40 liters.....	51
4.16 The normalized extinction spectra of silver nanoparticles diluted from 5,000 ppm silver nanoparticles synthesized from tubular flow reactor (the continuous flow processes) with various flow rates of	

Figure	Page
reactants.....	51
4.17 The illustration of the synthesized high silver nanoparticles from tubular flow reactor.....	53
4.18 The normalized extinction spectra of 5,000 ppm silver nanoparticles synthesized from tubular reactor with various diameter of tube.....	54
4.19 The normalized extinction spectra of silver nanoparticles diluted from 5,000 ppm silver nanoparticles obtained from batch reactor and flow reactor.....	56
4.20 The transmission electron microscopy (TEM) images of synthesized silver nanoparticles with (A) batch reactor and (B) tubular flow reactor.....	57
4.21 The normalized extinction spectra of silver nanoparticles obtained from tubular flow reactor ($\lambda_{\max} = 395 \text{ nm}$) and Commercial product ($\lambda_{\max} = 405 \text{ nm}$).....	58
4.22 TEM images of the synthesized silver nanoparticles: (A) tubular flow reactor synthesized silver nanoparticles (B) commercial product.....	59
4.23 The normalized extinction spectra of the same synthesized silver nanoparticles produced by tubular flow reactor measured immediately after synthesis and 6 months later.....	60
B 1 Procedure for the determination of the effects of silver nanoparticles on the reduction bacterial growth.....	79
B 2 The normalized extinction spectra of highly concentrated silver nanoparticles synthesized from our homemade silver nitrate and commercially available analytical grade silver nitrate.....	80
B 3 Photograph of antibacterial activity test of (A) <i>Escherichia coli</i> , (B) <i>Staphylococcus aureus</i> and (C) methicillin resistant <i>Staphylococcus aureus</i> (MRSA) with our synthesized silver nanoparticles (AgNPs),	

Figure	Page
and (D) our synthesis of silver nanoparticles was applied into commercial products.....	81
B 4 The antibacterial test of bacterial pathogens with silver nanoparticles padding on fabric: (A/B; Polyester), (C/D; Cotton) with AgNPs 50 ppm, Tested after 20 Wash: No Growth (NG), and (E/F; Polyester), and Control (Cotton) Tested after 20 Wash: Large Growth (LG) / Moderate Growth (MG).....	82

LIST OF ABBREVIATIONS

AgNO ₃	: silver nitrate
NaBH ₄	: sodium borohydride
LSPR	: localized surface plasmon resonance
nm	: nanometer
Ag	: Argentum (silver)
M	: Metal
FWHH	: Full width at half high
eV	: electron volt
TEM	: transmission electron microscopy
Re	: Reynolds numbers

LIST OF SYMBOLS

M	: metal
°C	: degree Celsius
ρ	: density of the fluid (kg/m^3)
D	: inert diameter of the tube (m)
v	: linear flow velocity (m/s)
ν	: kinematic viscosity of the fluid (m^2/s)
μ	: dynamic viscosity of the fluid ($\text{N}\cdot\text{s}/\text{m}^2$)

CHAPTER I

INTRODUCTION

The silver nanoparticles have been proved for their effective antibacterial activity. They have been integrated into many consumer products for the antibacterial applications, such as fabrics, food packaging, cleaning cloth, and cosmetics [1-6]. Many industries incorporated antibacterial properties into their products to increase the value of goods for the competitive advantage in the market. Nowadays, commercially available silver nanoparticles are very expensive and lab-scaled synthesized of silver nanoparticles is not sufficient for the industrial demand. Continuous process, large scale production and high concentration of silver nanoparticles are necessary for industrial applications. Thailand has not yet developed manufacturing techniques for the synthesis of highly concentrated colloidal silver nanoparticles for industrial applications.

Several studies have indicated that a conventional batch chemical reduction method could synthesize silver nanoparticles at the laboratory scale (100 – 2,000 mL) from batch reactor. The limitations of conventional processes are the requirement of high temperature and high pressure, the large particles with broad size distribution, high cost of production, and complicated process [7-13, 30]. At present, there is no tubular flow reactor for the continuous producing silver nanoparticles. To solve these problems, the present study is designed to develop the continuous flow reactor producing large-scale silver nanoparticles in high concentration via water – based system at room temperature.

The purpose of this research is to develop and to construct reactor for continuous producing large amount of controllable size, highly concentrated and highly stabilized silver nanoparticles. The process for continuous synthesis of high concentration silver nanoparticles was performed by a chemical reduction of silver salt solution mixing with the solution of reducing agent and produced silver nanoparticles at 20 to 40 liters per hour (20 - 40 L/hr). The synthesis of highly concentrated silver nanoparticles (i.e, greater than 10,000 ppm) was very stable (more than 6 months). The processes of highly concentrated silver nanoparticles were

performed at room temperature, atmospheric pressure. There were no by-products/chemical wastes.

1.1 Objectives of the Research

1. To develop a process for the synthesis of silver nanoparticles with easily scale-up to mass scale production at high concentration.
2. To produce high concentration silver nanoparticles colloids (10,000 – 100,000 ppm) in large amount (20 - 40 L/time) by chemical reduction method.
3. To design and to make the prototype of reactor for producing high concentration of silver nanoparticles for industrial applications.
4. To increase the value-added new products employing nanotechnology.

1.2 Scope of the Research

1. Synthesize silver nanoparticles with high concentration (i.e, greater than 10,000 ppm) and large amount (20 - 40 L/hr) of high stability with small size and narrow size distribution using chemical reduction method.
2. Develop the technique of silver nanoparticles synthesis with high concentration by optimizing conditions of reducing agent and stabilizer.
3. Design and fabricate reactor for producing high concentration of silver nanoparticles.

1.3 Benefits of the Research

1. Reduce imported nanomaterials.
2. Provide high quality at low price nanomaterials for industrial application.

3. Provide high quality nanomaterials for novel industrial application.
4. Improve competitive advantage of Thai products through nanotechnology.
5. Reduce the price of nano-enabled products through the utilization of homemade nanomaterials.

CHAPTER II

THEORETICAL BACKGROUND

2.1 Silver nanoparticles and synthesis of silver nanoparticles

Lyophobic colloids of noble metal nanoparticles such as silver nanoparticles have been used in many applications (scientific research and industrial application): optical sensors [14-15, 22], antibacterial agents [1-6], and conductive materials [16], due to the large surface area to volume ratio and size-dependent properties. The size effect of silver nanoparticles create a phenomenon based on the number of atom or molecules at the surface of nanoparticles and takes place in the range of 1-100 nm that produces the qualitative changing in physical, optical, and thermal properties.

The synthesis of silver nanoparticles method can be divided into 2 main methods: chemical reduction and physical reduction. The chemical reduction method (Bottom up approaches) is the most general method using silver salt solution mixed with the reducing solution agent. The nanoparticles started from small structures as atom/molecules grow to larger particles [17]. The physical reduction method (Top down approaches) started from large structure as macroscopic material and break down to small structures [12, 17].

Chemical reduction method involved the reduction of metal salt by various reducing agents such as borohydride, citrate, ethylene glycol and aldehyde or by the active species which generate by radiation with the stabilizer. The chemical reduction process, a multifactor process, depends on the difference between the redox potentials of the metal salt and the reducing agent, concentration of its components, temperature, and pH of medium.

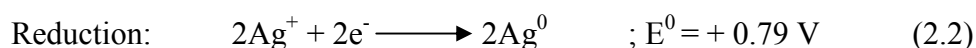
The behavior of metal particles is determined by the potential difference as follows [17]:

$$\Delta E = E - E_{\text{redox}} \quad (2.1)$$

where E is the redox potential of the particles and E_{redox} is the solution potential. The particles grow when $\Delta E > 0$ and dissolve when $\Delta E < 0$. The chemical

reduction depends on the difference between the redox potentials of the metal salt and reducing agent.

The reduction of silver nitrate (AgNO_3) by sodium borohydride (NaBH_4) can be written as [17]:



Redox reaction:



The chemical reduction method involved the reaction of metal salt with sodium borohydride as reducing agent. The growth of silver nanoparticles depicted in the following step as shown in Figure 2.1 [17-23]. Firstly, upon the reduction of silver ions, the seed was formed. The reaction called the nucleation of seed. And next, the nucleation can proceed in two pathways. If the seed combined with the other seed via the collision, the silver nanoparticles was formed with stable particles. If the seed combined with silver ion species, the autocatalytic pathways on the surface occurred. The silver nanoparticles grow into larger particles.

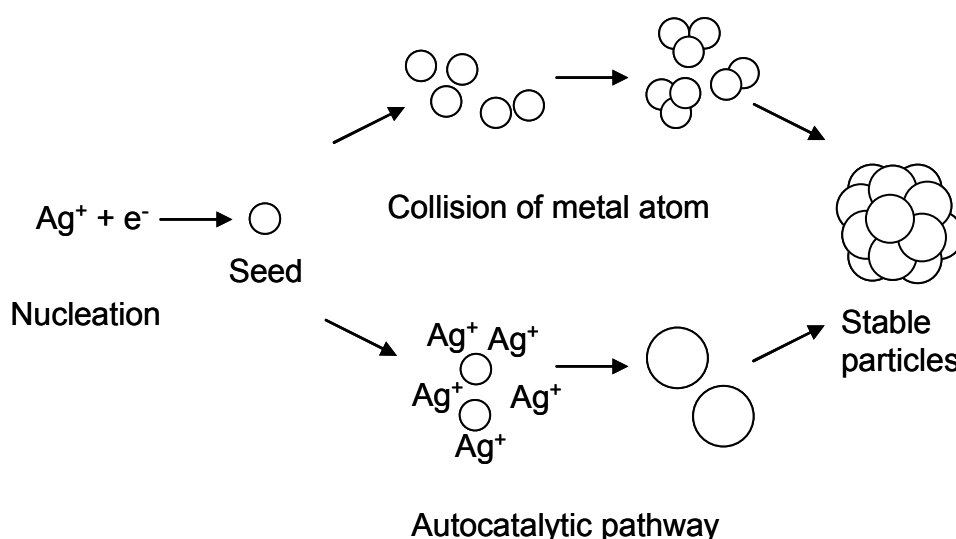


Figure 2.1 The proposed mechanism for stepwise formation of nanoparticles.

Physical reduction method, there are many methods for preparation of metal nanoparticles such as radiolytic reduction [12] and the burning droplets (spray pyrolysis) [24, 28]. The synthesized particle will be small particles and having the narrow particle size distribution. The radiolytic method is very dangerous because the use of gamma radiation at high intensity. The method is also high cost. However, the synthesized particle is of high purity with a narrow size distribution.

2.2 Colloids

Colloid is a small particles which dispersed in another phase. One of the components of a colloidal system will have dimension in the range of 1-1,000 nm. The terms used in describing colloidal systems can be classified into 3 groups: *Lyophilic colloid*, *Lyophobic colloid* and *Amphiphilic colloid* (Association colloid) [25]. Lyophobic and Lyophilic are used to describe the tendency of a surface or functional group that becomes wetting or solvating. For example, if the liquid medium is aqueous, lyophobic is hating liquid or hydrophobic while lyophilic is loving liquid or hydrophilic [25].

2.2.1 Lyophobic colloid

Lyophobic colloids are thermodynamically unstable and the particles will suddenly aggregate and settle [18, 25]. The formation of such colloid involves either degradation of bulk matter or aggregation of small molecules or ions. A higher degree of dispersion is oftenly obtainable by an aggregation method. The latter involves the formation of a molecular dispersion, supersaturated solution from which the dispersed phase precipitates in a suitably divided form. The formation of a new phase during precipitation involves two stages as *nucleation* and *growth* [18, 23, 25]. The relative rates of nucleation and growth determined particle size. A higher degree of dispersion is obtained when the nucleation rate is high and the rate of particles growth is low. Growth inhibitors can be exploited not only to obtain smaller particles, but also by acting selectively on the various crystal faces, to modify particles shape. If

the precipitated solid has a modest solubility, the dispersion will age, with the less soluble larger particles growing at the expense of the more soluble smaller ones.

The most important physical property of a colloidal dispersion has the tendency to aggregating particles by coagulation process. The coagulation or strong aggregation are flocculation to weak, easily reversed and tend to aggregate. To prevent the aggregation of particles, the peptization is need. Peptization is a process in which redispersion is achieved, with little or no agitation, by changing the composition of the dispersion medium.

2.2.2 Lyophilic colloid

Lyophilic is the solutions of macromolecules such as gelatin or starch in water [18, 25-27]. Their solubilities depend on the magnitude of their affinity for the solvent compared with their affinity for themselves. Macromolecules with a high solvent affinity will take on a fairly open configuration and have a high solubility, whereas those with more affinity for themselves than for the solvent will tend to coil up on themselves and show more limited solubility [25]. This balance of affinities will depend on factors such as pH, salt concentration, and temperature. Because of their great length and random coiling, dissolved macromolecules tend to immobilize relatively large amounts of solvent and their solutions are generally more viscous than ordinary solution. If all solvent becomes mechanically trapped and immobilized within the macromolecular network, the system as a whole takes on a solid appearance and is called a gel.

2.2.3 Amphiphilic colloid

Amphiphilic colloid is micelles or surfactant [18, 25, 29]. These molecules consist of a polar head group which is hydrophobic hydrocarbon region attached to a hydrophilic. Therefore, part of this molecule favors solubility in water while the other part favors insolubility in water. The satisfaction of both of these tendencies are for the molecule to adsorb at an aqueous interface oriented so that the hydrophilic head group is completely soluble in the water phase and the hydrocarbon part is out of

the water phase. The critical micelle concentration is above a certain concentration and another mechanism operates by which the same end is achieved.

Aggregated micelles, are formed in the bulk water phase oriented so that the hydrocarbon parts are in the center, away from water, and the polar head groups are on the outside, in contact with water. Micellization is a thermodynamically reversible process.

2.3 Colloid stability

The concept of colloid stability depends on the dispersion to prevent coagulation of particles [17, 23, 25]. A force barrier against colloids between the particles and possible coagulation subsequently and thermodynamic stability are the kinetic stability, coagulated states correspond to an increasing in free energy and, therefore, are thermodynamically unfavorable. According to thermodynamics, the spontaneous process occurs in the direction of decreasing Gibbs free energy, therefore we may conclude that the separation of a two-phase dispersed system have been occurred. The distinct layers is a change in the direction of decreasing Gibbs free energy. There is more surface energy in a two-phase system when dispersed in a highly subdivided state than when it is in a coarser state of subdivision. This suggests a correlation between the inherent instability of a high dispersed lyophobic system and the thermodynamics of the surface. For the present, it is important to note that lyophobic systems dislike their surroundings enough to separate out. On the other hand, Lyophilic systems are perfectly soluble in a solution. The two categories differ radically in their definitions of stability. We elaborate these individually in the following subsections.

The lyophobic stability depends on the balance between van der Waals (vdW) attraction and electric double layer repulsion between the particles, and the effects of surfactant or of polymeric additive [25, 30]. The vdW forces are best known as the attractive forces between molecules that cause gases to liquefy. The vdW energy between two atoms is both very weak and very short-range, varying inversely as the sixth power of the distance between the atoms. When the attractions between all atom pairs in two colloidal particles are summed, not only is the total interaction greatly

increased, but it is also much more long-range, varying inversely with somewhere between the first and second power of the distance between the particles. The electric double layer repulsion are known as the colloidal particles dispersed in a polar liquid such as water usually acquired a net electric charge at their surfaces. Ions in the dispersion medium of charge opposite to that of the particles are attracted toward the particles surface and ions of like charge repelled from the particles surface. This effect, together with the mixing tendency of thermal motion, leads to the formation of electric double layer made up of the charged particle surface and an excess of counter-ions over co-ions distributed in a diffuse manner in the dispersion medium.

The total interaction energy is the sum of the van der Waals attraction and electric double layer repulsion. Two extremely situations can be recognized. **At low electrolyte concentrations**, the electric double layer repulsion is long-range and an energy barrier to coagulation results (rather like the activation energy barrier to a chemical reaction). The rate of coagulation will be slowed correspondingly, and may be so slow that the colloid can be regarded as stable in the practical sense [25, 30]. **At high electrolyte concentrations**, the electric double layer repulsion is short-range and is exceeded by van der Waals attraction at all interparticle distances which has no energy barrier and coagulation is rapid [23, 25, 30]. The addition of electrolyte effected to transition between these extremes. The extra electrolyte required to lower the potential energy barrier—so that the coagulation time is reduced, say, from months to minutes—is relatively small. A critical coagulation concentration can be measured, and depends most of all on the valency of the counter-ions.

Surfactants which are powerful stabilizing agents, usually adsorb strongly on particle surfaces and make them more lyophilic. These adsorbed ionic surfactant often leads to enhance electrostatic stabilization.

2.4 Stabilizers

The stabilizers such as a substrate, often a donor ligands, polymers, and surfactants are used for stabilizing the silver nanoparticles in solution. In the absence of the stabilizer, silver nanoparticles can produce the formation of larger nanoparticles by van der Waals attraction force and Brownian motion [23, 25, 30].

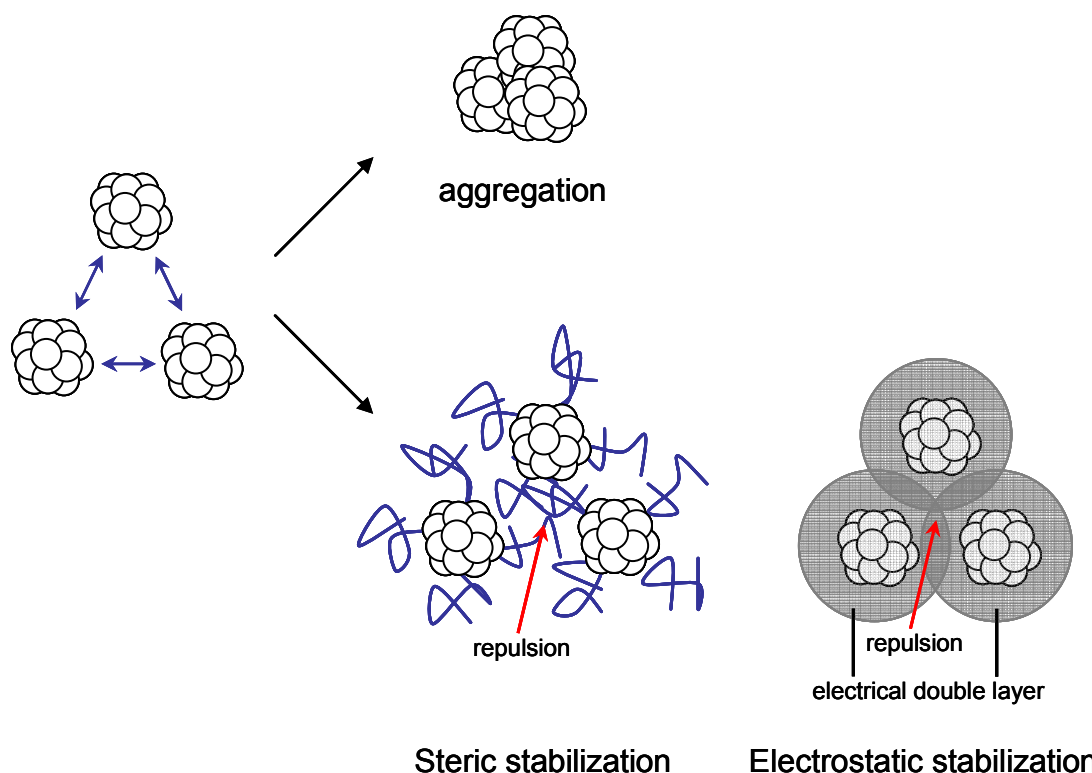


Figure 2.2 Schematic illustrations of aggregation, steric stabilization and electrostatic stabilization.

The formation of larger particles can be aggregated and precipitated as a metal. Therefore, the protection process can be described by 2 categories. Firstly, stabilizing by the steric effect and the stabilizer can stabilize silver nanoparticles. Secondly, the protection by the electrostatic repulsion, the stabilizer can prevent the aggregation of silver nanoparticles [25, 27, 30].

The stability of lyophobic colloid such as silver nanoparticles can often be enhanced by the addition of macromolecular material [23, 25]. The additional material can adsorb on the particles surface. This adsorbed material is a protective or stabilizing agent. The best protective agents are block copolymer, which have a lyophobic part that attaches the macromolecule strongly to the particles surface, and a lyophilic chain, which trails freely in the dispersion medium. The adsorbed macromolecule may influence stability by virtue of its effect on van der Waals and electric double layer interactions, but its most important role is likely to involve a

number of effects collectively termed steric stabilization. Basically, the conditions for dispersion stability will roughly be the same as the conditions for solubility of those parts of the stabilizing macromolecules that trail freely in the dispersion medium. If the particle aggregation takes place, it will be weak and easily reversed (flocculation), owing to the macromolecular material that still separates the particles. The balance between stability and flocculation is often a fine one that can be changed by raising or lowering the temperature.

For example, macromolecular materials are as follows:

Gelatin: weakly stabilized lyophobic colloid due to a weak binding between amino acids with silver nanoparticles. These weakly bound functional groups can easily be exchanged with donor ligands [26].

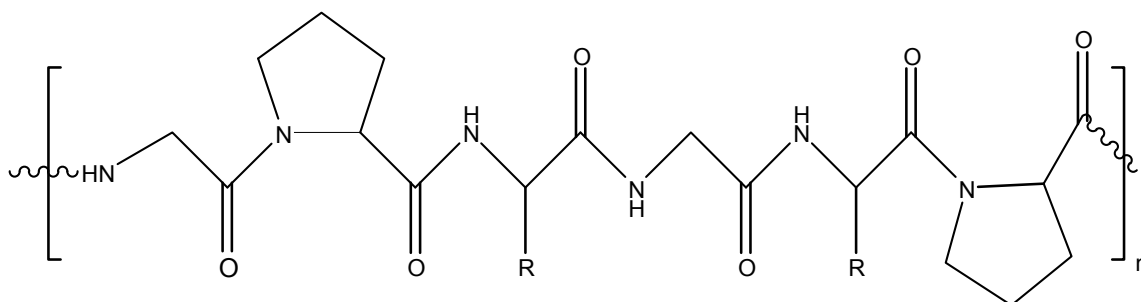


Figure 2.3 Structure of gelatin.

Methyl cellulose: the protective aggregation of lyophobic colloid comes from steric effect of long chain, slight branching like linear polymer [31].

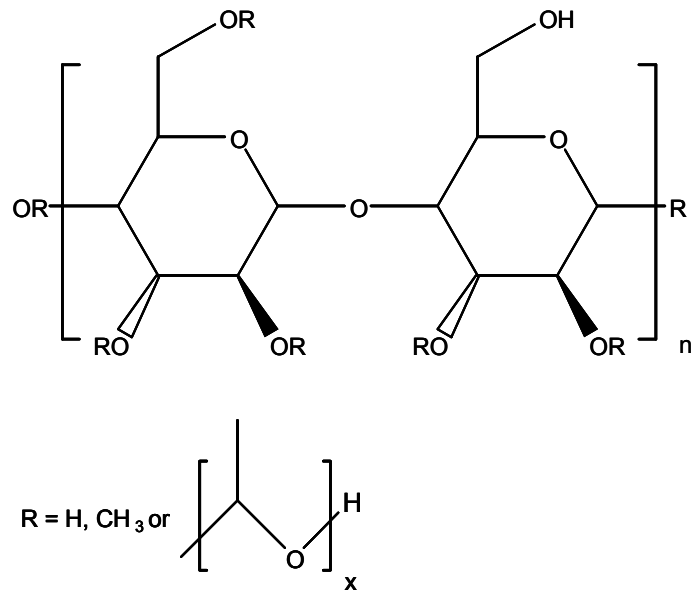


Figure 2.4 Structure of methyl cellulose.

Soluble starch: The steric effect and hydroxyl group of amylose component stabilized lyophobic colloid in unique and small size.

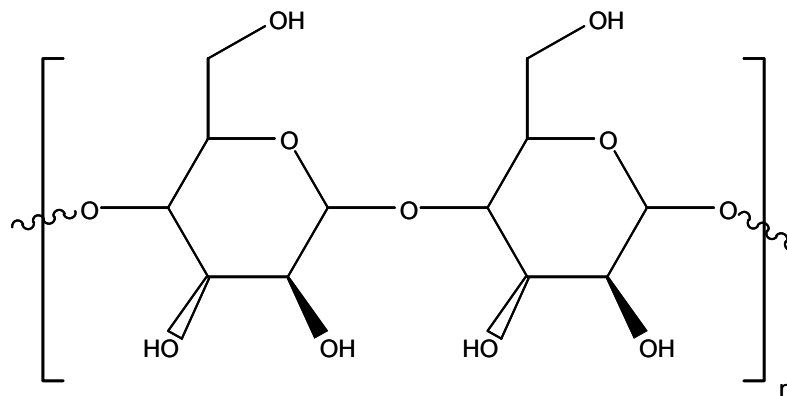


Figure 2.5 Structure of starch.

Colloidal dispersions are made more sensitive to aggregation by addition small quantities of macromolecular material or surfactant that would act as stabilizing agents if we used in larger amounts. The neutralizer surface charge of colloid particle is by addition of additive (for example, an ionic surfactant) which is the opposite

charge with colloid particle. This addition also increases steric effect on the surface of colloid.

Low concentration of macromolecules may bring about a rather loose flocculation by mean of a bridging mechanism in which the molecules are adsorbed with part of their length on two or more particles.

Particle aggregation has important consequences for the sedimentation and flow of dispersions. If sedimenting particles stick to one another, the final sediment volume will be high. Particle aggregation results in increasing viscosity and possible gelling.

2.5 Characterization of the synthesized silver nanoparticles

The localized surface plasmon resonance spectroscopy of silver nanoparticles was thoroughly exploited for the synthesis system development. When the incident photon frequency resonates with the collective oscillation of the conduction electron in the metal nanoparticles is frequency known as a *Localized Surface Plasmon Resonance* (LSPR) [14-17]. When the environment of metal nanoparticles was changed, LSPR shifts were observed. Electromagnetic field enhancement near the surface of nanoparticles is associated with extinction efficiency of nanoparticles, responsible for the intense signals.

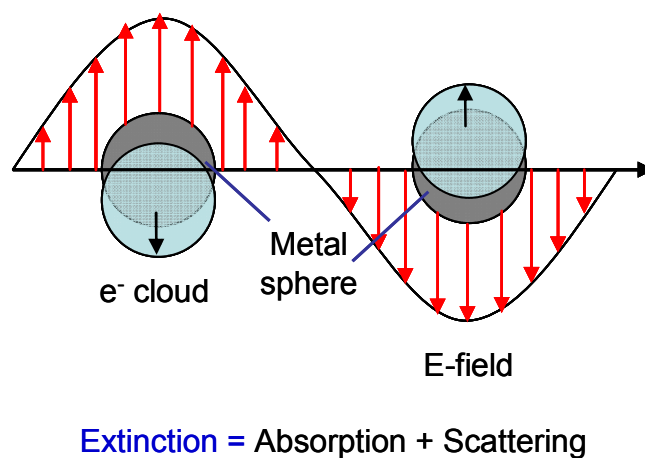


Figure 2.6 Localized Surface Plasmon Resonance (LSPR) phenomenon.

The particles shape, dimension, and particle size distribution are associated with the measured extinction spectra [14]. Therefore, we can obtain the direct particle information from the simple measurement, instead of the complex sample preparation and time – consuming TEM measurement for numerous sample measurements.

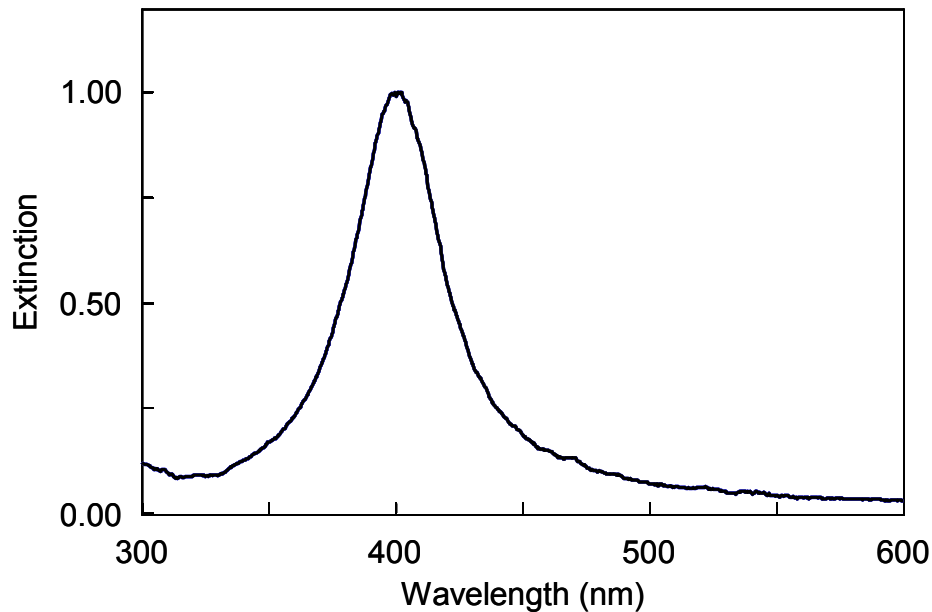


Figure 2.7 The extinction spectrum of silver nanoparticles.

The maximum and the full width at half height (FWHM) of plasmon band in UV-Visible were employed for characterizing silver nanoparticles. The specific optical properties of nanoparticles are caused by the collective oscillation of the electrons around the particles [14-15]. Results from extinction measurements were rapidly analyzed without complex sample preparation. According to the prior research, the narrow peak suggested the narrow particle size distribution. The shift of the peak to longer wavelength means the larger particle size. The symmetrical shape of plasmon band suggested the shape of particles was sphere [14, 31].

2.6 Tubular flow reactor

The influences of the flow patterns such as flow velocity, viscosity of the fluid and diameter of the tube, determined with Reynolds numbers, Re , were calculated using the following equation [9, 33]:

$$Re = \frac{\rho D v}{\mu} \quad (2.5)$$

where ρ is the density of the fluid (kg/m^3), D is the inert diameter of the tube (m), v is the linear flow velocity (m/s), ν is kinematic viscosity of the fluid (m^2/s), and μ is dynamic viscosity of the fluid ($\text{N}\cdot\text{s}/\text{m}^2$). This classifies the fluid flow patterns in 3 types that is the laminar flow pattern (Re is less than 2,000), transition flow pattern (Re is more than 2,000 and less than 4,000), and turbulent flow pattern (Re is more than 4,000).

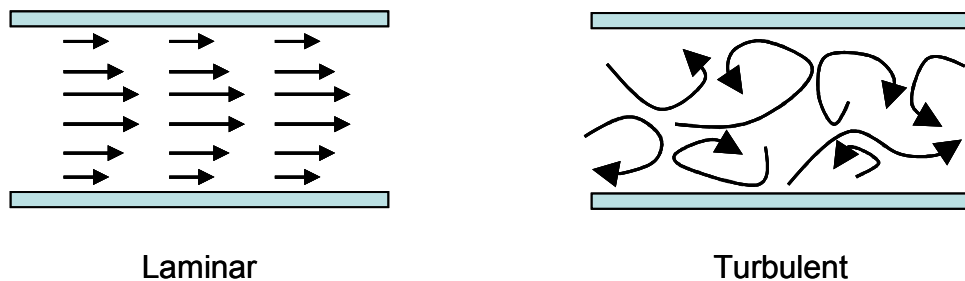


Figure 2.8 Illustration of the flow patterns of the fluid in a tube.

CHAPTER III

EXPERIMENTAL

3.1 Materials and Instruments

3.1.1 Materials

Silver metal (99.99%) was purchased from jewelry store. Silver nitrate, sodium borohydride, nitric acid and soluble starch were purchased from Merck[®]. Methyl cellulose and gelatin were purchased from Fluka[®]. Silver nitrate was achieved from our homemade.

3.1.2 Instruments

3.1.2.1 Ocean Optics Portable UV-Visible spectrometer equipped with a Deuterium-Halogen light source DH 2000 and USB 2.0 Fiber Optic spectrometer USB4000-UV-VIS detector.

3.1.2.2 EOL JEM-2010 analytical transmission electron microscope operated between 80 and 200kV at a point resolution of 0.23 nm, with a LaB₆ electron gun.

3.1.2.3 Novel reactor (homemade)

3.2 Novel reactor for preparation of highly concentrated colloid of silver nanoparticles

3.2.1 The Design, develop and invent reactor for the continuous system

The concepts; the design; develop and invent reactor for synthesis process can be divided to 3 categories: Firstly, the reactor is high efficient mixing because, the

reduction between silver nitrate with sodium borohydride is the spontaneous reaction; the efficient mixing effected the local concentration and concentration distribution of solution. This reaction is perfect homogenous concentration distribution of solution and perfect homogenous phase, the forming particles was uniform with narrow size distribution. Secondly, the reaction was no active silver ions in media solution; when the silver ions were reduced to silver nanoparticles, some active silver ions in media solution were reduced on the surface of silver nanoparticles and aggregation to form large particles by autocatalytic pathway. The formations of silver nanoparticles were non-uniform with a broad size distribution. Finally, the process was continuous production for the large amount of product.

3.2.1.1 Batch reactor

The batch reactor for the synthesis of large amount of high concentration silver nanoparticles is designed based on the mixing of silver salt solution with the solution of reducing agent has to mix with homogeneous and vigorous mixture in batch reactor under a vigorous stirring from mechanical stirrer was shown in Figure 3.1. The solution of silver nitrate was added to the sodium borohydride solution under a vigorous stirring. A dark cloud appeared and turned to yellowish brown within a few seconds. When all reactants were completely added, the solution turned dark brown.

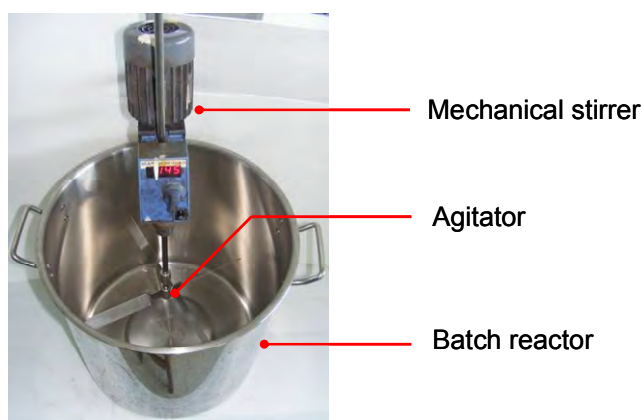


Figure 3.1 The batch reactor for the synthesis of high concentration silver nanoparticles

3.2.1.2 Jet Semi-Continuous Flow Reactor

This novel jet semi-continuous flow reactor for synthesizing silver nanoparticles is designed based on the mixing of silver salt solution with the solution of reducing agent has to mix with homogeneous and vigorous mixture in tubular reactor by air jet from air compressor, the time of the synthesized silver nanoparticles in the reactor could be very short, and the products rapidly flow out from reactor to storage as shown in Figure 3.2. To begin the operation, silver nitrate solution and sodium borohydride solution were filled into the container of silver salt solution and container of reducing agent. Then, these solutions were loaded into the reservoir of silver salt solution and the reservoir of reducing agent solution by gravitation. Next, the synthesized high concentration silver nanoparticles using the silver nitrate solution and the sodium borohydride solution in reservoirs were mixed within mixing chamber by air jet from air compressor and the product rapidly flow out from reactor to storage. A dark yellow solution appeared within a few seconds and the solution turned dark brown.

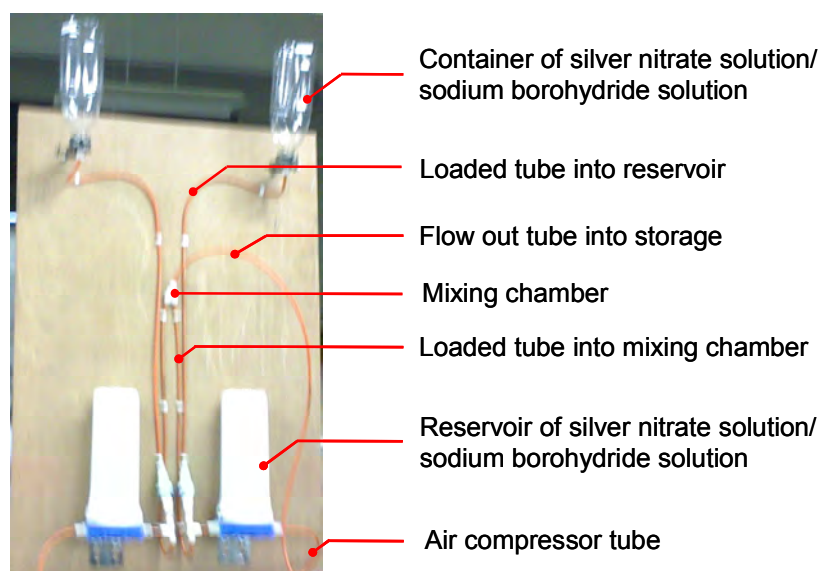


Figure 3.2 Jet semi-continuous flow reactor for the synthesis of high concentration silver nanoparticles.

3.2.1.3 Tubular flow reactor (The pulse flow processes)

The apparatus for novel tubular flow reactor (the pulse flow processes) for synthesizing silver nanoparticles is invented based on the mixing of silver salt solution with the solution of reducing agent has to mix with homogeneous and vigorous mixture in tubular reactor by the compressed pressure from connecting rod of cylinder, the time of synthesized silver nanoparticles in the reactor could be very short, and the products rapidly flow out from reactor to storage as shown in Figure 3.3. At the beginning of this operation, silver nitrate solution and sodium borohydride solution were filled into the container of silver salt solution and container of reducing agent. Then, these solutions were sucked from containers into the syringe of silver salt solution and the syringe of reducing agent solution by the compressed pressure from connecting rod of cylinder. Next, the synthesized high concentration silver nanoparticles using the silver nitrate solution and the sodium borohydride solution in syringes were mixed within mixing chamber by the compressed pressure from connecting rod of cylinder and the product rapidly flow out from reactor to storage. A dark yellow solution appeared within a few seconds and the solution turned dark brown. The pulse flow processes were repeated the synthesis of high concentration silver nanoparticles.

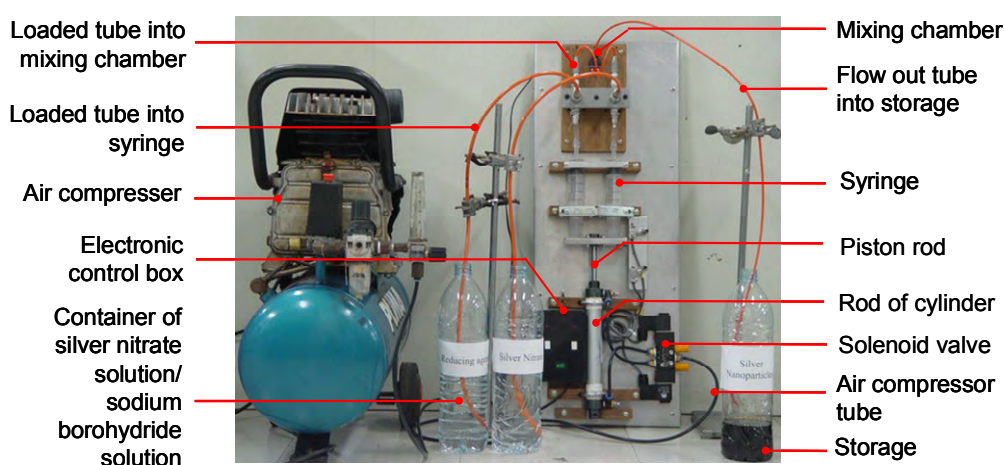


Figure 3.3 Tubular flow reactor (the pulse flow processes) for the synthesis of high concentration silver nanoparticles.

3.2.1.4 Tubular flow reactor (The continuous flow processes)

The novel tubular flow reactor (the continuous flow processes) for synthesizing silver nanoparticles is developed based on the mixing of silver salt solution with the solution of reducing agent has to mix with homogeneous and vigorous mixture in tubular reactor by pumping from diaphragm pump, the time of synthesized silver nanoparticles in the reactor could be very short, and the products rapidly flow out from reactor to storage as shown in Figure 3.4. In this work, silver nitrate solution and sodium borohydride solution were filled into the container of silver salt solution and container of reducing agent. Then, the synthesized high concentration silver nanoparticles by using the silver nitrate solution and the sodium borohydride solution in container were sucked and mixed within mixing chamber by pumping from diaphragm pump and the product rapidly flow out from reactor to storage. A dark yellow solution appeared within a few seconds and the solution turned dark brown. The flow processes was continuous the synthesis of high concentration silver nanoparticles.

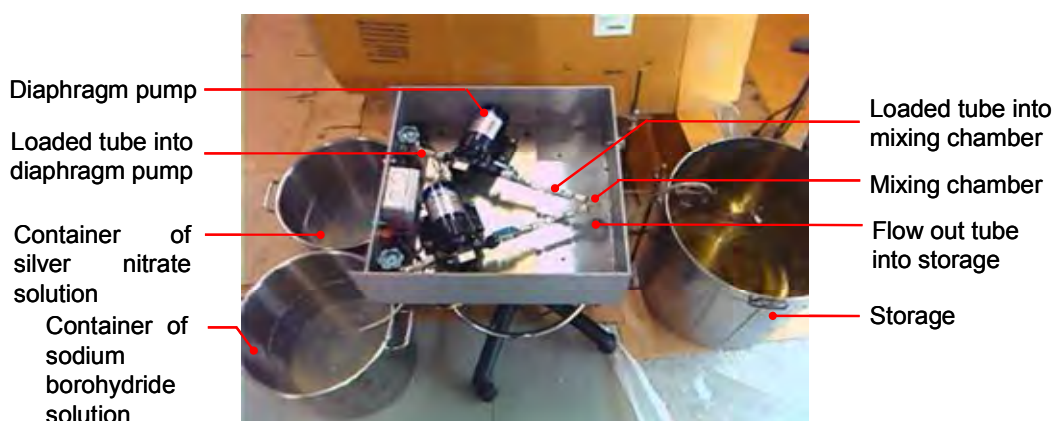


Figure 3.4 The tubular flow reactor for continuous synthesis of high concentration silver nanoparticles.

3.3 Synthesis of our homemade silver nitrate

A mixture of silver metal (99.99%, 100 g) and conc. nitric acid (200 mL) were heated until boiling at 100 – 120 °C for 2 hours and cool down at room temperature to give a white insoluble mass in nitric acid. The nitric acid was removed and the residue was filtered and crystallized from acetone. The crystal of silver nitrate was dried at 40 – 50 °C. The white solid (141.73 g, 90 % yield) with m.p. 212 – 213 °C was obtained.

Table 3.1 Comparison of silver nitrate properties and cost with our homemade and commercially available analytical grade.

Properties	Silver nitrate	
	Our homemade	Commercial product
Appearance	white solid	white solid
Melting point	212-213 °C	212 °C
pH	4 – 6	5 – 6
Cost (Baht/ 100 g)	1,338.7*	3,750**

* Estimated cost of our homemade silver nitrate summarized in Table A 1

** Merck®, AD 2009

3.4 Factors affecting the synthesis of high concentration silver nanoparticles

The highly concentrated silver nanoparticles (5,000 ppm) were synthesized by mixing silver salt solution with the solution of reducing agent for both batch reactors (Figure 3.1). An aqueous solution of 46 mM silver nitrate was prepared in 0.5 – 4.0% (w/v) stabilizer such as gelatin, methyl cellulose, and soluble starch. An aqueous solution of 23 - 70 mM sodium borohydride in the soluble starch solution was sequentially prepared. For the synthesis of silver nanoparticles by the batch reactor, the silver solution was added to the sodium borohydride solution under a vigorous stirring. A dark cloud appeared and turned to yellowish brown within a few seconds. When all reactants were completely added, the solution turned dark brown.

3.4.1 Influence of reducing agent

The various reducing agents (glucose and sodiumborohydride) were employed for silver nanoparticles synthesis. For the synthesis of silver nanoparticles using sodium borohydride as reducing agent, an aqueous solution of 4.6 mM silver nitrate was added to 4.6 mM of the sodium borohydride solution under a vigorous stirring. A dark cloud appeared and turned to yellowish brown within a few seconds. When all reactants were completely added, the solution turned dark brown. The synthesis of silver nanoparticles using glucose as reducing agent (excess), in the case of the reaction was heated up to the reaction temperature (about 90 °C) and maintained for 5 minutes. Then, the synthesis condition was similar to that reported using sodium borohydride as reducing agent. The brown color was from upon stirring mixture for 1 minute.

3.4.2 Influence of stabilizer

The stabilizers were varied form gelatin, methyl cellulose, and starch for synthesis of silver nanoparticles. An aqueous solution of 46 mM silver nitrate was prepared in gelatin solution. An aqueous solution of 46 mM sodium borohydride in the gelatin solution was sequentially prepared. For the synthesis of silver nanoparticles by the batch reactor, the silver solution was added to the sodium borohydride solution under a vigorous stirring. A dark cloud appeared and turned to yellowish brown within a few seconds. When all reactants were completely added, the solution turned dark brown. The conditions of silver nanoparticles synthesis by using methyl cellulose and starch were the same as that of using gelatin as stabilizer.

3.4.3 Influence of order of addition of reactant solution

To study the influence of order of addition of reactant solution on the synthesis of high concentration silver nanoparticles, the procedures are as follows: the stabilizer as soluble starch is prepared for synthesis of silver nanoparticles and the other experiments are synthesized the same as that of Section 3.4.2.

3.4.4 Influence of the concentration of reducing agent and stabilizer

The various concentrations of sodium borohydride (23, 35, 46 and 70 mM), and various concentrations of soluble starch (0.5, 2.0 and 4.0 %) were employed for synthesis of silver nanoparticles. The other synthesis condition was using the same as that of Section 3.4.2.

3.5 The factors affecting the production of large amount and high concentration silver nanoparticles

3.5.1 Comparison of synthesized silver nanoparticles from batch reactor with the reactor volume of 1 liter and 40 liters

To study the effect of reactor volume on the synthesized silver nanoparticles by batch reactor were varied from 1 liter and 40 liters, the synthesis condition of silver nanoparticles from the reactor volume of 1 liter using an aqueous solution of 46 mM silver nitrate (our synthesis) was prepared in 2.0% soluble starch, and an aqueous solution of 35 mM sodium borohydride in 2.0% the soluble starch solution was sequentially prepared. For the synthesis of silver nanoparticles by the batch reactor, the silver solution was added to the sodium borohydride solution under a vigorous stirring. A dark cloud appeared and turned to yellowish brown within a few seconds. When all reactants were completely added, the solution turned dark brown. The synthesis of silver nanoparticles from 40 liters batch reactor the using the novel batch reactor is shown in Figure 3.1. The reaction condition was as the same as synthesized silver nanoparticles from the reactor volume of 1 liter.

3.5.2 Synthesis of large amount and high concentration silver nanoparticles by novel reactor

3.5.2.1 Jet Semi-continuous flow reactor

The highly concentrated silver nanoparticles (5,000 ppm) were synthesized using an aqueous solution of 46 mM silver nitrate was prepared in 2.0% soluble starch, and an aqueous solution of 35 mM sodium borohydride in the 2.0% soluble starch solution was sequentially prepared. Silver nitrate solution and sodium borohydride solution were filled into the container of silver salt solution and container of reducing agent. The operation was the same as that of Section 3.2.1.2.

3.5.2.2 Tubular flow reactor (the pulse flow processes)

The large amounts of highly concentrated silver nanoparticles (5,000 ppm) were synthesized by tubular flow reactor (the pulse flow processes). The synthesis preparations were similar to that reporting in Section 3.5.2.1. The operation was the same as that of Section 3.2.1.3.

3.5.2.3 Tubular flow reactor (the continuous flow processes)

The preparation of the synthesized high concentration silver nanoparticles by tubular flow reactor (the continuous flow processes) were the same as that of Section 3.5.2.1. The operation was the same condition as that of Section 3.2.1.4.

3.5.3 Influence of flow rates on the synthesis of silver nanoparticles

To study the effect of the flow rate for producing silver nanoparticles by tubular flow, the reactor were varied as the flow rates of 3.1, 14.4, 800 and 4,000 mL/min. The length of tube was fixed at 20 cm and the diameter of tube was 6 mm. The preparation and the operation of the synthesized high concentration silver nanoparticles were the same as that of Section 3.5.2.3.

3.5.4 Influence of reactor diameter

The effect of reactor diameter for producing silver nanoparticles by tubular flow reactor were varied as 6, 8 and 10 mm. The preparation and the operation of the synthesized silver nanoparticles were similar to that reporting in Section 3.5.2.3.

3.5.5 Comparison of the synthesized silver nanoparticles from batch reactor with that of tubular flow reactor

The normalized extinction spectra of the synthesized silver nanoparticles by batch reactor (40 liters) and tubular flow reactor (40 liters) were measured. The results were compared with the size and size distribution.

3.6 Comparison of silver nanoparticles from our synthesis by tubular flow reactor with the available commercial product

The normalized extinction spectra of the synthesized silver nanoparticles from our synthesis by tubular flow reactor and the available commercial product were measured. The results were compared with the size and size distribution.

3.7 The stability of synthesized silver nanoparticles

The synthesized silver nanoparticles by tubular flow reactor kept for six months after synthesis were measured by UV-Vis spectrophotometer. The results were compared with the size and size distribution.

3.8 Economical point of view

Production costs of high concentration silver nanoparticles from our synthesis are summarized in Table 3.2

Table 3.2 Comparison cost of high concentration silver nanoparticles with our synthesis and the available commercial product

	Silver nanoparticles (commercial product)	Silver nanoparticles (our synthesis)	
		Type 1: Synthesized from commercial AgNO ₃	Type 2: Synthesized from Ag metal
Total cost (Baht/1liter)	8,500*	1,008.4**	622.8**

* Silver nanoparticles (available commercial product; 10,000 ppm/ 1liter) = 8,500 Baht,
<http://nanobio.bioneer.com/AccuSilversol.pdf>, AD 2010

** Estimated cost of our synthesized silver nanoparticles is summarized in Table A 2

3.9 Characterization of synthesized high concentration silver nanoparticles

3.9.1 UV-Visible spectroscopy

The plasmon absorptions of the synthesized silver nanoparticles were measured by Ocean Optics Portable UV-Visible spectrometer (USB4000-UV-VIS detector) equipped with the Deuterium-Halogen light source DH 2000. The sample was diluted with distilled water in order to get the final concentration of 10 ppm.

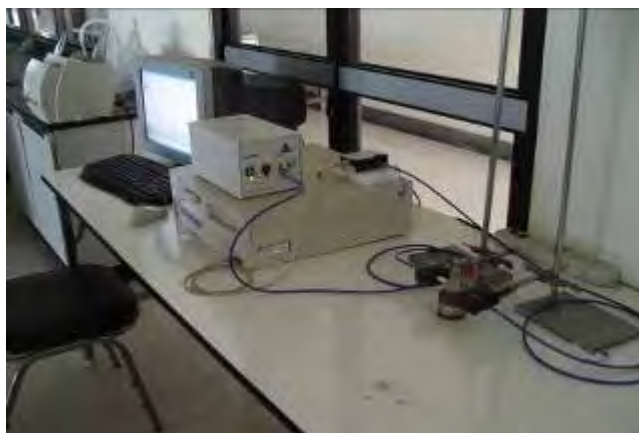


Figure 3.5 Ocean Optics Portable UV-Visible spectrometer.

3.9.2 Transmission electron microscope (TEM)

The particles morphology of the highly concentrated silver nanoparticles were measured via JEOL JEM-2010 analytical transmission electron microscope, which operated between 80 and 200 kV at a point resolution of 0.23 nm with the LaB₆ electron gun. The samples as silver nanoparticles were prepared by placing a drop of solution onto a carbon-coated copper grid. After the silver nanoparticles solutions were left dried out, TEM images of silver nanoparticles were collected.



Figure 3.6 JEOL JEM-2010 analytical transmission electron microscope.

3.10 Antibacterial activity testing and safety testing in laboratory animals with our synthesized silver nanoparticles

3.10.1 Antibacterial activity testing with our synthesized silver nanoparticles

Antibacterial activity of our synthesized silver nanoparticles was tested for its ability to reduce the growth of bacterial pathogens. In this experiment, *Escherichia coli* as Gram-negative bacteria, *Staphylococcus aureus* and methicillin resistant *Staphylococcus aureus* (MRSA) as Gram-positive bacteria were used. To compare the antibacterial activity, silver nanoparticles (50 ppm) were added into the tube that contained 5 mL of NSS (normal saline solution) and another tube that had only NSS

acted as a control. The experiment was performed in duplicate. The details of the experimental procedure modified from that of Hoffman et al. (2001), are shown in Figure B 1. Antibacterial activity of silver nanoparticles was determined under the supervision of Laboratory RM # 408, Department of Microbiology, Faculty of Science, Chulalongkorn University.

3.10.2 Safety testing in laboratory animals with our synthesized silver nanoparticles

Silver nanoparticles are investigated by the acute oral toxicity, the acute dermal toxicity and the acute eye irritation and corrosion of silver nanoparticles using the recommended Organization for Economic Cooperation and Development (OECD) guidelines No. 425, 434 and 405, respectively. And then, silver nanoparticles are investigating the acute pulmonary toxic test and the studies for describing the acute pulmonary pathological effects caused by intratracheal exposure to various doses of silver nanoparticles are shown in Appendix C. Our synthesized silver nanoparticles was investigated with safety testing in laboratory animals from Department of Pathology, Faculty of Veterinary Science, Chulalongkorn University.

3.11 Industrial applications of our synthesized silver nanoparticles

The synthesized silver nanoparticles were applied into commercial products and industrial applications. For examples of typical products: fabric as sportswear (Nan Yang Group Nan Yang Inspiration Center Co., Ltd.), colloid as deodorant (CutePress SSUP group Co., Ltd.), polymer as water filter (PURE Siam Cast Nylon Co., Ltd.) and detergent (Lion Co. (Thailand), Ltd.).

CHAPTER IV

RESULTS AND DISSCUSION

The region extinction spectra in UV-Visible were employed for characterizing synthesized silver nanoparticles. The specific optical properties of nanoparticles are the consequence of the characteristic collective oscillation of the electrons around the particles [17, 14]. The results were rapidly analyzed by considering peak shape, peak positions, and peak intensities. According to the prior research [18-20], the narrow peak suggested the narrow particle size distribution. The shift of the peak to longer wavelength implied the larger particle size. The symmetrical shape of extinction spectrum suggested the spherical particles [31-37].

4.1 Various factors affecting the synthesis of high concentration silver nanoparticles

The synthesis of high concentration silver nanoparticles by chemical reduction method was optimized with various reducing agents and stabilizer in order to optimal chemical reagents for producing stable silver nanoparticles in large amount. This process required the strong reducing agent for producing numerous metal nuclei in fast nucleation rate, and the stabilizer for protecting aggregation of synthesized nanoparticles.

4.1.1 The influence of reducing agents

The various reducing agents (glucose and sodium borohydride) were employed for silver nanoparticles synthesis. The results are shown in Figure 4.1. The maxima of normalized extinction spectra of synthesized silver nanoparticles obtained by glucose and sodium borohydride as reducing agents showed the peak at 416 nm and 390 nm, and have FWHH about 85 nm and 56 nm, respectively. These result suggested that the size of synthesized silver nanoparticles obtained from glucose as reducing agent were larger with broader size distribution than that of the synthesized

silver nanoparticles using sodium borohydride. It is known that glucose is the weak reducing agent; the nucleation rate is slow and the producing numerous metal nuclei is low. So, some ions could be inducted with irregularity on surface of nuclei. The formations of particles are non-uniform sizes and having the large particles with broad size distribution. In contrast, the sodium borohydride is the strong reducing agent. The reactions of sodium borohydride occur rapidly causing the immediate nucleation and the nucleation rate is high for the formation of silver particles. The obtained nanoparticles were small and had narrow size distribution. Therefore, the appropriate reducing agent using in this process is sodium borohydride.

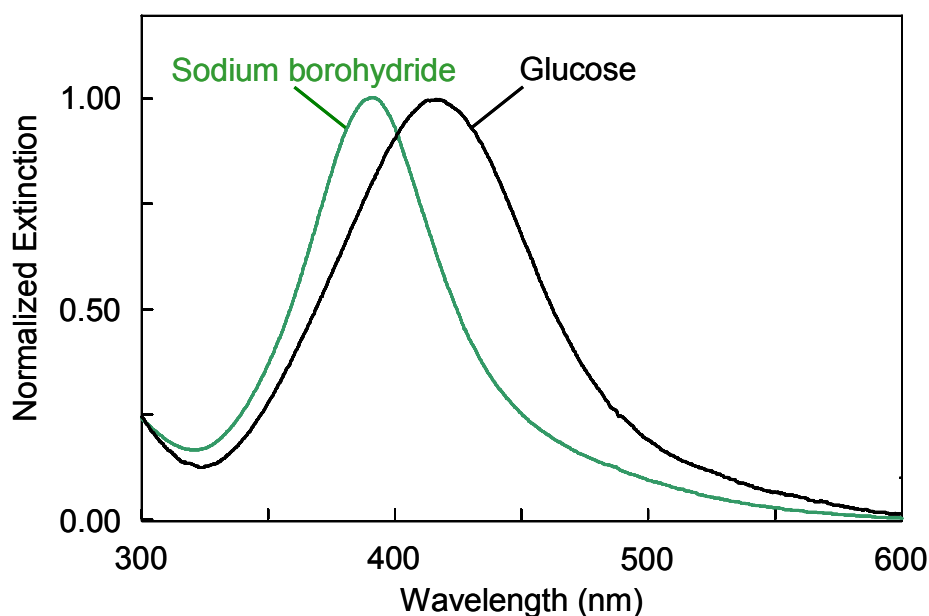


Figure 4.1 The normalized extinction spectra of highly concentrated silver nanoparticles (5,000 ppm) synthesized from batch reactor with various reducing agents.

Table 4.1 Extinction maxima and FWHH of extinction spectra of synthesized silver nanoparticles obtained from various reducing agents

Reducing agent	λ_{\max} (nm)	The full width at half height, FWHH (nm)
Glucose	416	85
Sodium borohydride	390	56

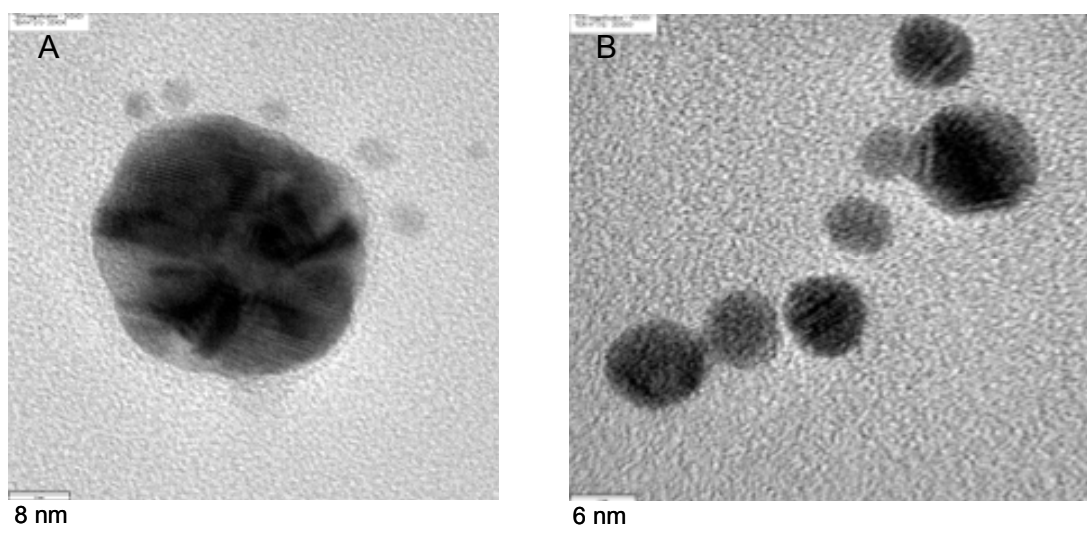


Figure 4.2 The transmission electron microscopy (TEM) images of the silver nanoparticles synthesized by various reducing agents: (A) glucose (B) sodium borohydride.

The proposed particle growth pathways are shown in Figure 4.3.

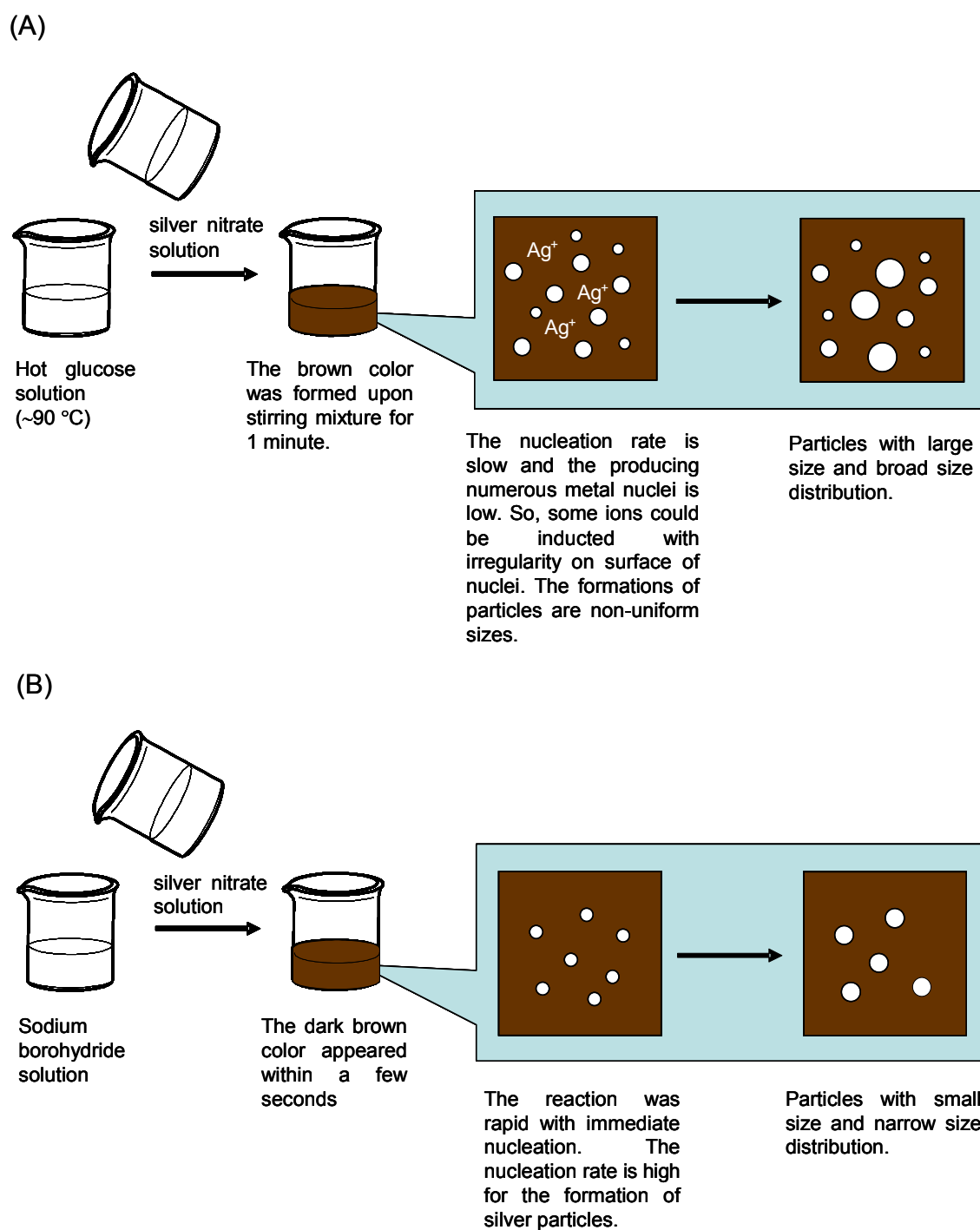


Figure 4.3 The proposed growth pathways of silver nanoparticles when (A) weak reducing agents and (B) strong reducing agents were employed as reducing agents.

4.1.2 The effect of stabilizers

The influence of stabilizer (gelatin, methylcellulose, and soluble starch) on particle shape, particles size and particles size distribution of synthesized silver nanoparticles were investigated. The results are shown in Figure 4.4. The maxima of normalized extinction spectra of silver nanoparticles stabilized by gelatin and methyl cellulose showed the peak at 430 and 417 nm, respectively. The quadrupole at 350 nm and tailing around 475 nm were observed. The FWHH of extinction spectra of silver nanoparticles stabilized with gelatin and methyl cellulose were 110 and 75 nm, respectively. These suggested a large size of synthesized silver nanoparticles with a broad size distribution, as well as the shape of imperfect spherical particles. The symmetrical extinction spectrum with the maximum located around 400 nm, and has FWHH about 45 nm were obtained from silver nanoparticles stabilized with soluble starch. – This represented the small size and narrow size distribution of spherical silver nanoparticles. It was found that the stability of silver nanoparticles with gelatin or methyl cellulose is the lowest. On the other hand, the stability of silver nanoparticles with soluble starch is the highest. It is known that sodium borohydride as reducing agent with silver nitrate is the spontaneous reaction. These reaction, the local concentration is perfect homogenous concentration distribution of solution and perfect homogeneous phase. So, the formations of particles are uniform sizes and narrow size distribution. For gelatin and methyl cellulose, the results suggested that the effect of low efficient mixing from heterogeneous phase of stabilizer as gelatin and methyl cellulose, while adding sodium borohydride with gelatin or methyl cellulose were obtained flood of foam in the solution. In addition, the stability of gelatin that provided amino functional groups for coordinating with silver metal. It can easily be exchanged with other metal due to the less steric in this stabilizer [10, 17-20]. Methyl cellulose utilized the steric effect for stabilizing silver nanoparticles. However, this stabilizer lacks of functional groups that stabilized silver nanoparticles. Methyl cellulose is sparingly soluble in water [11, 18]. Those results were decreased efficient stabilization of silver nanoparticles. The formations of particles from gelatin and methyl cellulose as stabilizer were non-uniform sizes and broad size distribution with imperfect spherical particles. In the case of soluble starch, it can be explained in

term of the solubility and stabilizer of starch with functional groups. The solutions were showed the high efficient stabilization of silver nanoparticles. Moreover, the combinations of steric effect and hydroxyl groups of amylose component stabilized silver nanoparticles in unique and small size [14, 22]. The formations of particles were uniform sizes and narrow size distribution. Therefore, the appropriate stabilizer used in this process was soluble starch.

Table 4.2 Extinction maxima and FWHH of extinction spectra of synthesized silver nanoparticles obtained from various stabilizers

Stabilizers	λ_{\max} (nm)	The full width at half height, FWHH (nm)
Gelatin	417	75
Methyl cellulose	430	110
Sodium borohydride	400	45

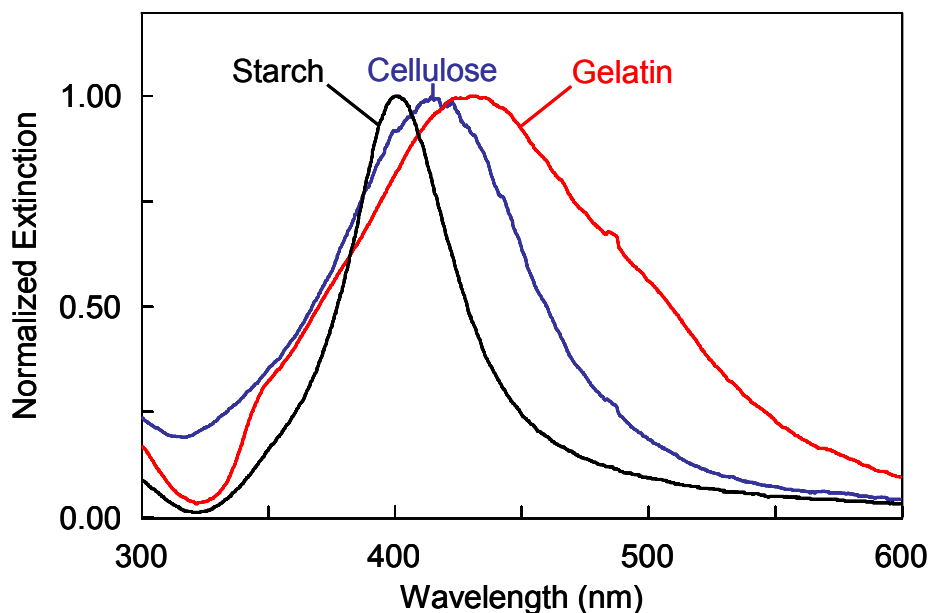


Figure 4.4 The normalized extinction spectra of 5,000 ppm silver nanoparticles synthesized from batch reactor with various stabilizers.

4.1.3 Influence of the order of addition of reactant solution

The order of addition of the sodium borohydride solution and silver nitrate solution also affect the size distribution. The influences of order of addition, on the synthesized silver nanoparticles are shown in Figure 4.5. The maximum and FWHH of normalized extinction spectrum of synthesized silver nanoparticles obtained with silver nitrate solution added to the sodium borohydride solution show the peak at 398 nm and 50 nm, respectively. The maximum of normalized extinction spectrum of synthesized silver nanoparticles obtained with sodium borohydride solution adding to silver nitrate solution was around 399 nm, and had FWHH about 55 nm. These results suggested that the size distribution of synthesized silver nanoparticles obtained from silver nitrate solution added to sodium borohydride were narrower.

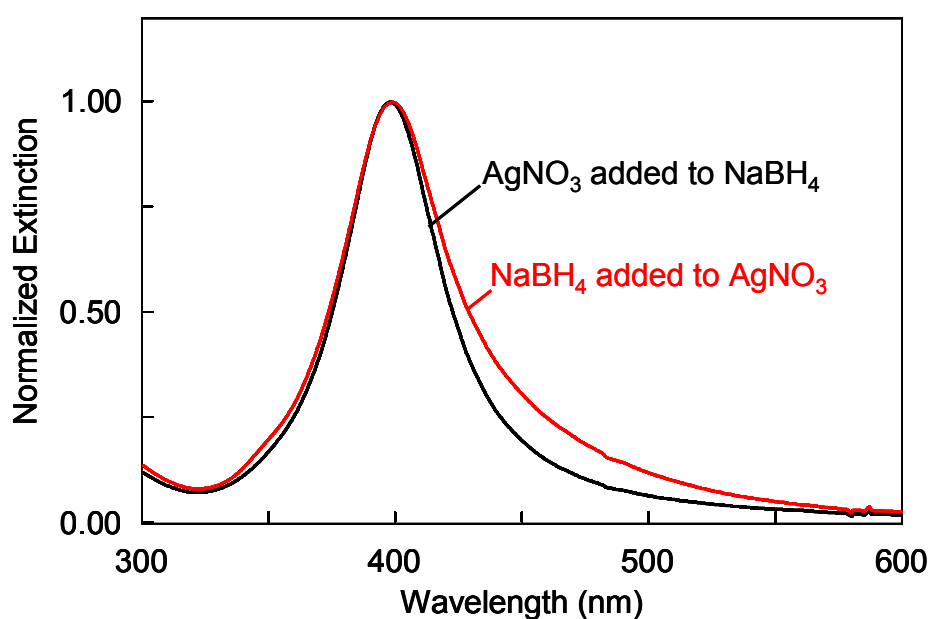


Figure 4.5 The normalized extinction spectra of synthesized silver nanoparticles when using different order of reactant addition.

The proposed particle growth pathways with different order of reactant addition for synthesizing high concentration silver nanoparticles are shown in Figure 4.6.

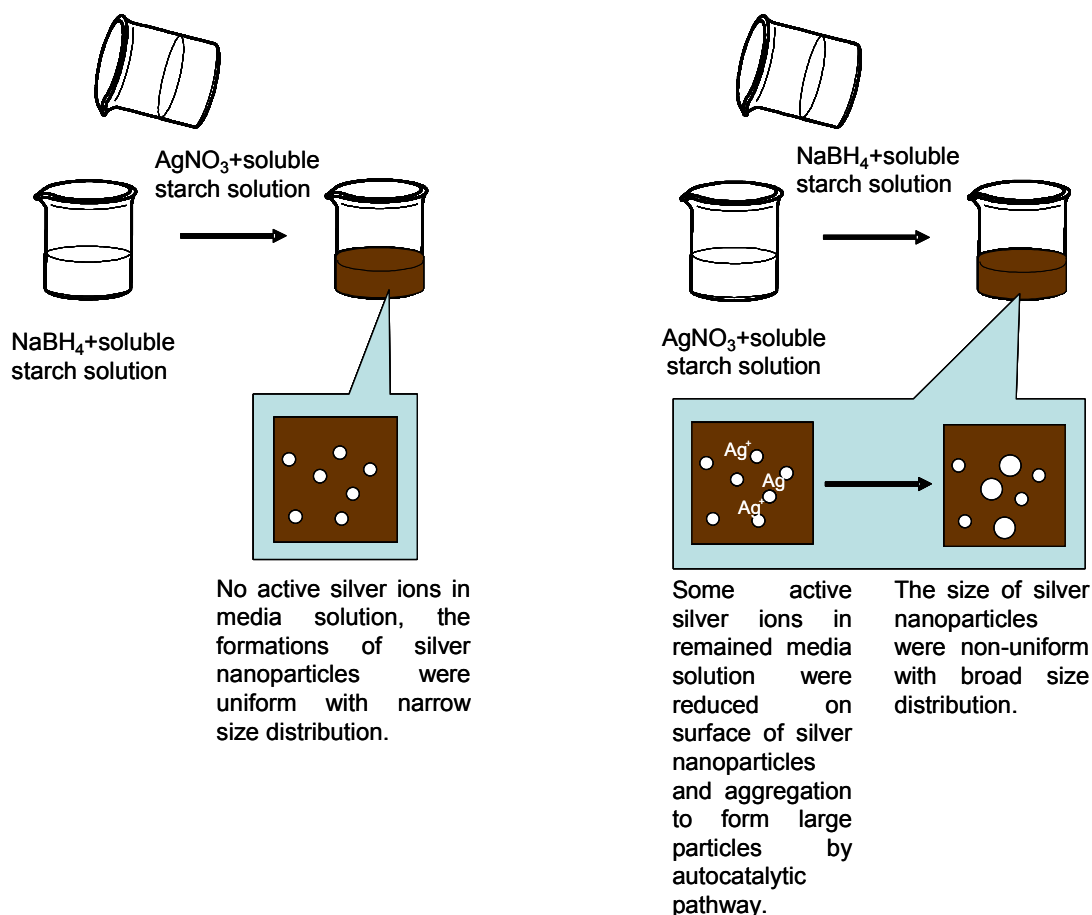


Figure 4.6 The illustration of order of addition for synthesizing high concentration silver nanoparticles.

When silver nitrate solution was added to the sodium borohydride, the particles size distribution was narrow because, the silver ions were completely reduced to silver nanoparticles. No active silver ions in media solution reduced on surface of silver nanoparticles by with narrow size distribution.

Vice versa, when sodium borohydride solution was added to the silver nitrate solution, some active silver ions in media solution were reduced on the surface of silver nanoparticles and aggregated to form large particles by autocatalytic pathway. So, the formations were non-uniform with a broad size distribution.

4.1.4 The effect of the concentration of reducing agent & stabilizer

The concentration of sodium borohydride (reducing agent) and concentration of soluble starch (stabilizer) were optimized. The normalized extinction spectra of highly concentrated silver nanoparticles (5,000 ppm; 46 mM) synthesized from batch reactor with various concentration of sodium borohydride (23, 35, 46 and 70 mM), and various concentration of soluble starch (0.5, 2.0 and 4.0 %) are shown in Figure 4.7. The maxima of normalized extinction spectra of silver nanoparticles obtained with 23 mM sodium borohydride, and 2.0 and 4.0% soluble starch were around 400 nm having the symmetrical shape with the FWHH about 47 and 50nm, respectively. The maxima of normalized extinction spectra of silver nanoparticles obtained with 35 mM sodium borohydride, and 2.0 and 4.0% soluble starch were at 400 nm, having symmetrical shape with the FWHH about 42 and 52nm, respectively. When 0.5% soluble starch was used; silver nanoparticles with 23 and 35 mM sodium borohydride showing the peak around 400 nm. The quadrupole at 350 nm and the tailing around 450 nm were found as well as the FWHH was about 63 and 64 nm, respectively. These results suggested that the size distribution of synthesized silver nanoparticles was broader with imperfect spherical shape comparable to those obtained from 23 and 35 mM sodium borohydride, and 2.0 and 4.0% soluble starch. It meant that the concentration of 0.5% soluble starch was not enough for stabilizing silver nanoparticles. In addition, there are the formations of the larger silver nanoparticles. However, the concentration of 4.0% soluble starch is improper as the stabilizer, because the increased concentration of soluble starch was obtained flood of foaming as the heterogeneous phase solution. The stability of silver nanoparticles was weak and aggregating when 23 mM sodium borohydride was used and the broad size distribution of silver nanoparticles were found after 7 days.

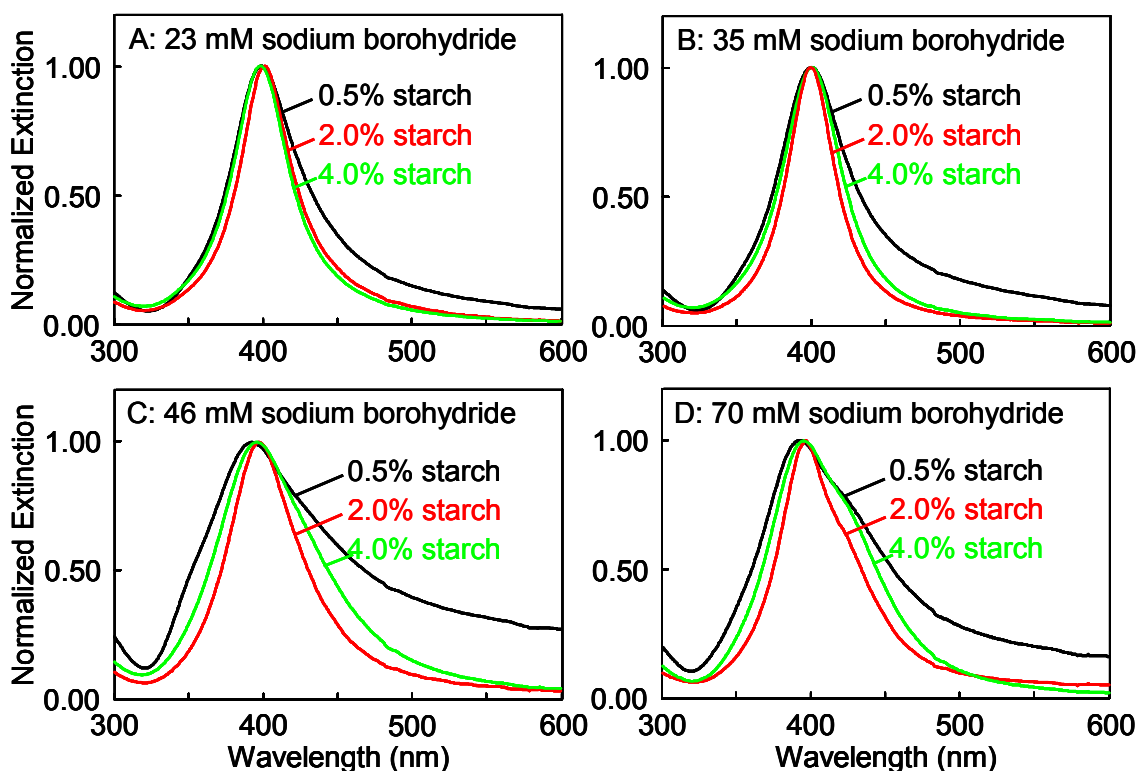


Figure 4.7 The normalized extinction spectra of highly concentrated silver nanoparticles (5,000 ppm) synthesized from batch reactor with various concentration of soluble starch (0.5, 2.0 and 4.0 %) and various concentration of sodium borohydride (A) 23 mM, (B) 35 mM, (C) 46 mM and (D) 70 mM.

The maximum of normalized extinction spectrum of silver nanoparticles obtained with 46 mM sodium borohydride, and 2.0% soluble starch was at 398 nm. The symmetrical peak shape had the FWHH about 63 nm. The maximum of normalized extinction spectra of silver nanoparticles obtained with 46 mM sodium borohydride, and 0.5% and 4.0% starch showed the peak around 395 nm with the quadrupole situated at 350 nm and the tailing around 450 nm. The FWHH was about 136 and 89 nm, respectively. This result suggested that the size distribution of synthesized silver nanoparticles was broad and the particle shape was imperfect sphere.

The maximum of normalized extinction spectra of silver nanoparticles obtained with 70 mM sodium borohydride and 0.5%, 2.0% and 4.0% soluble starch

showed the peak around 395, 398 and 395 nm with the FWHH about 106, 64 and 82 nm, respectively. These implied that the use of high concentration of sodium borohydride (70 mM) obtained complete and fast reaction for producing small size of silver nanoparticles. However, the concentration of stabilizer was insufficient for stabilizing silver nanoparticles from aggregation into large particles size.

From those studies, the optimal condition for synthesizing silver nanoparticles was 35 mM sodium borohydride (reducing agent) and 2.0% soluble starch as stabilizer for producing large amount as well as high concentration and stable silver nanoparticles.

This research was the synthesized silver nitrate for reducing the cost of import silver nitrate and producing low cost of silver nanoparticles. The synthesis of silver nanoparticles from silver nitrate was in similarity with our homemade comparable to that obtained with available commercial product as shown in Figure B 2.

Summary

- √ The silver nanoparticles were reproducibility of the synthesized by chemical reduction of silver nitrate with sodium borohydride for producing large amount high concentration silver nanoparticles.
- √ The optimal molar ratio of silver nitrate to sodium borohydride was 1.00 to 0.75.
- √ The optimal concentration of soluble starch 2% (w/v) were used as a stabilizer.
- √ The synthesized silver nanoparticles were narrow size distribution with FWHH about 42 nm and spherical with the mean size of 10 nm.
- √ The synthesized silver nanoparticles was in similarity with that getting started from our homemade silver nitrate comparable to that obtained with getting started from silver nitrate as commercially available analytical grade.

4.2 The various factors affecting the production of large amount and high concentration silver nanoparticles

4.2.1 Comparison of the synthesized silver nanoparticles from batch reactor with the reactor volume of 1 liter and 40 liters

The normalized extinction spectra of 5,000 ppm silver nanoparticles synthesized from batch reactor with the reactor volume of 1 and 40 liters are shown in Figure 4.8. The maximum of normalized extinction spectra of silver nanoparticles obtained from the reactor volume of 1 liter was at 400 nm, symmetrical shape with the FWHH about 50 nm. However, the maximum of normalized extinction spectrum of silver nanoparticles obtained from 40 liter batch reactor shows the peak around 395 nm, the FWHH is about 64 nm, and the tailing around 450 nm. This result suggests that the size distribution of synthesized silver nanoparticles is broader compared batch reactor with the synthesized highly concentrated silver nanoparticles obtained from 1 liter.

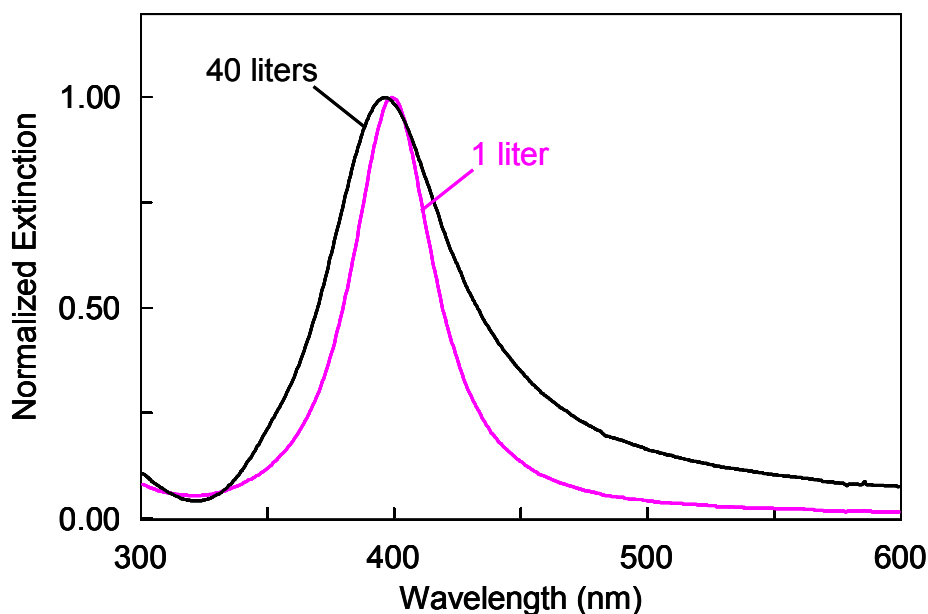


Figure 4.8 The normalized extinction spectra of 5,000 ppm silver nanoparticles synthesized from batch reactor with 1 liter and 40 liters reactor volume.

Transmission electron microscopy (TEM) images presenting silver nanoparticles synthesized from 1 liter and 40 liters batch reactor are shown in Figure 4.9. The particle shape of the silver nanoparticles obtained from the 40 liters batch reactor were imperfect sphere with borader size distribution than that of the silver nanoparticles obtained from the 1 liter batch reactor.

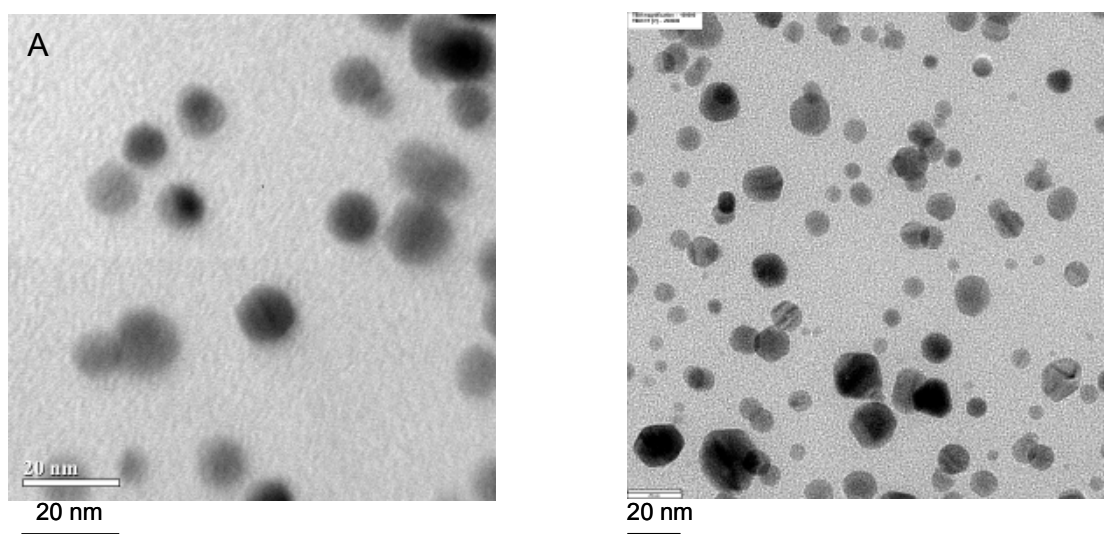


Figure 4.9 The TEM images representing silver nanoparticles synthesized from batch reactor with (A) 1 liter and (B) 40 liters reactor volume.

The proposed particles growth pathways of batch reactor are shown in Figure 4.10.

At 1 liter - batch reactor, the size of synthesized silver nanoparticles was small with narrow size distribution. The reduction between silver nitrate with sodium borohydride is the spontaneous reaction. The efficient mixing was effected the local concentration and concentration distribution of solution. The efficient mixing is high. The reaction is perfect homogenous concentration distribution of solution and perfect homogeneous phase. Therefore, the nanoparticles formations were uniform with narrow size distribution.

From 40 liters batch reactor, the mixing was poor with large volume; the efficient mixing is low, so the local concentration between silver ions and sodium

borohydride is non-homogeneous concentration distribution of solution and non-homogeneous phase. Some active silver ions in media solution were reduced on surface of silver nanoparticles and aggregation to form large particles by autocatalytic pathway. Therefore, synthesized nanoparticles were non-uniform with broad size distribution. The particles shape was imperfect sphere.

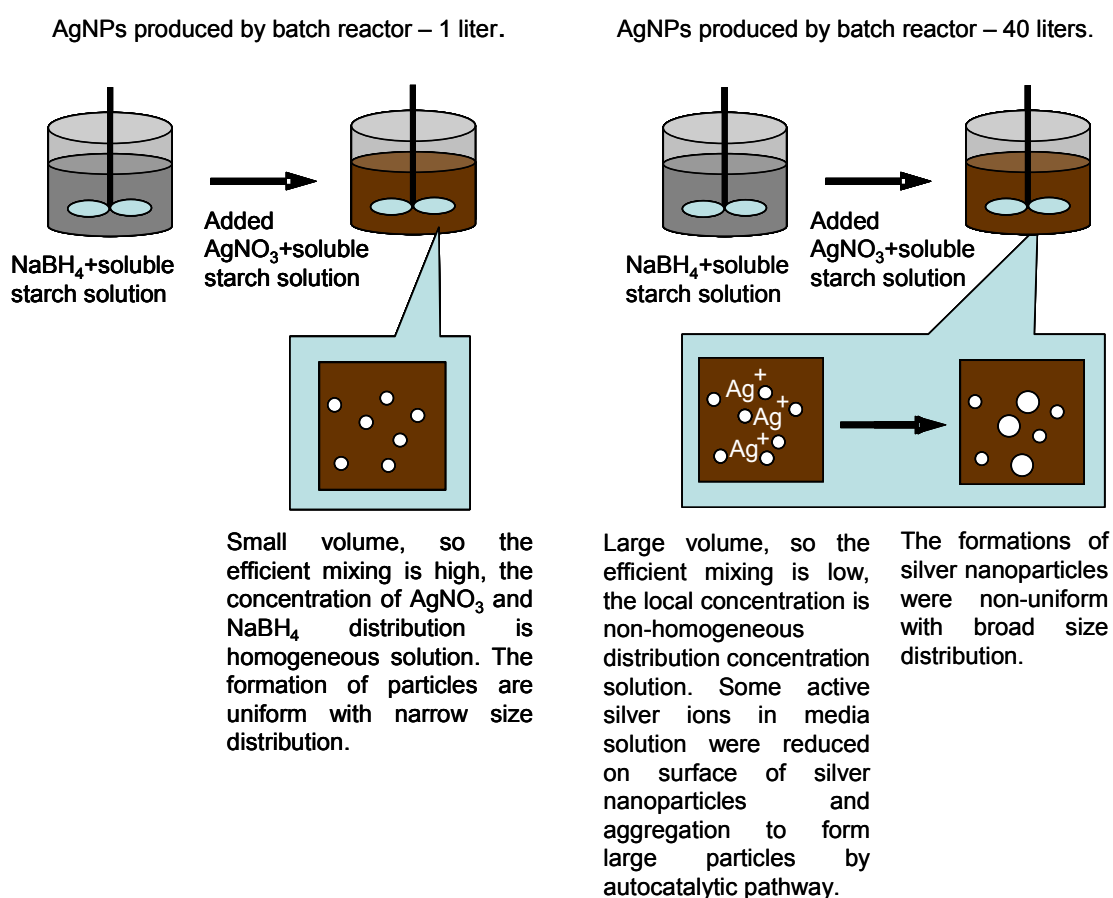


Figure 4.10 The illustrations of the high concentration silver nanoparticles synthesized from batch reactor.

4.2.2 Synthesis of large amount and high concentration silver nanoparticles by novel reactor

The maximum of production by batch reactor with the capacity about 40 liters per hour is not continuous production of silver nanoparticles and not overcome the large amount for support industrial. With increasing the large amount of high concentration silver nanoparticles by batch reactor (1 liter up to 40 liters), the efficient mixing is low, the formation of particles were non-uniform with broad size distribution. To solve problems of this research, the novel reactor was designed to resolve and develop for producing large amount of high concentration silver nanoparticles with narrow size distribution of particles.

The concepts, the design, develop and invent reactor for synthesis process can be divided to 3 categories: Firstly, the reactor is high efficient mixing because, the reduction between silver nitrate with sodium borohydride is the spontaneous reaction; the efficient mixing was effected the local concentration and concentration distribution of solution. This reaction is perfect homogenous concentration distribution of solution and perfect homogenous phase, the forming particles was uniform with narrow size distribution. Secondly, the reaction was no active silver ions in media solution; when the silver ions were reduced to silver nanoparticles, some active silver ions in media solution were reduced on the surface of silver nanoparticles and aggregation to form large particles by autocatalytic pathway. The formations of silver nanoparticles were non-uniform with a broad size distribution. Finally, the process was continuous production for large amount of product.

4.2.2.1 Jet semi-continuous flow reactor

At the beginning of the development and the invention of reactor, the jet semi-continuous flow reactor was designed for synthesis of large amount of high concentration silver nanoparticles had narrow size distribution of particles by using flow system. The reaction was flow in tube; it decreased some active silver ions in media solution that prevented the autocatalytic reaction.

The normalized extinction spectrum of 5,000 ppm silver nanoparticles was synthesized with the jet semi-continuous flow reactor by using primary mixing chamber as three-ways connection tube and, primary mixing chamber as three-ways connection tube with external mixing chamber are shown in Figure 4.11 A and B. The maximum of normalized extinction spectrum of silver nanoparticles obtained from the jet semi-continuous flow reactor by using primary mixing chamber as three-ways connection tube show the peak around 403 nm, and tailing around 475 nm were observed. The symmetrical shape and the maximum of normalized extinction spectrum of silver nanoparticles obtained from the jet semi-continuous flow reactor by using primary mixing chamber as three-ways connection tube with external mixing chamber show the peak around 403 nm and the quadrupole at 350 nm. The FWHH of silver nanoparticles obtained from the jet semi-continuous flow reactor by using primary mixing chamber as three-ways connection tube, and primary mixing chamber as three-ways connection tube with external mixing chamber were 97 and 57 nm, respectively. The smaller with narrow size distribution and blue-shift in the maxima of normalized extinction spectrum of the silver nanoparticles were synthesized from 1 liter batch reactor observed the symmetrical shape and the maximum of normalized extinction spectrum of this solution show peak around 400 nm with FWHH 50 nm are compared to that obtained from the jet semi-continuous flow reactor are show in Figure 4.11D. These results suggested that the larger with broad size distribution of silver nanoparticles obtained from the jet semi-continuous flow reactor by using primary mixing chamber as three-ways connection tube due to the effect of efficient mixing, while the primary mixing chamber as three-ways connection tube showed the low efficient mixing and be poor for mixing. In addition, the narrow size distribution of silver nanoparticles obtained from the jet semi-continuous flow reactor by using primary mixing chamber as three-ways connection tube with external mixing chamber due to the effect of increased efficient mixing, while the external mixing showed the thoroughly mixed. However, this efficient mixing did not complete showed the normalized extinction spectrum of silver nanoparticles obtained from the jet semi-continuous flow reactor by using primary mixing chamber as three-ways connection tube with external mixing chamber were the imperfect spherical shape with broader size distribution than that from 1 liter batch reactor.

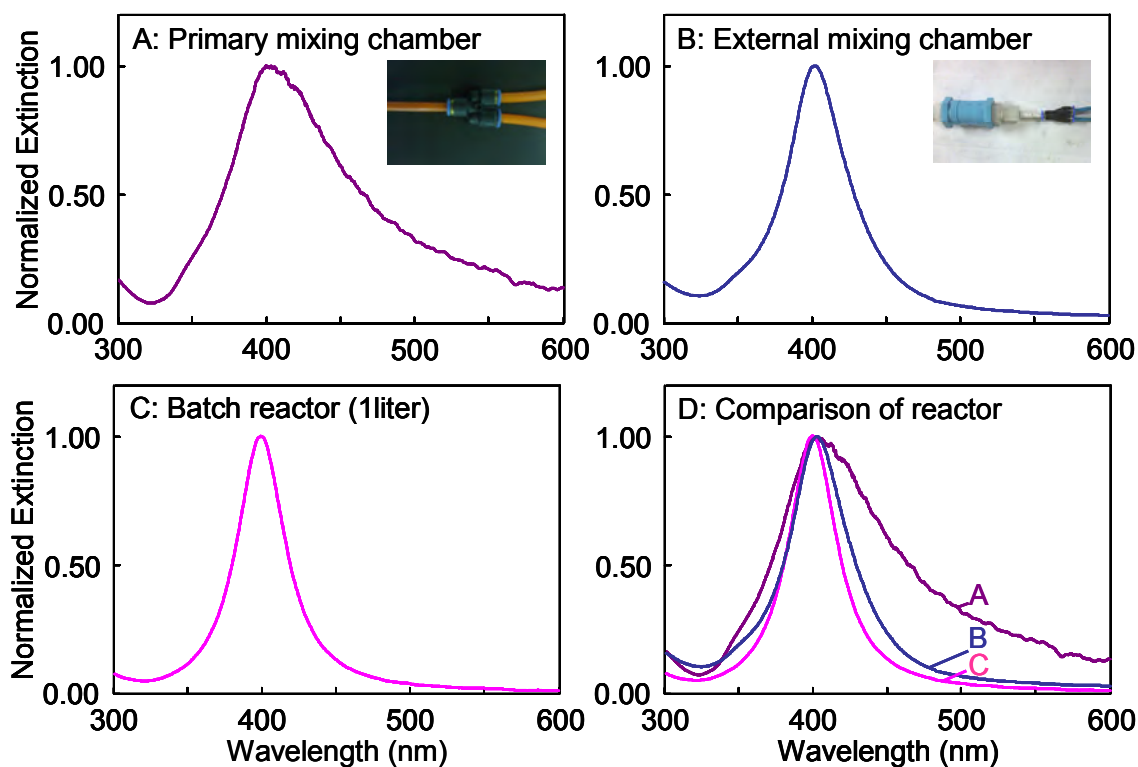


Figure 4.11 The normalized extinction spectrum of 5,000 ppm silver nanoparticles synthesized from (A) the jet semi-continuous flow reactor by using primary mixing chamber as three-ways connection tube, (B) the jet semi-continuous flow reactor by using primary mixing chamber as three-ways connection tube with external mixing chamber, (C) batch reactor with 1 liter and (D) the comparison of the normalized extinction spectra of silver nanoparticles synthesized from the jet semi-continuous flow reactor by using primary mixing chamber as three-ways connection tube and as three-ways connection tube with external mixing chamber, and batch reactor with 1 liter.

The normalized extinction spectrum of silver nanoparticles diluted from the high concentration ca. 5,000 ppm synthesized with the jet semi-continuous flow reactor is shown in Figure 4.12. The red-shift in the maximum of normalized extinction spectra of the silver nanoparticles (46 mM/5,000 ppm) were synthesized from jet semi-continuous flow reactor with 35 mM sodium borohydride, and 2.0% soluble starch and observed the maximum of normalized extinction spectrum of this

solution show peak around 403 nm with the quadrupole at 350 nm and the FWHH about 57 nm are compared to the symmetrical peak shape had the maximum of normalized extinction spectrum of silver nanoparticles obtained from 1 liter batch reactor showing the peak around 400 nm with FWHH 50 nm was observed. However, the size distribution of silver nanoparticles was narrower from the jet semi-continuous flow reactor by using primary mixing chamber as three-ways connection tube with external mixing chamber compared to that obtained from 40 liters batch reactor.

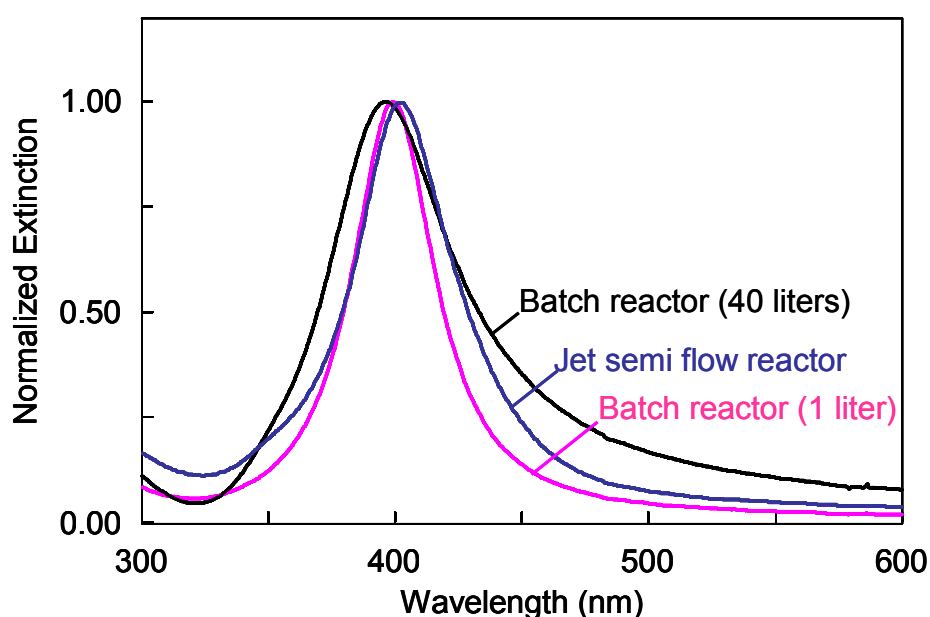


Figure 4.12 The normalized extinction spectra of 5,000 ppm silver nanoparticles synthesized from the batch reactor with 1 liter, the jet semi-continuous flow reactor by using primary mixing chamber as three-ways connection tube with external mixing chamber and the batch reactor with 40 liters.

4.2.2.2 Tubular flow reactor (the pulse flow processes)

The normalized extinction spectrum of silver nanoparticles diluted from the high concentration ca. 5,000 ppm was synthesized with the tubular flow reactor (the pulse flow processes) by using primary mixing chamber as three-ways connection tube with external mixing chamber, primary mixing chamber as modified from hypodermic syringe and primary mixing chamber as custom-made modified

from hypodermic syringe are shown in Figure 4.13A-C. The maximum of normalized extinction spectrum of silver nanoparticles obtained from the tubular flow reactor (the pulse flow processes) by using primary mixing chamber as three-ways connection tube with external mixing chamber show the peak around 401 nm with the quadrupole at 350 nm were observed. The symmetrical shape and the maximum of normalized extinction spectrum of silver nanoparticles obtained from the tubular flow reactor (the pulse flow processes) by using primary mixing chamber as modified from hypodermic syringe show the peak around 399 nm with the quadrupole at 350 nm. The FWHH of silver nanoparticles obtained from the tubular flow reactor (the pulse flow processes) by using primary mixing chamber as three-ways connection tube with external mixing chamber and as modified from hypodermic syringe were 59 and 55 nm, respectively. The narrow size distribution of normalized extinction spectrum of the silver nanoparticles were synthesized from the tubular flow reactor (the pulse flow processes) by using primary mixing chamber as custom-made modified from hypodermic syringe observed the symmetrical shape and the maximum of normalized extinction spectrum of this solution show peak around 401 nm with FWHH 53 nm. These result compared to that obtained from the tubular flow reactor (the pulse flow processes) by using primary mixing chamber as three-ways connection tube with external mixing chamber and as modified from hypodermic syringe are show in Figure 4.13D. These result suggested that the efficient mixing of tubular flow reactor (the pulse flow processes) by using primary mixing chamber as custom-made modified from hypodermic syringe were high efficient mixing and showed the spherical shape with narrow size distribution of silver nanoparticles, while the efficient mixing of tubular flow reactor (the pulse flow processes) by using primary mixing chamber as three-ways connection tube with external mixing chamber and as modified from hypodermic syringe were low efficient mixing and showed the imperfect spherical shape with broader size distribution of silver nanoparticles, it could be seen that the tubular flow reactor (the pulse flow processes) by using primary mixing chamber as custom-made modified from hypodermic syringe showed the high efficient mixing.

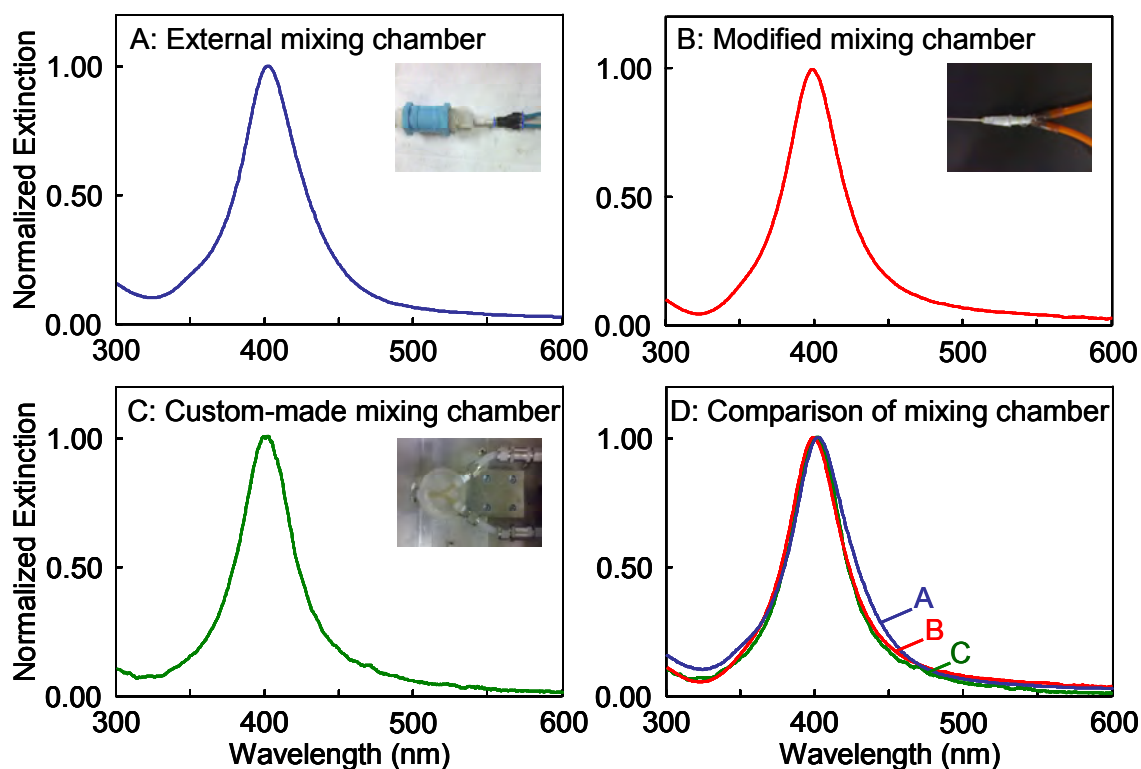


Figure 4.13 The normalized extinction spectrum of 5,000 ppm silver nanoparticles synthesized from the tubular flow reactor (the pulse flow processes) by using (A) primary mixing chamber as three-ways connection tube with external mixing chamber, (B) primary mixing chamber as modified from hypodermic syringe, (C) primary mixing chamber as custom-made modified from hypodermic syringe and (D) the comparison of the normalized extinction spectra of silver nanoparticles synthesized from the tubular flow reactor (the pulse flow processes) with various mixing chamber.

The normalized extinction spectra of silver nanoparticles diluted from the high concentration ca. 5,000 ppm synthesized with the tubular flow reactor (the pulse flow processes) are shown in Figure 4.14. The maximum of normalized extinction spectra of silver nanoparticles obtained from tubular flow reactor (the pulse flow processes) with the same condition as that from the jet semi-continuous flow reactor was at 401 nm. The symmetrical peak shape had the FWHH about 53 nm. The

symmetrical peak shape had the maximum of normalized extinction spectrum of silver nanoparticles obtained from 1 liter batch reactor showing the peak around 400 nm with FWHH 50 nm. The result suggests that the size of synthesized silver nanoparticles obtained from tubular flow reactor (the pulse flow processes) are slightly broad size distribution than that of the synthesized silver nanoparticles from 1 liter batch reactor. However, the size distribution of silver nanoparticles was narrower from the tubular flow reactor (the pulse flow processes) compared to that obtained from 40 liters batch reactor.

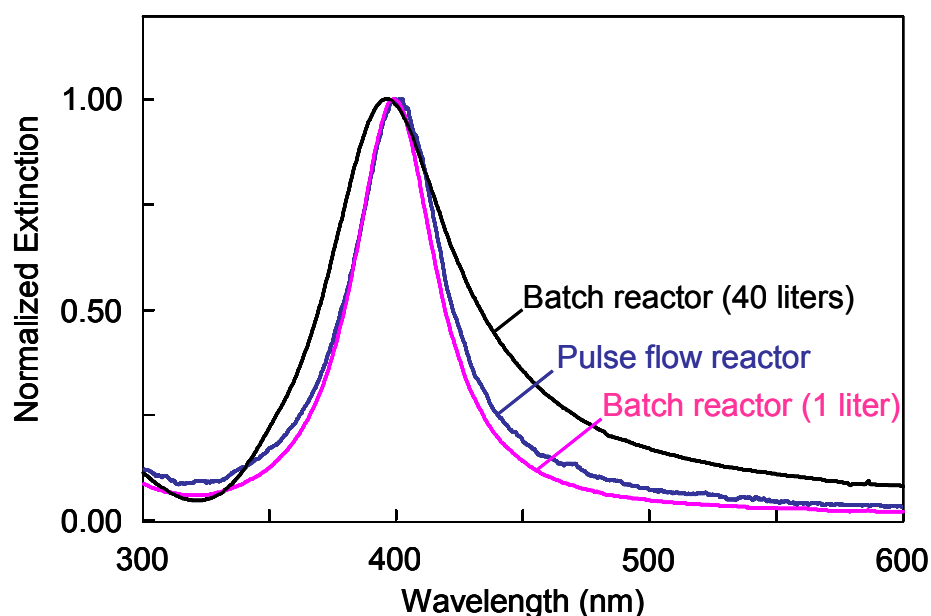


Figure 4.14 The normalized extinction spectra of silver nanoparticles synthesized from batch reactor with 1 liter batch reactor, the tubular flow reactor (the pulse flow processes) by using primary mixing chamber as custom-made modified from hypodermic syringe and batch reactor with 40 liters.

4.2.2.3 Tubular flow reactor (the continuous flow processes)

The normalized extinction spectra of synthesized silver nanoparticles obtained from the 1 liter - batch reactor and tubular flow reactor (the continuous flow processes) are compared as shown in Figure 4.15. These results suggested that the size of synthesized silver nanoparticles obtained from tubular flow reactor (the

continuous flow processes) are slightly broad size distribution than that of the synthesized silver nanoparticles from the 1 liter - batch reactor. However, the size distribution of silver nanoparticles was narrower from the tubular flow reactor (the continuous flow processes) compared to that obtained from 40 liters batch reactor.

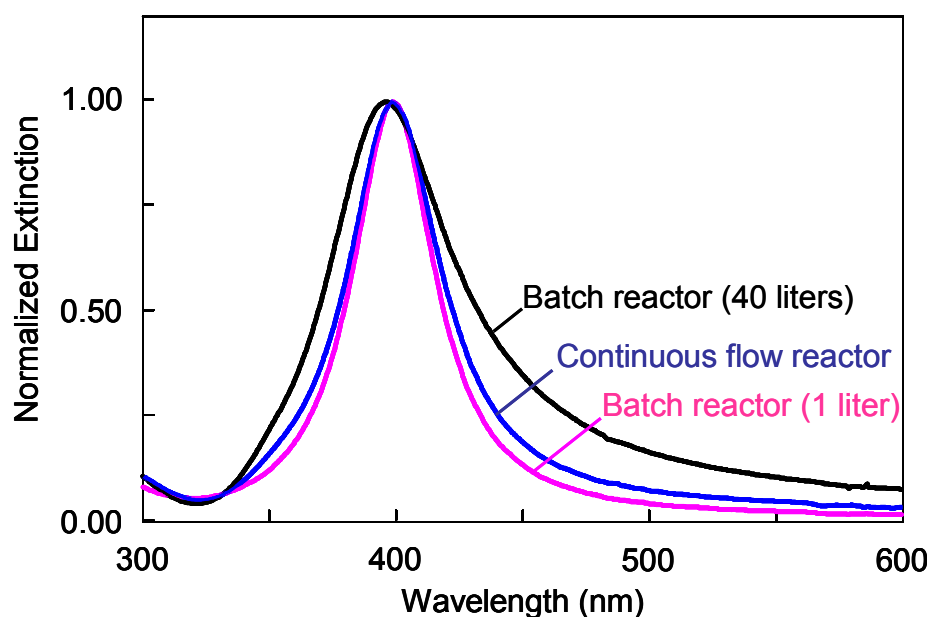


Figure 4.15 The normalized extinction spectra of silver nanoparticles synthesized from batch reactor with 1 liter, tubular flow reactor (the continuous flow processes) by using primary mixing chamber as custom-made modified from syringe and batch reactor with 40 liters.

4.2.3 Influence of flow rates on the synthesis of silver nanoparticles

In order to produce the large amount, controllable size distribution, highly concentrated and stabilized silver nanoparticles, the flow system was developed. The tubular flow reactor for the synthesized silver nanoparticles is shown in Figure 3.4. The FWHH for the normalized extinction spectra of silver nanoparticles diluted from 5,000 ppm silver nanoparticles synthesized with various flow rates of reactants are shown in Figure 4.16. The maxima of normalized extinction spectra of silver nanoparticles obtained from the flow rate of 3.1 and 14.4 mL/min were located around 400 nm, and the tailing around 475 nm with the FWHH of 76 and 58 nm, respectively. These suggested a small size of synthesized silver nanoparticles with a broad size distribution and also the shape of imperfect spherical particles. The maximum of normalized extinction spectrum of silver nanoparticles for the flow rate of 87.7 mL/min shows the peak around 400 nm and tailing around 450 nm with the FWHH about 51 nm.

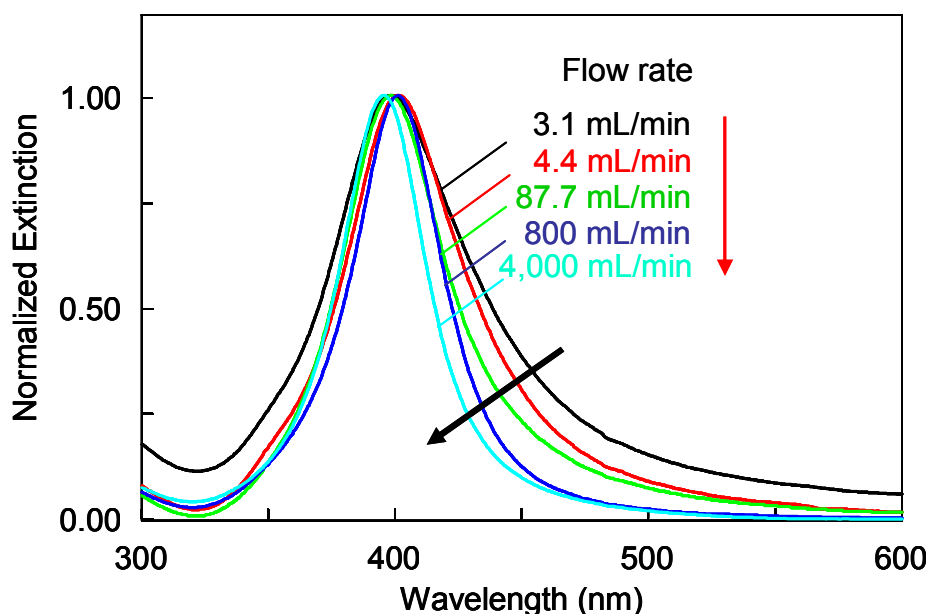


Figure 4.16 The normalized extinction spectra of silver nanoparticles diluted from 5,000 ppm silver nanoparticles synthesized from tubular flow reactor (the continuous flow processes) with various flow rates of reactants.

This result suggested the small size and broader size distribution of synthesized silver nanoparticles. At the flow rate of 800 and 4,000 mL/min, the symmetrical shape of the normalized extinction spectra has the maxima at 400 nm and 395 nm, and had FWHH about 44 nm and 42 nm, respectively. These presented the spherical particles with small size and narrow size distribution of silver nanoparticles.

Table 4.3 Reynolds numbers, Re, at various flow rates.

Flow rate (mL/min)	Diameter of tube (mm)	Re	FWHH (nm)
3.1	6	11	76
14.4	6	51	58
87.7	6	310	51
800.0	6	2,828	44
4,000.0	6	14,141	42

The Reynolds numbers calculated from the experimental parameters were shown in Table 4.3. The values of Re for the flow rate of 3.1 and 14.4 mL/min are 11 and 51, respectively. Since, Re are below the value of 2,100, flow patterns are laminar (smooth flow) [9, 33]. So, it is possible that the mixing is poor; the efficient mixing is low. The reaction is imperfect homogeneous concentration distribution of solution and imperfect homogeneous phase. Some active silver ions in media solution could be reduced on surface of silver nanoparticles and aggregate by autocatalytic pathway. The forming particles were growing to larger and non-uniform particles with broad size distribution [18]. The values of Re at the flow rate of 800.0 and 4,000.0 mL/min are 2,828 and 14,141, respectively. Re are above 4,000; the turbulent flow patterns, rough flow [9, 33], caused the efficient mixing is high. The reaction is perfect homogenous concentration distribution of solution and perfect homogeneous phase. There were no active silver ions left in media solution that triggered the autocatalytic reaction. The small sizes of synthesized silver nanoparticles were uniform with a narrow size distribution.

The proposed particle growth pathways for flow reactors are shown in Figure 4.17.

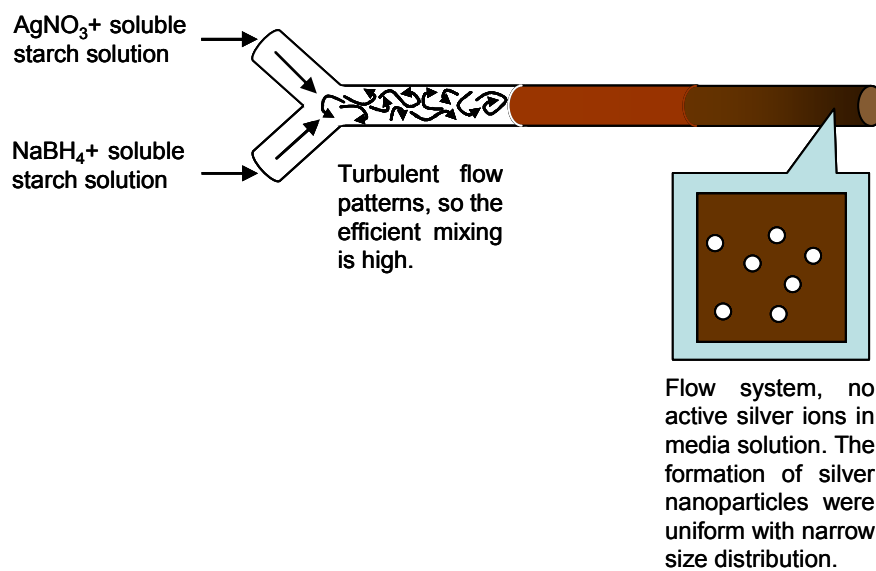


Figure 4.17 The illustration of the synthesized high silver nanoparticles from tubular flow reactor.

4.2.4 Influence of reactor diameter

The normalized extinction spectra of the synthesized silver nanoparticles when various diameter of reactor tube were used for the synthesis are shown in Figure 4.18. The maximum of the normalized extinction spectra of silver nanoparticles when reactor tube were 6, 8 and 10 mm located around 395 nm and had the symmetrical shape with the FWHH of 42, 43 and 45 nm, respectively. This suggested that the shape of particles were sphere and the particle size of the synthesized silver nanoparticles obtained from diameter of 6, 8 and 10 mm were nearly superimposable with the narrow size distribution.

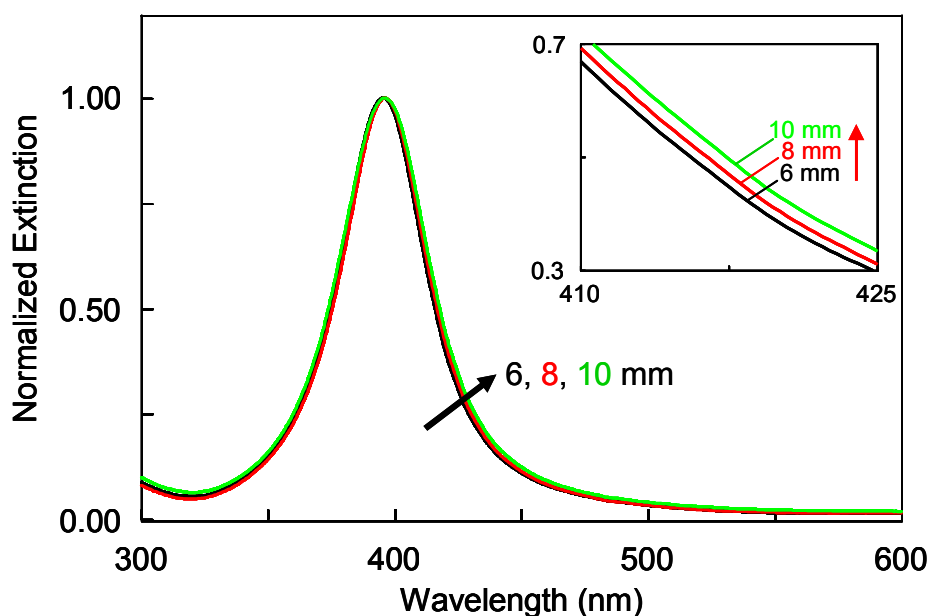


Figure 4.18 The normalized extinction spectra of 5,000 ppm silver nanoparticles synthesized from tubular reactor with various diameter of tube.

Table 4.4 Reynolds numbers, Re, at various reactor tube diameter.

Flow rate (mL/min)	Diameter of tube (mm)	Re	FWHH (nm)
4,000	6	14,141	42
4,000	8	10,606	43
4,000	10	8,485	45

The Reynolds numbers calculated from the experimental parameters as shown in Table 4.4. The values of Re for the diameter of tube about 6, 8 and 10 mm are 14,141, 10,606 and 8,485, respectively. The results suggested that increasing diameter of tube decreasing the values of Re, the values of Re was below. From the experimental, the increasing diameter of tube with the flow rate of 4,000 mL/min, the values of Re were obtained the turbulent flow patterns. This indicates that the turbulent flow patterns were highly efficient mixing for homogeneous concentration distribution solution. The formation of particles was uniform with narrow size distribution. These experimental, the increasing diameter of tube as 6, 8 and 10 mm were no effected efficient mixing of reactants.

4.2.5 Comparison of synthesized silver nanoparticles from batch reactor and tubular flow reactor.

The normalized extinction spectra of silver nanoparticles which diluted from 5,000 ppm silver nanoparticles obtained from batch and tubular flow reactor are compared as shown in Figure 4.19. The normalized extinction spectrum of silver nanoparticles obtained from 40 liters batch reactor is 395 nm and the tailing around 450 nm are observed. The FWHH is 64 nm. For the tubular flow reactor at flow rate of 4,000 mL/min, the symmetrical shapes of the normalized extinction spectrum of the synthesized silver nanoparticles with the maxima at 395 nm and having FWHH about 42 nm was obtained. These suggested that the synthesized silver nanoparticles were smaller with narrow size distribution comparable to the synthesized silver nanoparticles by the batch reactor.

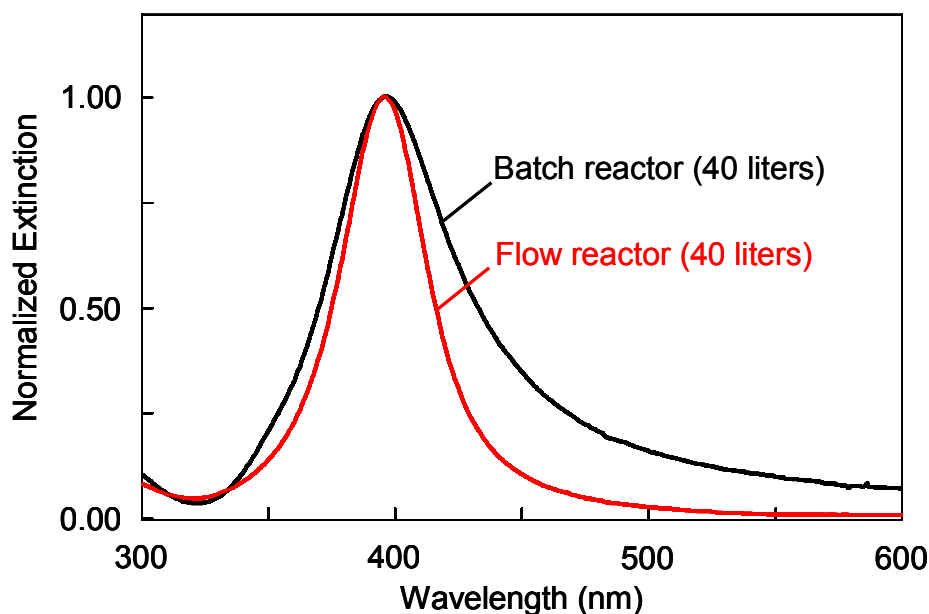


Figure 4.19 The normalized extinction spectra of silver nanoparticles diluted from 5,000 ppm silver nanoparticles obtained from batch reactor and flow reactor.

The TEM images of silver nanoparticles synthesized by batch and tubular flow reactor are shown in Figure 4.20. From the TEM images, the particles size distribution of batch reactor is broader than the silver nanoparticles synthesized by tubular reactor.

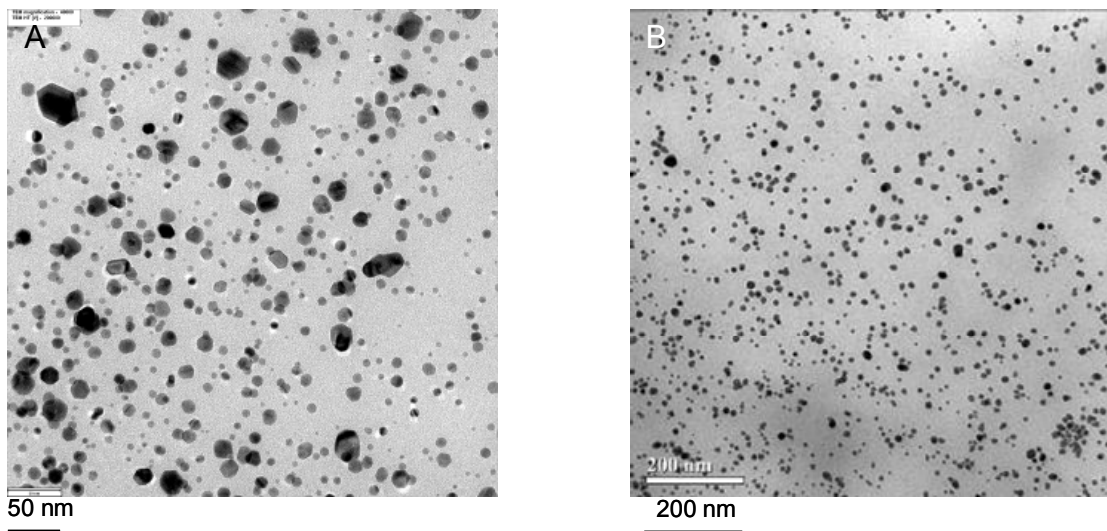


Figure 4.20 The transmission electron microscopy (TEM) images of synthesized silver nanoparticles with (A) batch reactor and (B) tubular flow reactor.

4.3 Comparison of silver nanoparticles from our synthesis by tubular flow reactor with the available commercial product

From Figure 4.21, the normalized extinction spectra of diluted colloidal silver nanoparticles have maxima of 395 and 405 nm for silver nanoparticles synthesized by the tubular flow reactor and the commercial silver nanoparticles, respectively. This indicates that the synthesized particles by the tubular flow reactor have smaller particle size than that of the commercial product. In addition, FWHH of the normalized extinction spectra of the flow reactor synthesized silver nanoparticles indicates a narrower size distribution than that of commercial product.

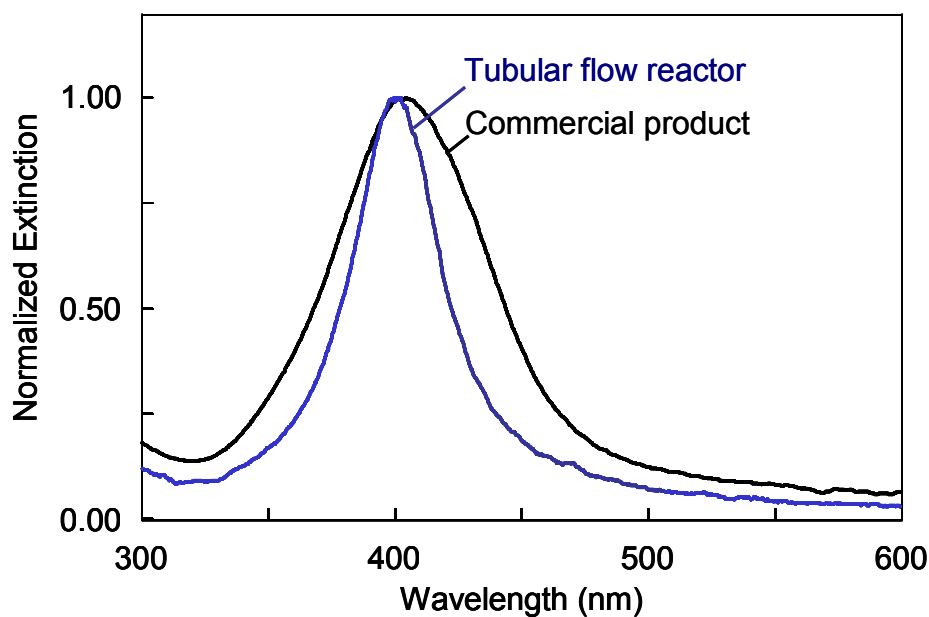


Figure 4.21 The normalized extinction spectra of silver nanoparticles obtained from tubular flow reactor ($\lambda_{\max} = 395$ nm) and Commercial product ($\lambda_{\max} = 405$ nm).

The TEM images of silver nanoparticles synthesized by the tubular flow reactor and the commercial product are compared in Figure 4.22.

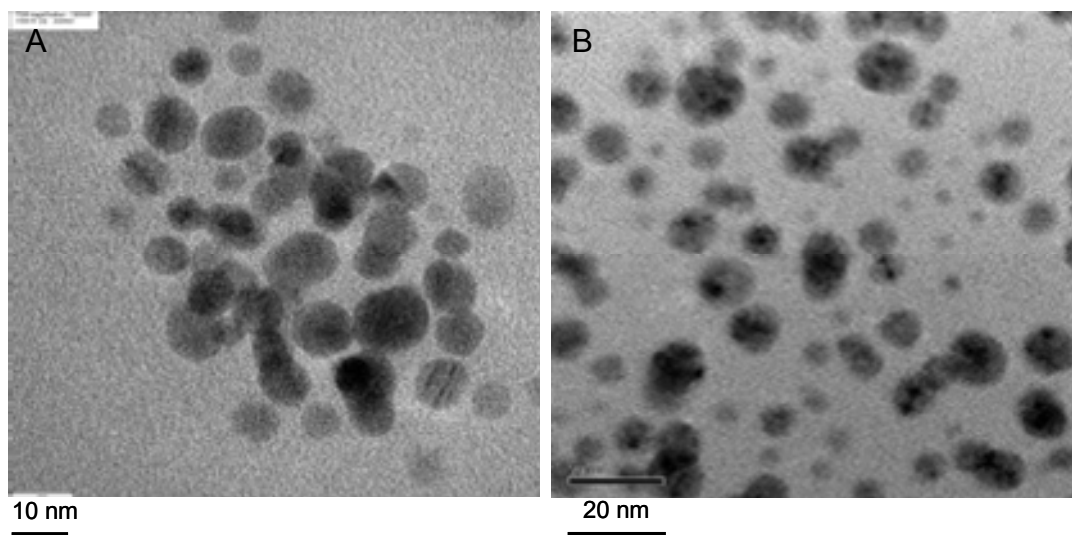


Figure 4.22 TEM images of the synthesized silver nanoparticles: (A) tubular flow reactor synthesized silver nanoparticles (B) commercial product.

4.4 The stability of synthesized silver nanoparticles

In Figure 4.23, the normalized extinction spectra of synthesized nanoparticles from the tubular flow reactor measured immediately after synthesis and 6 months later show the peak around 395 nm and FWHH about 42 nm, respectively. They were nearly superimposable. This indicates that the synthesized silver nanoparticles were stable. They were not decomposed, aggregated, and precipitated after, 6 months of storage at ambient conditions.

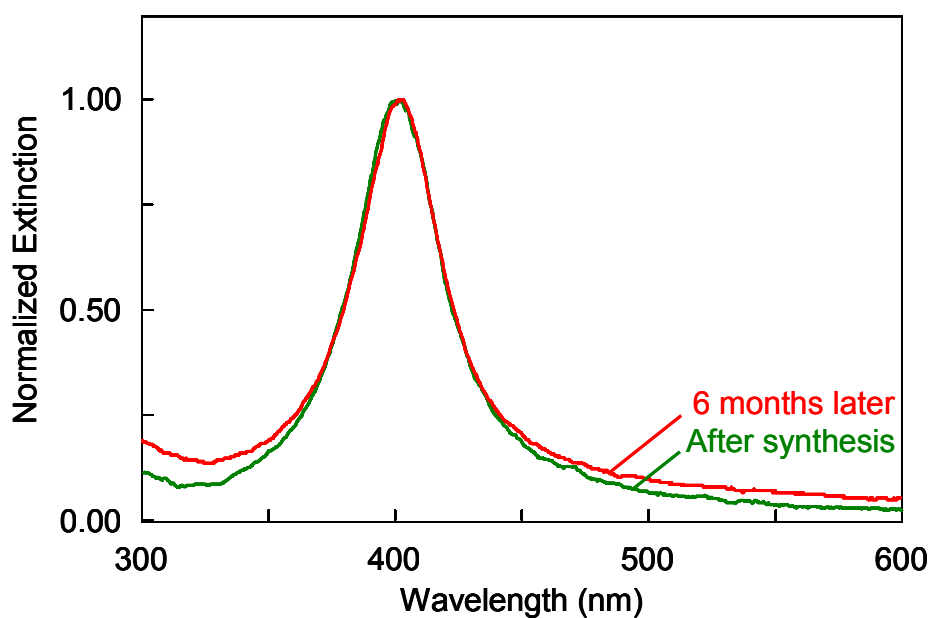


Figure 4.23 The normalized extinction spectra of the same synthesized silver nanoparticles produced by tubular flow reactor measured immediately after synthesis and 6 months later.

Summary

- √ The synthesized silver nanoparticles were controlled quality and reproducibility for producing large amount high concentration and stable silver nanoparticles.
- √ Development of tubular flow reactor (the continuous flow processes) at the flow rate of 4 liters / min was continuously produced silver nanoparticles in 240 liters per hour (240 L/hr).
- √ The synthesized silver nanoparticles were spherical shape with average diameter of 10 nm.
- √ The particles size distribution was narrow with FWHH about 42 nm.
- √ The synthesized silver nanoparticles was stable for at least 6 months.

4.5 Antibacterial activity testing and safety testing in laboratory animals with our synthesized silver nanoparticles

4.5.1 Antibacterial activity testing

Our synthesized silver nanoparticles was chosen for this experiment. Effect of the silver nanoparticles on the reduction of *Escherichia coli* as Gram-negative bacteria, *Staphylococcus aureus* and methicillin resistant *Staphylococcus aureus* (MRSA) as Gram-positive bacteria were compared with only normal saline solution as control. The viability of all tested bacteria could be confirmed from the result of control. The reduction of *E. coli* from 125000 CFU/mL to 103500 CFU/mL (17.2%), *S. aureus* from 70000 CFU/mL to 7350 CFU/mL (89.5%), and methicillin resistant *S. aureus* (MRSA) from 162000 CFU/mL to 34000 CFU/mL (79.01%), at 24 hours were determined. More reduction of *S. aureus* and methicillin resistant *S. aureus* (MRSA) maybe due to they could not maintain cell integrity in normal saline solution. While our synthesis of silver nanoparticles could reduce *E. coli*, *S. aureus* and methicillin resistant *S. aureus* (MRSA) from 125000, 70000, and 162000 CFU/mL, respectively to 0 CFU/mL (100%), at 24 hours.

From the results, three bacterial pathogens were effectively inhibited with 100% reduction of growth by our synthesis of silver nanoparticles (50 ppm) are shown in Table 4.5. It can conclude that silver nanoparticles had the antimicrobial activity as bactericidal functioning *in vitro*; however, the antimicrobial activity *in vivo* should be investigated for further application as a commercial product.

Table 4.5 The antibacterial test^{*, **}.

	<i>Escherichia coli</i> CFU/mL			
	24	Average	% reduction	
Control 0 hr.	136000	114000	125000	
Control 24 hr.	100000	107000	103500	
Silver nanoparticles	0	0	0	
	100			
	<i>Staphylococcus aureus</i> CFU/mL			
	24	Average	% reduction	
Control 0 hr.	104000	36000	70000	
Control 24 hr.	8600	6100	7350	
Silver nanoparticles	0	0	0	
	100			
	methicillin resistant <i>Staphylococcus aureus</i> (MRSA) CFU/mL			
	24	Average	% reduction	
Control 0 hr.	184000	140000	162000	
Control 24 hr.	47000	21000	34000	
Silver nanoparticles	0	0	0	
	100			

* The photograph of antibacterial activity test of three bacterial pathogens with AgNPs is shown in Figure B 3

** The antibacterial test of bacterial pathogens with AgNPs padding on fabric is shown in Figure B 4

4.5.2 Safety testing in laboratory animals with our synthesized silver nanoparticles

The effects of silver nanoparticles on safety testing on laboratory animals are shown in Table 4.6.

Table 4.6 The toxicity test in laboratory animals *

Toxicity test	Results
Acute oral toxicity test; (OECD/OCDE 425)	No death No toxicological effects (LD ₅₀ (Lethal dose), TD ₅₀ (Toxic dose) >5,000 mg/kg)
Acute dermal toxicity test; (OECD/OCDE 434)	No significant changes in the general appearance and skin condition No toxicological effects (LD ₅₀ (Lethal dose), TD ₅₀ (Toxic dose) >5,000 mg/kg)
Acute eye irritation and corrosion test; (OECD/OCDE 405)	No any sign of eye irritation No toxicological effects (LD ₅₀ (Lethal dose), TD ₅₀ (Toxic dose) >5,000 mg/kg)
Acute pulmonary toxic test	(LD ₅₀ (Lethal dose), TD ₅₀ (Toxic dose) >2,000 mg/kg)



* Effects of silver nanoparticles with safely testing in laboratory animals are shown in Appendix C

4.6 Industrial applications of our synthesized silver nanoparticles

Our synthesized silver nanoparticles were commercially available, and now they have been integrated into many commercial products. Some examples are shown in table 4.7

Table 4.7 The applications of synthesized silver nanoparticles in some commercial products.

Company	Industrial applications	Typical products	Commercial products
 CutePress SSUP group Co., Ltd. (89/1 Soi Ratchataphan, Ratchaprarop road, Makkasan, Ratchathevee, Bangkok 10400)	Cosmetics industrial	Deodorant and talcum powder	 “Cute press Deodorant & Cute press Perfumed Talc with NANO SILVER “
 Lion Co. (Thailand), Ltd. (666 Rama 3 road, Yannawa, Bangkok 10120)	Consumer product	Detergent	 “ Pao silver nano”

Company	Industrial applications	Typical products	Commercial products
 <p data-bbox="252 712 671 815">Nan Yang Group Nan Yang Inspiration Center Co., Ltd.</p> <p data-bbox="252 875 671 965">(71 Moo 12 Phetkasem 71 road, Nongkham Bangkok 10160)</p>	Textiles industrial	Sportswear, Shirt and fabric	 <p data-bbox="1145 831 1326 853">"Shirt silver nano"</p>

Summary

- √ Our synthesized silver nanoparticles could perform antibacterial activity; three bacterial pathogens were effectively inhibited with 100% reduction of growth by silver nanoparticles (50 ppm).
- √ Our synthesized silver nanoparticles were no toxicological effects.
- √ Our synthesized silver nanoparticles could really apply to commercial products and industrial applications such as textiles industrial, cosmetics industrial and consumer products.

CHAPTER V

CONCLUSIONS

The silver nanoparticles (1,000-10,000 ppm) were controlled quality and reproducibility of the synthesis by chemical reduction of silver nitrate with sodium borohydride. The optimum molar ratio of silver nitrate to sodium borohydride was 1.00 to 0.75. The soluble starch was used as a stabilizer; the optimal concentration of soluble starch was 2% (w/v). The synthesized silver nanoparticles were spherical with the mean size of 10 nm. The particle size distribution was very narrow with FWHH about 42 nm. Our synthesized silver nanoparticles were highly stable. They can be kept at ambient temperature without any aggregation, decomposition, and precipitation for at least 6 months.

Development of tubular flow reactor with the length of tube was fixed at 20 cm, the diameter of tube was 6 mm and the flow rate of 4 L/min was continuously produced silver nanoparticles in 240 liters per hour (240 L/hr). The maximum of the normalized extinction spectrum of silver nanoparticles obtained from the synthesis was located around 395 nm with FWHH at 42 nm. The TEM images of synthesized silver nanoparticles showed that they were spherical shape with diameter range between 5-20 nm and an average diameter of 10 nm.

Moreover, the estimated cost of our synthesis of high concentration silver nanoparticles (10,000 ppm/1 liter) was about 620 Baht/1 liter.

In this study, 100% reduction of the three bacterial pathogens such as *Escherichia coli* as Gram-negative bacteria, *Staphylococcus aureus* and methicillin resistant *Staphylococcus aureus* (MRSA) as Gram-positive bacteria were observed when they were tested against 50 ppm silver nanoparticles. In addition, our synthesis of silver nanoparticles did not show any toxicological effects such as the acute oral toxicity, acute eye irritation and corrosion, and acute dermal toxicity test-fixed dose procedure at the LD₅₀ or TD₅₀ > 5,000 mg/kg, and acute pulmonary toxicity test at TD₅₀ > 2,000 mg/kg.

Nowadays, our silver nanoparticles could really apply into commercial products and industrial applications. For examples, sportswear and fabric for textiles

industrial (Nan Yang Group Nan Yang Inspiration Center Co., Ltd.), deodorant products for cosmetics industrial (CutePress SSUP group Co., Ltd.), water filter for consumer products (PURE Siam Cast Nylon Co., Ltd.) and detergent for consumer products (Lion Co. (Thailand), Ltd.).

All in all, it was concluded that the aims of this research work was fully fulfilled.

REFERENCES

- [1] Jeong S. H.; Yeo S. Y.; and Yi S. C. The effect of filler particle size on the antibacterial properties of compounded polymer/silver fibers J. Mater. Sci. 40 (2005): 5407-5411.
- [2] Kolar M.; Urbanek K.; and Latal T. Antibiotic selective pressure and development of bacterial resistance Int. J. Antimicrob. Agents. 17 (2001): 357-363.
- [3] Ulkur E.; Oncul O.; Karagoz H.; Yeniz E.; and Celikoz B. Comparison of silver-coated dressing (ActicoatTM), chlorhexidine acetate 0.5% (Bactigrass1), and fusidic acid 2% (Fucidin1) for topical antibacterial effect in Methicillin-resistant Staphylococci-contaminated, full-skin thickness rat burn wounds Burns 31 (2005): 874-877.
- [4] Chou W. L.; Yu D. G.; and Yang M. C. The preparation and characterization of silver-loading cellulose acetate hollow fiber membrane for water treatment Polym. Adv. Technol. 16 (2005): 600-607.
- [5] Pal S.; Tak Y. K.; and Song J. M. Does the antibacterial activity of silver nanoparticles depend on the shape of the nanoparticle? A Study of the Gram-Negative Bacterium Escherichia coli Appl. Environ. Microbiol. 73 (2007): 1712-1720.
- [6] Sondi I.; and Salopek-Sondi B. Silver nanoparticles as antimicrobial agent: a case study on E. coli as a model for Gram-negative bacteria J. Colloid Interface Sci. 275 (2004): 177-182.
- [7] Pillai Z. S.; and Kamat P. V. What factors control the size and shape of silver nanoparticles in the citrate ion reduction method J. Phys. Chem. B 108 (2004): 945-951.
- [8] Rodriguez-Snachez L. Electrochemical Synthesis of Silver Nanoparticles J. Phys. Chem. B 104 (2000): 9683-9688.
- [9] Lin X. Z.; Terepka A. D.; and Yang H. Synthesis of silver nanoparticles in a continuous flow tubular microreactor Nanoletters 4 (2004): 227-2232.

- [10] Zhang Z.; Patel R. C.; Kothari R.; Johnson C. P.; and Friberg S. E. Stable silver clusters and nanoparticles prepared in polyacrylate and inverse micellar solutions J. Phys. Chem. B 104 (2000): 1176-1182.
- [11] Bingsheng Y.; and Houyi M. Electrochemical synthesis of silver nanoparticles under protection of poly(N-vinylpyrrolidone) J. Phys. Chem. B 107 (2003): 8898-8904.
- [12] Treguer M.; Cointet C. D.; Remita H.; and Khatouri J. Dose rate effects on radiolytic synthesis of gold-Silver bimetallic clusters in solution J. Phys. Chem. B 102 (1998): 4310-4321.
- [13] Huang Z. Y.; Mills G. T.; and Hajek B. Spontaneous formation of silver particles in basic 2-propanol J. Phys. Chem. 97 (1993): 11542-11550.
- [14] Willets K. A.; and Van Duyne R. P. Localized surface plasmon resonance spectroscopy and sensing Annu. Rev. Phys. Chem. 58 (2007): 67-97.
- [15] Kelly K. L.; Coronado E.; Zhao L. L.; and Schatz G. C. The optical properties of metal nanoparticles: the influence of size, shape, and dielectric environment J. Phys. Chem. B 107 (2003): 668-677.
- [16] Ryu B. et al. Synthesis of highly concentrated silver nanosol and its application to inkjet printing Colloid and Surface A 270 (2005): 345-351.
- [17] Sergeev G. B. Nanochemistry New York: Elsevier, 2006.
- [18] Van Hyning D. L.; Klemperer W. G.; and Zukoski C. F. Silver nanoparticle formation: predictions and verification of the aggregative growth model Langmuir 17 (2001): 3128-3135.
- [19] Shirtcliffe N.; Nickel U.; and Schneider S. Reproducible preparation of silver sols with small particle size using borohydride reduction: for use as nuclei for preparation of larger particles J. Colloid Inter. Sci. 211 (1999): 122-129.
- [20] Wang H.; Qiao X.; Chen J.; and Ding S. Preparation of silver nanoparticles by chemical reduction method Coll. Surf. A 256 (2005): 111-115.
- [21] Raghuraman K.; and Katti K. K. Methods for producing silver nanoparticles, US Patent 0045916A1 (2006).

- [22] Zhao J.; Zhang X.; Yonzon C. R.; Haes A. J.; and Van Duyne R. P. Localized surface plasmon resonance biosensors Nanomedicine 1 (2006): 219-228.
- [23] Turkevich J. Colloidal gold part I: historical and preparative aspects, morphology and structure Gold Bull. 18 (1985): 86–9.
- [24] Tsai S. C.; Song Y. L.; and Tsai C. S. Ultrasonic spray pyrolysis for nanoparticles synthesis J. Mater. Sci. 39 (2004): 3647-3657.
- [25] Shaw D. J. Introduction to colloid and surface chemistry oxford: Butterworth, 1983.
- [26] Mohan Y. M.; Lee K.; Premkumar T.; and Geckeler K. E. Hydrogel networks as nanoreactors: a novel approach to silver nanoparticles for antibacterial applications Polymer 48 (2007): 158-164.
- [27] Can-Amarens M. V.; Garcia-Ramos J. V.; and Gomez-Varga J. D. Comparative study of the morphology, aggregation, adherence to glass, and surface-enhanced Raman scattering activity of silver nanoparticles prepared by chemical reduction of Ag⁺ using citrate and hydroxylamine Langmuir 21 (2005): 8546-8553.
- [28] Pluym T. C.; Powell Q. H.; Gurav A. S.; Ward T. L.; Kodas T. T.; Wang L. M.; and Glicksman H. D. Solid silver particle production by spray pyrolysis J. Aerosol Sci. 24 (1993): 383-392.
- [29] Henglein A.; and Giersig M. Formation of colloidal silver nanoparticles: capping action of citrate J. Phys. Chem. B 103 (1999): 9533-9539.
- [30] Ju-Nam Y.; and Lead J. R. Manufactured nanoparticles: an overview of their chemistry, interactions and potential environmental implications Sci Total Environ. 400 (2008): 396-414.
- [31] Poovathinthodiyil R.; Jie F.; and Scott L. W. Completely “Green” synthesis and stabilization of metal nanoparticles J. Am. Chem. Soc. 125 (2003): 13940-13941.
- [32] Zukoski C. F. Formation mechanisms and aggregation behavior of borohydride reduced silver particles Langmuir 14 (1998): 7034-7046.
- [33] Holman, J. P. In Heat Transfer 6th ed. New York: McGraw-Hill, 1986.

- [34] Wiley B. J. et al. Maneuvering the surface plasmon resonance of silver nanostructures through shape-controlled synthesis J. Phys. Chem. B 110 (2006): 15666-15675.
- [35] Kreibig U.; and Vollmer M. Optical properties of metal clusters Berlin, Germany: Springer, 1995.
- [36] Haes A. J. et al. A nanoscale optical Biosensor: the long range distance dependence of the localized surface Plasmon resonance of noble metal nanoparticles J. Phys. Chem. B 108 (2004): 109-116.
- [37] Ales P.; Libor K.; and Robert P. Silver colloid nanoparticles: synthesis, characterization, and their antibacterial activity J. Phys. Chem. B 110 (2006): 16248-16253.
- [38] Pradhan N.; Pal A.; and Pal T. Silver nanoparticles catalyzed reduction of aromatic nitro compounds Colloid and Surface A 196 (2002): 247-257.
- [39] Panáček A. et al. Silver colloid nanoparticles: synthesis, characterization, and their antibacterial activity J. Phys. Chem. B 110 (2006): 16248-16253
- [40] Draine T. B.; and Flatau P. J. Discrete-dipole approximation for scattering calculations J. Opt. Soc. Am. A 11 (1994): 1491-1499.
- [41] Silvert P. Y.; Herrera-Urbina R.; and Tekaiia-Elhsissena K. Preparation of colloidal silver dispersions by the polyol process Part 2. Mechanism of particle formation J. Mater. Chem. 7 (1997): 293-299.
- [42] Panacek A. et al. Silver colloid nanoparticles: synthesis, characterization, and their antibacterial activity J. Phys. Chem. B 110 (2006): 16248-16253.
- [43] Panigrahi S.; Kundu S.; Ghosh S. K.; Nath S.; and Pal T. General method of synthesis for metal nanoparticles J. Nanoparticle Res. 6 (2004): 411-414.
- [44] Pal T.; Sau T. K.; and Jana N. R. Reversible formation and dissolution of silver nanoparticles in aqueous surfactant media Langmuir 13 (1997): 1481-1485.
- [45] Huang H. H. et al. Photochemical formation of silver nanoparticles in Poly(N-vinylpyrrolidone) Langmuir 12 (1996): 909-912.
- [46] Gutierrez M.; and Henglein A. formation of colloidal silver by "Push-Pull" reduction of Ag^+ J. Phys. Chem. 97 (1993): 11368-11370.

- [47] Mafune F.; Kohno J.; Takeda, Y.; and Kondow T. Structure and stability of silver nanoparticles in aqueous solution produced by laser ablation J. Phys. Chem. B 104 (2000): 8333-8337.
- [48] Djokić S. Synthesis and antimicrobial activity of silver citrate complexes Bioinorg. Chem. Appl. (2008): 1-7.
- [49] Mpourmpakis G.; and Vlachos D. G. Insights into the Early Stages of Metal Nanoparticles Formation via First-Principle Calculation: the Roles of Citrate and Water Langmuir 24 (2008): 7465-7473.

APPENDICES

APPENDIX A

Table A 1 Estimated cost of our homemade silver nitrate.

Material cost	Cost per unit	Production costs of our homemade silver nitrate	
		Amount used	Cost (Baht)
Ag metal	18,000 Baht / 1,000 g [*]	100 g	1,800
Conc. Nitric acid	815 Baht / 2,500 mL ^{**}	200 mL	65
Acetone	600 Baht / 2,500 mL ^{**}	100 mL	24
Electrical cost	Electrical power (kW)	Time used (hr)	Electricity consumed (unit); Electricity charge (Baht) ^{***}
Heater	1.6 (kW)	2	3.2(unit); 8.4 (B)
Total cost			1897.4
Cost of silver nitrate (Baht / 100 g)			= <u>1,338.7</u> ^{****}

* Ag metal (99.99%, jewelry store), AD 2009

** Merck®, AD 2009

*** 2.63 Baht / unit (According to the electricity tariff applicable to business and residential industry (12 kV and low), AD 2000)

**** Silver nitrate (141.73 g; 90% yield, getting started from Ag metal 100 g)

Table A 2 Estimated cost of our synthesis of high concentration silver nanoparticles (10,000 pm/1 liter).

		Production costs of our synthesis of high concentration silver nanoparticles			
Material cost	Cost per unit	Type 1: Getting started from AgNO ₃ (commercial product)		Type 2: Getting started from AgNO ₃ (our synthesis)	
		Amount used	Cost (Baht)	Amount used	Cost (Baht)
AgNO ₃ (our synthesis)	~1340 Baht / 100 g*	-	0	16 g	214.4
AgNO ₃ (Commercial)	3,750 Baht / 100 g**	16 g	600	-	0
Reducing agent (NaBH ₄)	7,700 Baht / 100 g**	2.6 g	200	2.6 g	200
Stabilizer (Soluble Starch)	7,500 Baht / 1,000 g**	20 g	150	20 g	150
DI Water	200 Baht / 4,000 mL	1,000 mL	50	1,000 mL	50
Electrical cost	Electrical power (kW)	Time used (hr)	Electricity consumed (unit); Electricity charge (Baht)***	Time used (hr)	Electricity consumed (unit); Electricity charge (Baht)***
Heater	1.6	2	3.2 (unit); 8.4 (B)	2	3.2 (unit); 8.4 (B)
Total cost			<u>1,008.4</u>		<u>622.8</u>

* Cost of our synthesis of silver nitrate, AD 2009

** Merck®, AD 2009

*** 2.63 Baht / unit (According to the electricity tariff applicable to business and residential industry (12 kV and low), AD 2000)

APPENDIX B

Add 0.1 mL of the inoculums (10^6 CFU/mL) to each of the tubes containing the silver nanoparticles (0.05 g) and only normal saline solution as a control



Put the tubes on an orbital shaker (100 rpm) and orbitally shake at room temperature (~ 25 °C)



Collect 100 μ L samples after 0 and 24 hours, dilute, and spread in triplicate on TSA agar plate.



Incubate the plates at 37 °C until the growth of the test organism was observed.



Count the number of colonies on each plate and report as CFU/mL.

Figure B 1 Procedure for the determination of the effects of silver nanoparticles on the reduction bacterial growth.

Comparison of synthesized silver nanoparticles from our homemade silver nitrate and commercially available analytical grade silver nitrate

From Figure B 2, the maxima of normalized extinction spectra of highly concentrated silver nanoparticles synthesized from our homemade silver nitrate and available commercial product were around 400 nm and the FWHH about 39 and 41 nm, respectively. The two spectra are nearly super imposable. The results suggested that the synthesized silver nanoparticles possessed the same shape, size, and size distribution, and were independent from the source of the silver nitrate used.

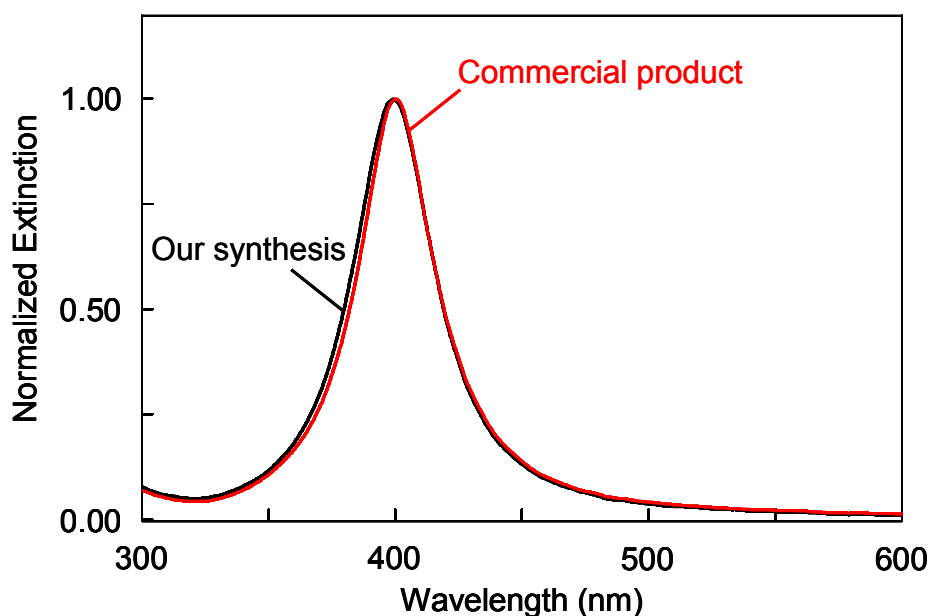


Figure B 2 The normalized extinction spectra of highly concentrated silver nanoparticles synthesized from our homemade silver nitrate and commercially available analytical grade silver nitrate.

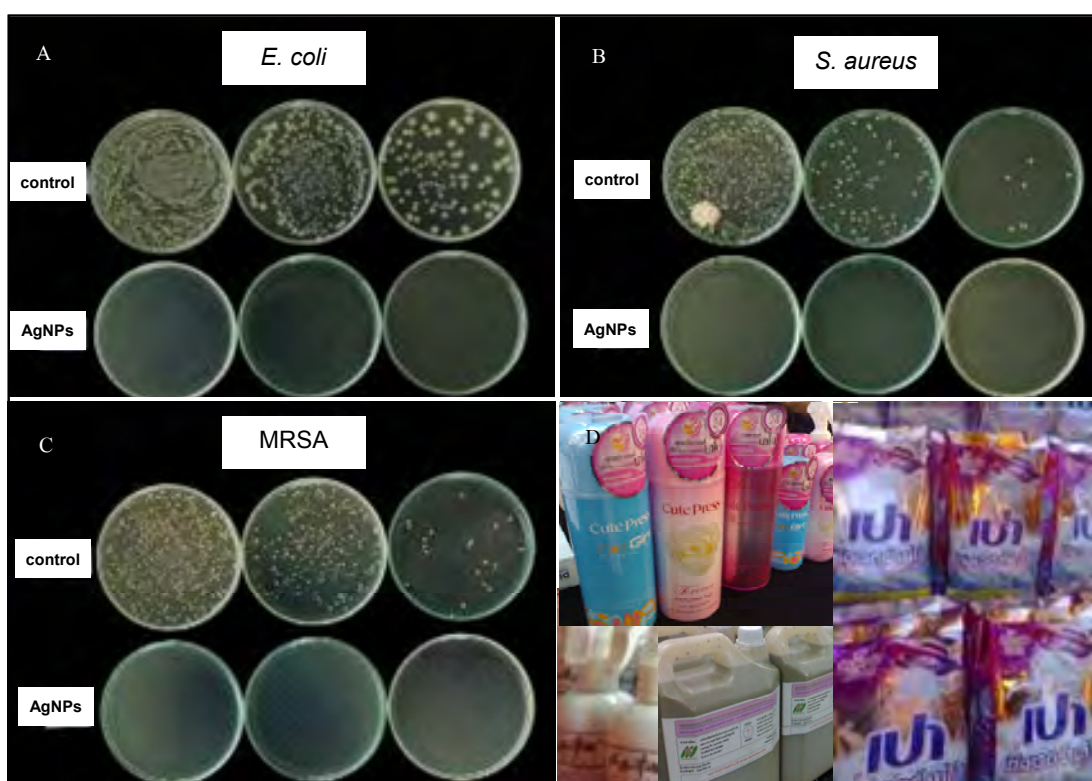
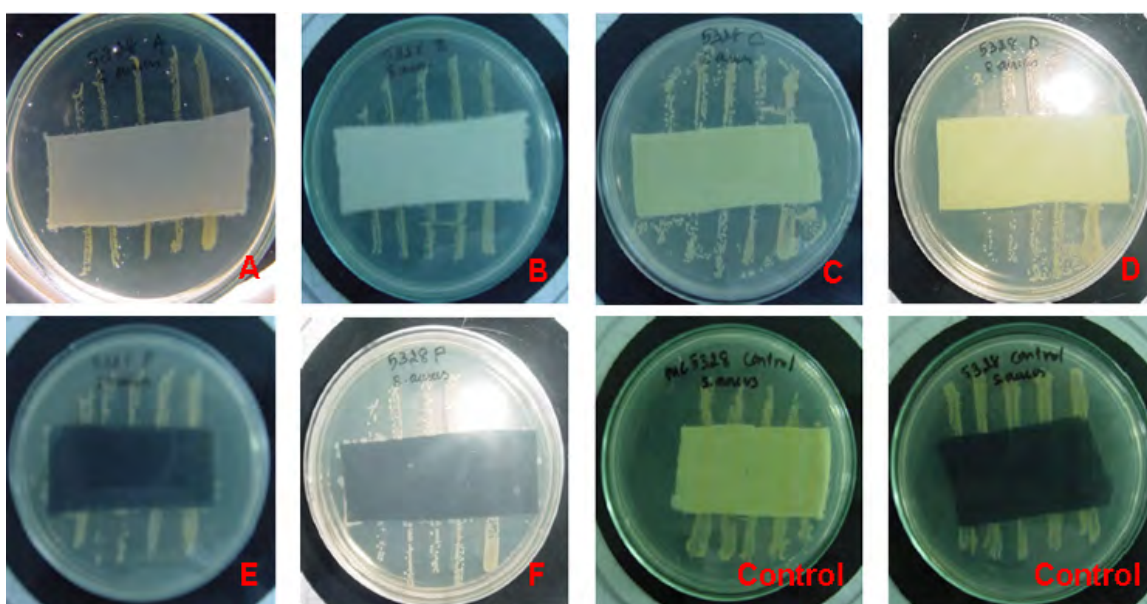


Figure B 3 Photograph of antibacterial activity test of (A) *Escherichia coli*, (B) *Staphylococcus aureus* and (C) methicillin resistant *Staphylococcus aureus* (MRSA) with our synthesized silver nanoparticles (AgNPs), and (D) our synthesis of silver nanoparticles was applied into commercial products.

Antibacterial test against *Staphylococcus Aureus* (ATCC 6538) by Parallel Streak method.

AATCC test method 147-1998 (the American Association of Textile Chemists Colorists, 2004).



Tested by Nanyang Knitting Factory Co., Ltd. And Intertex Testing Services (Thailand) Limited.

Figure B 4 The antibacterial test of bacterial pathogens with silver nanoparticles padding on fabric: (A/B; Polyester), (C/D; Cotton) with AgNPs 50 ppm, Tested after 20 Wash: No Growth (NG), and (E/F; Polyester), and Control (Cotton) Tested after 20 Wash: Large Growth (LG) / Moderate Growth (MG).

APPENDIX C

Acute Oral Toxicity Test of Colloidal Silver Nanoparticles

T. Kaewamatawong^{1*}, W. Banlunara¹, S. Ekgasit², P. Maneewattanapinyo²

¹Department of Pathology, Faculty of Veterinary Science, ²Department of Chemistry, Faculty of Science, Chulalongkorn University, Bangkok, Thailand 10330 *Corresponding author: Theerayut71@hotmail.com

Keywords: acute, oral, colloidal silver nanoparticles, mouse toxicity

Introduction

Engineered nanoparticles (NP) are defined as materials produced within the range of 1-100 nm in length or diameter. Nanoparticles have the increased structural integrity as well as unique physical and chemical properties (3). Although the applications and benefits of these engineered nanomaterials are extensively and currently being widely used in modern technology, there is a severe lack of information concerning the human health and environmental implications of occupational exposure during the manufacturing and handling process (2). Silver nanoparticles (Ag-NPs) have been known to have inhibitory and bactericidal effects as well as the effective in retarding the growth of mold, harmful spores and germs (1). Ag-NPs are found to be a popular constituent in health applications and ink industry. Despite the varied uses of these Ag-NPs in many commercial products that launched into the market recently, there is a lack of information on the basic toxicity of silver nanoparticles. Thus, the objective of this study is to investigate the acute oral toxicity of silver nanoparticles using the recommended Organization for Economic Cooperation and Development (OECD) guidelines for testing of chemicals for safety evaluation. Furthermore, lethal Dose 50 (LD50) or Toxic Dose 50 (TD50) is evaluated in this study.

Materials and Methods

Particles: Colloidal silver nanoparticles were obtained as a gift from Sensor Research Unit, Department of Chemistry, Faculty of Science, Chulalongkorn University, Thailand. The Ag-NPs were suspended in water in various concentrations and had a primary particle diameter of 5-20 nm.

Experimental design: The acute oral toxicity of Ag-NPs was evaluated in mice using the up and down procedure (4). Mice of either sex (nine females and nine males, weight: 28-35 g, age: 10-12 weeks) received colloidal Ag-NPs at the limited dose of 5,000 mg/kg (100,000 ppm) orally using a suitable intubation cannula. The animals were observed for toxic symptoms continuously for the first 3 hr after dosing. Finally, the number of survivors was noted after 24 hr and these animals were then maintained for further 14 days with observations made daily. At 1, 7 and 14 days after gavage, six mice in each group were sacrificed. Whole blood was collected for routine clinical pathology and blood chemical parameters including aspartate aminotransferase (AST), serum creatinine, cholesterol and total protein. Various organs such as lung, hilar lymph node, heart,

liver and kidney were collected in 10% buffered neutral formalin for routine histopathological evaluations.

Results and Discussion

Clinical and general signs: No death was recorded in the 14 days of observation period in the male and female animals given 5000 mg/kg of the colloidal Ag-NPs orally. The animals did not show any significant changes in the general appearance during the 14 days observation period.

Body weight: There were no significant differences in the percentage of weight gain between control and treatment groups of both sexes.

Blood analysis: Routine hematological analysis and leukocyte differential count showed no significant changes in the male and female treatment groups compared to the control groups. The result of blood chemistry study also showed no significant differences in any of the parameters examined in either the control or the animals treated with Ag-NPs.

Tissue analysis: There were no detectable abnormalities on gross findings in any observation time. Histopathological examination of various organs in the control and treated animals showed no remarkable lesions that could be attributed to the effect of oral exposure of Ag-NPs on mice for 14 days observation period.

Conclusion: The results of acute toxicity study indicated that the LD50 or TD50 of the colloidal Ag-NPs is greater than 5000 mg/kg or 100,000 ppm in line with the 5000 mg/kg limit dose recommend by OECD 425 (4). It is therefore concluded that the acute oral administration of colloidal Ag-NPS at 5000 mg/kg body weight for 14 consecutive days to male and female ICR mice did not induce any toxicological effects. However, further long-term or chronic exposure of Ag-NPs should be performed.

Acknowledgement

This work was supported by a grant from The National Research Council of Thailand, 2008.

References

1. Chen and Schluesener, 2008. Toxicol. Letters 176(1): 1-12.
2. Hoet et al., 2004. J. Nanobiotechnology 1: 12.
3. Thomas and Sayre, 2005. Toxicol Sci 2: 316-321.
4. OECD guidelines No. 425, 2009. Organization for Economic Cooperation and Development 1(4): 1-27.

Acute Dermal Toxicity Test of Colloidal Silver Nanoparticles

T. Kaewamatawong^{1*}, W. Banlunara¹, S. Ekgasit², P. Maneewattanapinyo²

¹Department of Pathology, Faculty of Veterinary Science, ²Department of Chemistry, Faculty of Science, Chulalongkorn University, Bangkok, Thailand 10330 *Corresponding author: Theerayut71@hotmail.com

Keywords: acute, colloidal silver nanoparticles, dermal, guinea pig, toxicity

Introduction

Engineered nanoparticles (NP) are defined as materials produced within the range of 1-100 nm in length or diameter. Nanoparticles have the increased structural integrity as well as unique physical and chemical properties (3). Although the applications and benefits of these engineered nanomaterials are extensively and currently being widely used in modern technology, there is a severe lack of information concerning the human health and environmental implications of occupational exposure during the manufacturing and handling process (2). Silver nanoparticles (Ag-NPs) have been known to have inhibitory and bactericidal effects as well as the effective in retarding the growth of mold, harmful spores and germs (1). Ag-NPs are found to be a popular constituent in health applications and ink industry. Despite the varied uses of these Ag-NPs in many commercial products that launched into the market recently, there is a lack of information on the basic toxicity of silver nanoparticles. Thus, the objective of this study is to investigate the acute dermal toxicity of silver nanoparticles using the recommended Organization for Economic Cooperation and Development (OECD) guidelines for testing of chemicals for safety evaluation. Furthermore, lethal Dose 50 (LD50) or Toxic Dose 50 (TD50) is evaluated in this study.

Materials and Method

Particles: Colloidal silver nanoparticles were obtained as a gift from Sensor Research Unit, Department of Chemistry, Faculty of Science, Chulalongkorn University, Thailand and had a primary particle diameter of 5-20 nm. The Ag-NPs were suspended in water in various concentrations.

Experimental design: Male guinea pigs (500-650 g) were randomly divided into 3 groups containing 3 animals each in the following manner: group 1, distilled water (vehicle control); group 2 and group 3, 50 and 100,000 ppm of colloidal Ag-NPs, respectively. All treated groups received the above chemicals at 2 ml. The procedure used for determining the dermal toxicity of the above chemicals followed the procedures as recommended and documented by OECD 434; acute dermal toxicity-fixed dose procedure (4). Briefly, the Ag-NPs were dissolved in distilled water and applied to a shaved area of skin, approximately 7x10 cm². The chemical was left in contact with the skin with a porous gauze dressing and non-irritating tape for 24 hours. All animals were observed for toxic symptoms continuously at 1, 3, 7 and 14 hr after dosing. After 24-hr exposure period, any residue was removed by washing with distilled water. The number of survivors was noted after 24 hr and these animals were then maintained and observed for toxic signs for further 14 days with observations made daily. At 1, 3 and 7 days after exposure, skin biopsy was performed for routine histopathological evaluations. All animals were sacrificed after a 14 day observation period and collected the skin for histopathological examination.

Results and Discussion

Clinical and gross findings: All control and treated animals, there were no exposure-related clinical signs in any observation time. Grossly, the control, 50 and 100,000 ppm colloidal Ag-NPs did not show any significant changes in the general appearance and skin condition during the 14 days observation period (Fig. 1).

Histopathology: No significant lesions were observed in the skins from treatment groups compared to the control animals at all observation times (Fig. 2).

The results of acute dermal toxicity study indicated that the LD₅₀ or TD₅₀ of the colloidal Ag-NPs is greater than 100,000 ppm. It is therefore concluded that the acute oral administration of colloidal Ag-NPs at 50 or 100,000 ppm for 14 consecutive days did not induce any toxicological effects. However, further long-term or chronic repeated exposure of Ag-NPs should be performed.

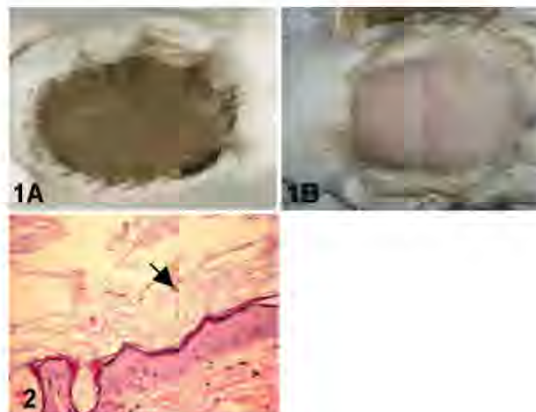


Fig. 1 Skin appearance of 100,000 ppm group at 0 hr post-exposure (A) and 24 hr post-exposure after residue removing (B)

Fig. 2 Skin biopsy from 100,000 ppm group, Ag-NPs cover on the keratin layer (arrow) H&E, x390.

Acknowledgement

This work was supported by a grant from The National Research Council of Thailand, 2008.

References

1. Chen and Schluesener, 2008. Toxicol. Letters 176(1): 1-12.
2. Hoet et al., 2004. J. Nanobiotechnology 1: 12.
3. Thomas and Sayre, 2005. Toxicol. Sci. 2: 316-321.
4. OECD guidelines No. 434. 2004. Available: www.oecd.org/dataoecd/63/24/32037747.pdf

Acute Eye Irritation and Corrosion Test of Colloidal Silver Nanoparticles

T. Kaewamatawong^{1*}, W. Banlunara¹, S. Ekgasit², P. Maneewattanapinyo²

¹Department of Pathology, Faculty of Veterinary Science, ²Department of Chemistry, Faculty of Science, Chulalongkorn University, Bangkok, Thailand 10330 *Corresponding author: Theerayut71@hotmail.com

Keywords: acute, colloidal silver nanoparticles, eye, irritation, mouse

Introduction

Engineered nanoparticles (NP) are defined as materials produced within the range of 1-100 nm in length or diameter. Nanoparticles have the increased structural integrity as well as unique physical and chemical properties (3). Although the applications and benefits of these engineered nanomaterials are extensively and currently being widely used in modern technology, there is a severe lack of information concerning the human health and environmental implications of occupational exposure during the manufacturing and handling process (2). Silver nanoparticles (Ag-NPs) have been known to have inhibitory and bactericidal effects as well as the effective in retarding the growth of mold, harmful spores and germs (1). Ag-NPs are found to be a popular constituent in health applications and ink industry. Despite the varied uses of these Ag-NPs in many commercial products that launched into the market recently, there is a lack of information on the basic toxicity of silver nanoparticles. Thus, the objective of this study is to investigate the acute eye irritation and corrosion of colloidal silver nanoparticles using the recommended Organization for Economic Cooperation and Development (OECD) guidelines for testing of chemicals for safety evaluation.

Materials and Methods

Particles: Colloidal silver nanoparticles were obtained as a gift from Sensor Research Unit, Department of Chemistry, Faculty of Science, Chulalongkorn University, Thailand and had a primary particle diameter of 5-20 nm. The Ag-NPs were suspended in water in various concentrations.

Experimental design: Male guinea pigs (500-650 g) were randomly divided into 2 groups containing 4 animals each in the following manner: group 1, 50 ppm of colloidal Ag-NPs and group 2, 5,000 ppm of colloidal Ag-NPs. The procedure used for determining the ocular toxicity of the above chemicals followed the procedures as recommended and documented by OECD 405; acute eye irritation and corrosion (4). Briefly, the 0.1 ml of colloidal Ag-NPs suspension was placed in the conjunctival sac of one eye of each animal after gently pulling the lower lid away from the eyeball. Another eye, which remains untreated, serves as a control by instilling with 0.1 ml of distilled water. All animals were observed for toxic symptoms continuously at 1, 12, 24, 48 and 72 hr after dosing. The eye reactions of iris, conjunctivae, cornea and chemosis were graded following the grading system of OECD 405 guideline. The animals were then maintained and observed for toxic signs for further 14 days with observations made daily.

Results and Discussion

Clinical and general signs: The animals from control and treated animals did not show any toxic signs in the clinical and general appearance during the 14 days observation period.

Ocular reactions: No any significant lesion was observed in the control and 50 ppm Ag-NPs treated animals throughout the observation period (Fig. 1). During first 24 hr observation time, some animals from 5,000 ppm Ag-NPs treated group showed grade 1 of conjunctivae irritation, which some blood vessels hyperemia in conjunctivae were observed (Fig. 2). However, no any sign of eye irritation was found in all treated animals after 48 hr post-exposure.

The results of acute eye administration of colloidal Ag-NPs at 50 or 5,000 ppm for 14 consecutive days did not induce any toxicological effects. However, the animals from 5,000 ppm groups showed transient mild conjunctival irritation at early 24 hr post-exposure. It is therefore concluded that the acute ocular toxic dose of the colloidal Ag-NPs might be greater than 5,000 ppm. Further long-term or chronic repeated exposure of Ag-NPs should be performed.

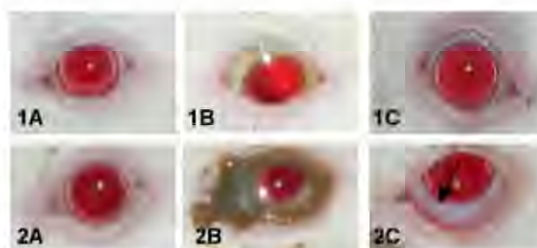


Fig. 1 Ocular appearance of 50 ppm groups; (A) control, (B) 0 hr post-exposure, (C) 12hr post-exposure

Fig. 2 Ocular appearance of 5,000 ppm groups; (A) control, (B) 0 hr post-exposure, (C) 12hr post-exposure. Arrow revealed blood vessels hyperemia in conjunctivae.

Acknowledgements

This work was supported by a grant from The National Research Council of Thailand, 2008.

References

1. Chen and Schluessener, 2008. *Toxicol. Letters* 176(1): 1-12.
2. Hoet et al., 2004. *J. Nanobiotechnology* 1: 12.
3. Thomas and Sayre, 2005. *Toxicol. Sci.* 2: 316-321.
4. OECD guideline No. 405, 2009. Organization for Economic Cooperation and Development 1(4): 1-14.

Acute Pulmonary Toxicity Caused by Single Intratracheal Instillation of Colloidal Silver Nanoparticles in Mice

T. Kaewamatawong^{1*}, W. Banlunara¹, S. Ekgasit², P. Maneewattanapinyo²

¹Department of Pathology, Faculty of Veterinary Science, ²Department of Chemistry, Faculty of Science, Chulalongkorn University, Bangkok, Thailand 10330 *Corresponding author: Theerayut71@hotmail.com

Keywords: acute, colloidal silver nanoparticles, lung, mouse, toxicity

Introduction

Engineered nanoparticles (NP) are defined as materials produced within the range of 1-100 nm in length or diameter. Nanoparticles have the increased structural integrity as well as unique physical and chemical properties (3). Although the applications and benefits of these engineered nanomaterials are extensively and currently being widely used in modern technology, there is a severe lack of information concerning the human health and environmental implications of occupational exposure during the manufacturing and handling process (2). Silver nanoparticles (Ag-NPs) have been known to have inhibitory and bactericidal effects as well as the effective in retarding the growth of mold, harmful spores and germs (1). Ag-NPs are found to be a popular constituent in health applications and ink industry. Despite the varied uses of these Ag-NPs in many commercial products that launched into the market recently, there is a lack of information on the basic toxicity of silver nanoparticles. Moreover, data of the pulmonary pathological effects of Ag-NPs have not been reported to our knowledge. The purpose of this study is to describe acute pulmonary pathological effects caused by intratracheal exposure to various doses of Ag-NPs.

Material and Methods

Particles: Colloidal silver nanoparticles were obtained as a gift from Sensor Research Unit, Department of Chemistry, Faculty of Science, Chulalongkorn University, Thailand and had a primary particle diameter of 5-20 nm. The Ag-NPs were suspended in water in various concentrations.

Experimental design: 60 Male ICR mice were single intratracheally instilled with 50 μ l aqueous suspensions of 20, 200, 2000 or 20,000 ppm of Ag-NPs suspended in distilled water. The control groups of mice were instilled with 50 μ l of distilled water. At 1, 3, 7 and 14 days after instillation, the animals in each group were sacrificed. Various organs such as lung, hilar lymph node, heart, liver and kidney were collected in 10% buffered neutral formalin for routine histopathological evaluations.

Results and Discussion

Clinical and gross findings: In control, 20 and 200 ppm of Ag-NPs treated animals, there were no exposure-related clinical signs in any observation time. Some mice in 2,000 and 20,000 ppm treated animals showed a sign of dyspnea shortly after instillation. However, this sign was recovered after 6 hr post-exposure. Grossly, instillation of 20 and 200 ppm Ag-NPs treated animals caused mild congestion and edema in lung compared to the control groups. In both 2,000 and 20,000 ppm Ag-NPs treated animals, tiny pin-head sized or patchy black brown foci were scattered in lung lobes throughout the experiment.

The degree of lesions described above in 20,000 ppm treated groups was more severe than 2,000 ppm treated groups (Fig. 1). **Histopathology:** At 1 day after instillation, accumulation of free aggregated particles was found in the alveoli and bronchiolar lumens of all treated groups. Some of aggregated particles were present within alveolar macrophages, and occasionally present within alveolar epithelial cells with increasing number of cells in alveolar wall (Fig. 2A). The animal instilled with 2,000 and 20,000 ppm Ag-NPs had a moderate to severe accumulation of Ag-NPs laden alveolar macrophages and inflammatory cells in lung parenchyma. At 3 days after instillation, moderate to severe focal alveolitis characterized by accumulation of numerous active AMs, particle-laden AMs, inflammatory cells was observed (Fig. 2B). Changes in the lungs of mice killed at 7 and 14 days post-exposure were distributed to the appearance of the alveolitis with some necrotic areas (Fig. 2C). The magnitude lesions in 20,000 ppm groups were greater than 2,000 ppm groups.

An acute pulmonary instillation Ag-NPs above 2,000 ppm for 14 consecutive days can induce lung inflammation and tissue injury in a dose dependent manner.

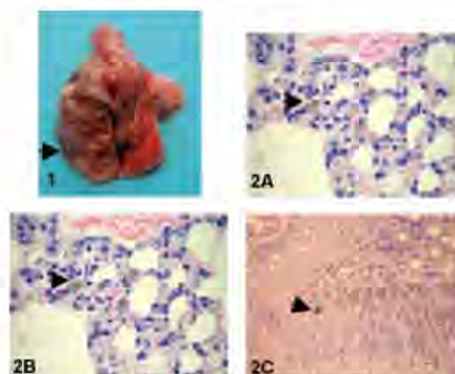


Fig. 1 Multifocal black foci (arrow); 20,000 ppm groups

Fig. 2 Lungs from various doses of Ag-NPs, H&E, x 390.

- A) 200 ppm groups at 1 day post-exposure
 B) 20,000 ppm groups at 1 day post-exposure
 C) 20,000 ppm groups at 14 day post-exposure; arrows showed Ag-NPs

Acknowledgement

This work was supported by a grant from The National Research Council of Thailand, 2008.

References

- Chen and Schluesener, 2008. *Toxicol. Letters* 176(1): 1-12.
- Hoet et al., 2004. *J. Nanobiotechnology* 1: 12.
- Thomas and Sayre, 2005. *Toxicol. Sci.* 2: 316-321.

APPENDIX D

Inhibition of Human Cytochrome P450 Enzymes by Metallic Nanoparticles: A Preliminary to Nanogenomics

¹A. Sereemaspun, ²P. Hongpiticharoen, ³R. Rojanathanes, ³P. Maneewattanapinyo,
³S. Ekgasit and ²W. Warisnoicharoen

¹Department of Anatomy, Faculty of Medicine, Chulalongkorn University,
Phyathai Road, Pathumwan, Bangkok 10330, Thailand

²Pharmaceutical Technology (International) Program, Faculty of Pharmaceutical Sciences,
Chulalongkorn University, Phyathai Road, Pathumwan, Bangkok 10330, Thailand.

³Department of Chemistry, Faculty of Science, Chulalongkorn University,
Phyathai Road, Pathumwan, Bangkok 10330, Thailand

Abstract: The effect of nanoparticles on the biological functions or the relative toxicity is not well-understood and becomes the major public concerns. This study determined the *in vitro* effect of gold and silver nanoparticles as the two most frequently used metallic nanomaterials for therapeutics and diagnostic on the microsomes containing wild-type cDNA expressed human CYP450 enzymes CYP1A2, 2C9, 2C19 and 3A4. Results demonstrated that all of the CYP450s activities were down-regulated by metallic nanoparticles. These findings suggest the inhibition of oxidation based biological process by penetration of metallic nanosized particles across the microsomal membrane.

Key words: Cytochrome P450, gold nanoparticles, silver nanoparticles, metabolism

INTRODUCTION

It is widely recognized that nanomaterials produce extensive influences in general public including economical, technological and medicinal purposes (Farokhzad and Langer, 2006). The concern of negative consequence on health and environment of nanomaterials is continuously raised, whereas the knowledge on their biological effects remains unclear. The study related to the toxicity or biological activities of the Synthetic Nanoparticles (NPs) is an urgent need if such materials are aimed to further implement in human.

Gold and silver nanoparticles are the metal-based nanocarriers commonly used in various applications including drug delivery, diagnosis and therapy (Biju *et al.*, 2008). Recently, the self-assembly metallic nanoparticles were reported to alter or inhibit the biological functions (Fischer *et al.*, 2002; Mukherjee *et al.*, 2005). Gold nanoparticles (AuNPs) were found to inhibit the chymotrypsin activity and vascular endothelial growth factor of endothelial cells (Fischer *et al.*, 2002; Mukherjee *et al.*, 2005). Importantly, AuNPs might play a role in cell cycle by upregulating the p21 and p27 proteins

expressed in the G1 phase (Bhattacharya *et al.*, 2007). Additionally, silver nanoparticles (AgNPs) showed ability to bind with the glycoprotein subunits of HIV-1 leading to deactivation of HIV-1 virus (Elechiguerra *et al.*, 2005).

To explore whether AuNPs and AgNPs can interfere with the metabolic or biotransformation process of drug and xenobiotics, we performed an inhibition assay of NPs on some cDNA expressed human cytochrome P450 monooxygenases (P450), namely CYP1A2, CYP2C9, CYP2C19 and CYP3A4, as key oxidative enzymes in a first stage of metabolism (Coleman, 2005).

MATERIALS AND METHODS

Materials: Tetrachloroauric acid (HAuCl₄) was purchased from Acros Organics (Morris Plains, NJ). Trisodium citrate dihydrate (Na₃C₆H₅O₇·2H₂O), silver nitrate (AgNO₃) and sodium borohydride (NaBH₄) were supplied from Merck (Darmstadt, Germany). Microsomes from baculovirus-infected cells containing wild-type cDNA expressed human CYP1A2, CYP2C9, CYP2C19 or CYP3A4 and NADPH-cytochrome P450 reductase (P450 Baculosomes[®]), NADPH regeneration system containing

Corresponding Author: Warangkana Warisnoicharoen, Faculty of Pharmaceutical Sciences, Chulalongkorn University,
Phyathai Road, Pathumwan, Bangkok 10330, Thailand Tel: +66-2-2188332 Fax: +66-2-2188332

glucose-6-phosphate dehydrogenase (G-6-PD) and glucose-6-phosphate (G-6-P), NADP⁺, fluorogenic Vivid[®] EOMCC substrate (7-ethyloxymethoxy-3-cyanocoumarin) for CYP1A2/2C19 or Vivid[®] BOMCC substrate (7-benzyloxymethoxy-3-cyanocoumarin) for CYP2C9/3A4 and potassium phosphate buffer (reaction buffer) were from Invitrogen (Madison, WI). All other chemicals used were the highest commercial grade available.

Synthesis and characterization of AuNPs and AgNPs:

AuNPs were synthesized from HAuCl₄ using Na₂C₂H₂O₇·2H₂O as a reducing agent and AgNPs were made by reducing AgNO₃ with NaBH₄ as earlier described (Enüstün and Turkevich, 1963; Van Hyning and Zukoski, 1998). The final concentration of Au atom in AuNP solution was 44 ppm. The AgNP solution was 20-fold diluted to obtain 50 ppm of Ag atom prior to use. The NPs were characterized using Transmission Electron Microscopy (TEM) H-7650 (Hitachi, Japan) and UV-visible spectroscopy (Shimadzu, Japan). The zeta potential or the surface charge of NPs was determined by Zetasizer NanoZS (Malvern, UK).

CYP P450 inhibition assay: The inhibition assay was conducted in black, flat-bottom, 96-well plate (PerkinElmer, Waltham, MA) for a 100 µL reaction per well according to the standard protocol described (<http://www.invitrogen.com/contents/sfs/panvera/L0504.pdf>). For inhibition assay of CYP1A2 or CYP2C19, a 50 µL buffer solution (pH 8.0) containing P450 Baculosomes[®] at assay concentrations of 5 nM CYP450, 0.3 U mL⁻¹ G-6-PD and 3.33 mM G-6-P was added to 40 µL of the solution of AuNPs (44 ppm) or AgNPs (50 ppm). The plate was incubated for 20 min at room temperature before adding 10 µL a mixture of EOMCC substrate (3 µM for CYP1A2 or 10 µM for CYP2C19) and 100 µM NADP⁺ solution. The same procedure was used for inhibition studies of CYP2C9 or CYP3A4 except for 10 µM BOMCC substrate was used and the assay concentrations of CYP2C9 and CYP3A4 were 10 and 5 nM, in orderly. The enzymatic reaction was stopped by addition of 5 µL of 0.5 M Tris base (pH 10.5) to all wells after 30 min incubation at room temperature. The relative fluorescence unit (RFU) was read on a Victor³ V plate reader (PerkinElmer, Waltham, MA) using the fluorescent excitation filter at 390 nm and a bandwidth of 20 nm and emission wavelength at 450 nm and a bandwidth of 10 nm. Percent inhibition was then calculated by comparison of RFU to those wells using water instead of sample.

RESULTS AND DISCUSSION

Characterization of the metallic NPs: The visual appearance of synthesized AuNPs was in deep red color and AgNPs was in yellow color (Fig. 1a). The characteristic Surface Plasmon Resonance (SPR) bands of AuNPs at 525 nm and AgNPs at 440 nm were clearly observed by UV-Vis suggesting the formation of spherical NPs (Fig. 1b). The TEM images showed the average particle diameter of 9 nm for AuNPs and 15 nm for AgNPs (Fig. 1c, d). The zeta potential (Mean±SD, n = 3) of AuNPs were -30.8±2.4 mV. The AgNPs had slightly negative zeta potential, -14.4±1.1 mV.

P450 inhibitory potency of metallic NPs: The P450 metabolism cleaves the quenched substrates, resulting in a highly fluorescent metabolite of 3-cyano-7-hydroxycoumarin. P450 inhibitory effects of AuNPs and AgNPs were identified by their ability to prevent formation of fluorescent signal in the assay. The wild-type P450 isozymes were chosen to be studied as being dominant genes in the population (Coleman, 2005). The results clearly showed that the P450s were down-regulated by AuNPs and AgNPs with the greater extent being seen with the AgNPs (Table 1).

So far, there are no any evidences on how the NPs interact with the P450 proteins. We propose here in the possible ways in which the metallic NPs inhibit the P450 activity, NPs having the binding affinity to P450 due to the lipophilicity of the NPs and the hydrophobicity of the haem environment in P450 molecule, hence being the competitor of enzyme substrate (Lewis *et al.*, 2004). NPs forming mixed micelles with the microsomal membrane leading to the change in membrane integrity and the inactivity of the enzyme.

From the results, the metallic NPs were surface charged as seen from the zeta potential; hence, the NPs might be less lipophilic than the value required for the P450 binding affinity. However, the data obtained from molecular modeling such as hydrogen bond and π-π stacking interaction energy of the NP molecule are needed for proper justification of the first hypothesis. For the assumption on membrane perturbation of NPs, it is known that the inactivation of P450 is well succeeded with the amphiphilic molecule (i.e., surfactants). The earlier study reported that the formation of micelles of glycocholic/phospholipid or taurocholate/phospholipid caused 80 to 100% inhibition of human CYP3A4 *in vitro* (Mountfield *et al.*, 2000). Metallic NPs were considered to be amphiphilic, thus being able to fluidize

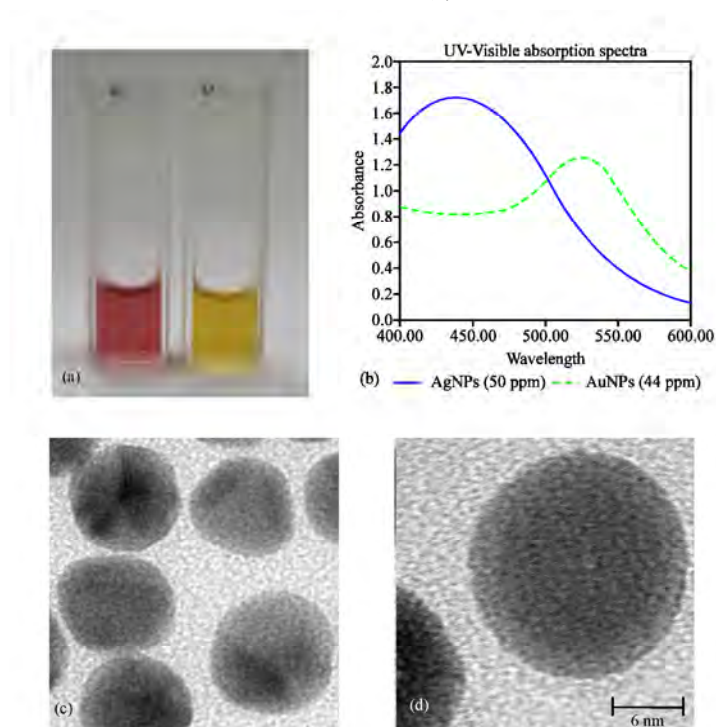


Fig. 1: Synthetic colloidal gold nanoparticles (AuNPs) and silver nanoparticles (AgNPs); (a) Visual detection of the AuNPs (left) and the AgNPs (right), (b) UV absorption spectrum of AgNPs and AuNPs and (c, d) Electron micrographs of AuNPs (c) and AgNPs (d) at the same magnification (scale bar = 6 nm both)

Table 1: Inhibitory effect of gold nanoparticles (AuNPs) and silver nanoparticles (AgNPs) on wild-type human P450 (Mean \pm SD, n = 4)

CYP 450 isozymes	Inhibition (%)	
	AuNPs	AgNPs
1A2	6.3 \pm 2.6	95.0 \pm 0.8
2C9	28.5 \pm 2.9	83.5 \pm 2.4
2C19	32.0 \pm 5.4	97.8 \pm 3.2
3A4	26.0 \pm 5.9	98.7 \pm 0.5

and penetrate the microsomal membrane. Additionally, other nanomaterials such as carbon nanotubes were capable of passing through a transmembrane configuration (Lopez *et al.*, 2004).

CONCLUSION

Conclusively, to our knowledge, this is the first report of AuNPs and AgNPs influence on human P450 proteins. The preliminary findings implied that metallic NPs had an inhibitory potential on the oxidative metabolism. Any changes in P450-NP interaction due to the polymorphic variances of P450 isozymes are under our further investigations.

ACKNOWLEDGMENTS

The authors would like to thank Kasama Rakphetmanee and Duangjai Punyapojak for their technical assistance. The partial support from Center of Innovative Nanotechnology Chulalongkorn University is gratefully acknowledged.

REFERENCES

- Bhattacharya, R., C.R. Patra, R. Verma, S. Kumar and P.R. Greipp *et al.*, 2007. Gold nanoparticles inhibit the proliferation of multiple myeloma cells. *Adv. Mater.*, 19: 711-716.
- Biju, V., T. Itoh, A. Anas, A. Sujith and M. Ishikawa, 2008. Semiconductor quantum dots and metal nanoparticles: Syntheses, optical properties, and biological applications. *Anal. Bioanal. Chem.*, 391: 2469-2495.
- Coleman, M.D., 2005. *Human Drug Metabolism*. 1st Edn., John Wiley and Sons, Chichester, ISBN-13 978-0-470-86353-6.

Int. J. Pharmacol., 4 (6): 492-495, 2008

- Elechiguerra, J.L., J.L. Burt, J.R. Morones, A. Camacho-Bragado and X. Gao *et al.*, 2005. Interaction of silver nanoparticles with HIV-1. *J. Nanobiotechnol.*, 3: 1-10.
- Entüstün, B.V. and J. Turkevich, 1963. Coagulation of colloidal gold. *J. Am. Chem. Soc.*, 85: 3317-3328.
- Farokhzad, O.C. and R. Langer, 2006. Nanomedicine: Developing smarter therapeutic and diagnostic modalities. *Adv. Drug Deliv. Rev.*, 58: 1456-1459.
- Fischer, N.O., C.M. McIntosh, J.M. Simard and V.M. Rotello, 2002. Inhibition of chymotrypsin through surface binding using nanoparticle-based receptors. *Proc. Natl. Acad. Sci. USA.*, 99: 5018-5023.
- Lewis, D.F.V., M.N. Jacobs and M. Dickins, 2004. Compound lipophilicity for substrate binding to human P450s in drug metabolism. *Drug Discov. Today*, 9: 530-537.
- Lopez, C.F., S.O. Nielsen, P.B. Moore and M.L. Klein, 2004. Understanding nature's design for a nanosyringe. *Proc. Natl. Acad. Sci. USA.*, 101: 4431-4434.
- Mountfield, R.J., S. Senepin, M. Schleimer, I. Walter and B. Bittner, 2000. Potential inhibitory effects of formulation ingredients on intestinal cytochrome P450. *Int. J. Pharm.*, 211: 89-92.
- Mukherjee, P., R. Bhattacharya, P. Wang, L. Wang and S. Basu *et al.*, 2005. Antiangiogenic properties of gold nanoparticles. *Clin. Cancer Res.*, 11: 3530-3534.
- Van Hying, D.L. and C.F. Zukoski, 1998. Formation mechanism and aggregation behavior of borohydride reduced silver particles. *Langmuir*, 14: 7034-7046.



Contents lists available at ScienceDirect

Sensors and Actuators B: Chemical

journal homepage: www.elsevier.com/locate/snb

Novel potentiometric approach in glucose biosensor using silver nanoparticles as redox marker

Wittaya Ngeontae^{a,b}, Wanwisa Janrungratsakul^a, Pattwat Maneewattanapinyo^a, Sanong Ekgasit^a, Wanlapa Aeungmaitrepirom^d, Thawatchai Tuntulani^{d,*}

^a Department of Chemistry, Faculty of Science, Chulalongkorn University, Bangkok 10330, Thailand

^b Department of Chemistry and Center of Excellence for Innovation in Chemistry, Faculty of Science, Khon Kaen University, Khon Kaen 40002, Thailand

ARTICLE INFO

Article history:

Received 14 September 2008

Received in revised form 4 November 2008

Accepted 4 November 2008

Available online 13 November 2008

Keywords:

Silver selective electrode

Silver nanoparticles

Glucose biosensor

Potentiometric redox marker

ABSTRACT

A new approach in glucose biosensor based on polymeric membrane Ag-ISE fabricated from benzothiazole calix[4]arene was investigated. Silver nanoparticles (AgNPs) were synthesized and demonstrated for the first time to be used as a potentiometric redox marker in a glucose biosensor. The linear relationship between logarithmic of H₂O₂ concentration and activity of free Ag⁺ releasing from silver nanoparticles was observed by direct potentiometry. Basically, the enzyme–substrate reaction between β-D-glucose and glucose oxidase (GOx) produced H₂O₂ as a product. The generated H₂O₂ was able to oxidize AgNPs to free Ag⁺ ions. The amount of Ag⁺ ions corresponded to the concentration of glucose could be directly monitored using the Ag-ISE. The working linear range was 0.1–3 mM in 10 mM magnesium acetate buffer pH 6.0. Parameters affected the reaction rate such as pH and the amount of GOx and AgNPs were explored. The lower detection limit was 1.0 × 10⁻⁵ M. The sensors exhibited very good repeatability with %R.S.D. < 7 and high sensor-to-sensor reproducibility. The proposed sensor provided a double selective function and could be used to determine glucose in beverages with good accuracy and precision.

© 2008 Elsevier B.V. All rights reserved.

1. Introduction

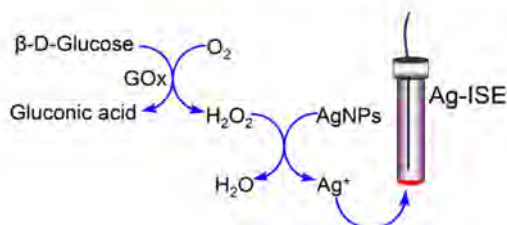
Glucose biosensors have long been developed. Up until now, three generations of glucose biosensors using (i) natural oxygen co-substrate and generation and detection of hydrogen peroxide, (ii) synthetic electron mediators, and (iii) direct electron transfer between GOx and the electrode, have been reported [1]. Amperometry is the main detection technique used in glucose biosensors due to good sensitivity and low detection limit. To improve the performance of glucose biosensors, various nanomaterials such as carbon nanotube (CNT) and metal nanoparticles have been incorporated into the biosensor platform.

Wang and Musameh have shown that a CNT-modified sensor strip facilitates low potential amperometric measurements of H₂O₂ and NADH [2]. Luong and colleagues demonstrated that coupling of CNT with Pt nanoparticles could improve the detection limit and response time of GOx-based glucose biosensors (0.5 mM and 3 s, respectively) [3]. Willner and co-workers showed that the gold nanoparticle, immobilized onto the gold electrode by means of a thiol linker acted as an electrical nanoplug for the electrical wiring of the redox center of GOx [4,5]. Later, the same group used platinum nanoparticles as catalytic labels for detecting biorecognition

events through the electrocatalyzed reduction of H₂O₂ [6]. Another efficient probe for GOx employed aligned single walled CNT modified gold electrode has been reported by Gooding and colleagues [7]. This approach allowed more efficient electron transfer to the FAD with a rate constant of 9 s⁻¹. Recently, detection of glucose by a CdS-nanoparticles modified electrode has been demonstrated by Huang et al. to give significantly enhanced electron transfer activity [8].

Despite its numerous uses, the amperometric technique seems to exhibit some disadvantages such as selectivity due to the interference of other reducible species in blood. Potentiometry such as ion selective electrode (ISE) has an advantage over amperometry in selectivity. However, a quite important drawback of ISEs is that only charge molecules can be directly detected using the ISEs. To overcome this obstacle, an analyte must undergo a reaction that produces an ion in an amount proportional to the concentration of the analyte in the sample. The ion generated or "the marker" is then detected using an appropriate ISE. Górski et al. used F⁻ selective electrodes based on zirconium(IV) 5,10,15,20-tetraphenylporphyrin as a detector for glucose in a FIA system [9]. Meyerhoff has demonstrated the determination of glucose using a coupled-enzymatic reaction with fluoride selective optical sensing polymeric film coated in microliter plate wells [10]. Iodide selective electrode has also been used as a new glucose sensor detecting the decreasing amount of I⁻ upon the release of H₂O₂ [11].

* Corresponding author. Tel.: +66 2 2187643; fax: +66 2 2187598.
E-mail address: thawatc@chula.ac.th (T. Tuntulani).



Scheme 1. Use of AgNPs as a new potentiometric redox marker in a glucose biosensor.

Thus far, no reports regarding the use of cation as marker have been found. This reason stems from the lack of cation markers available. Recently, metal nanoparticles such as gold and silver nanoparticles have been used as nanomaterial labels or “markers” in electrochemical biosensors and immunosensors [12–14]. Our group has fabricated a silver ion selective electrode or Ag-ISE using benzothiazole calix[4]arene as ionophore [15]. This Ag-ISE can be used in speciation analysis of silver nanoparticles (AgNPs). The key idea of this paper is to use AgNPs as cation marker in glucose biosensors as shown in Scheme 1. The enzyme–substrate reaction between glucose oxidase and glucose is well known to yield H_2O_2 . The oxidizing power of H_2O_2 is sufficient to convert Ag^0 of AgNPs to free Ag^+ . The activity of Ag^+ is immediately measured by a Ag-ISE.

2. Materials and methods

2.1. Materials

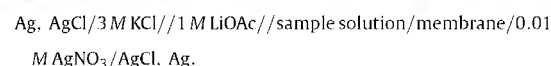
Glucose oxidase from *Aspergillus niger* (GOx, EC 1.1.3.4, 208.17 U mg^{-1}), magnesium acetate tetrahydrate, fructose, sucrose, high molecular weight polyvinyl chloride (PVC), *o*-nitrophenyl octyl ether (*o*-NPOE), potassium tetrakis (4-chlorophenyl) borate (KTPCIPB) and tetrahydrofuran (THF) were obtained from Fluka. Urea and glycine were purchased from Merck. β -D-Glucose was obtained from Sigma–Aldrich. The ionophore **CU1** [15] was prepared according to previously published procedures. The aqueous solutions were prepared from Milli-Q (Bedford, MA, USA) water purification system (Millipore).

Water colloids of high concentration silver nanoparticles (10,000 ppm) were synthesized via the chemical reduction process adapted from previous reports [16–18]. An aqueous solution of silver nitrate, 0.094 M (Merck) was prepared with methyl cellulose (Shin-Etsu) as a stabilizer. An aqueous solution of 0.07 M sodium borohydride reducing agent (Merck) with the methyl cellulose solution as a solvent was sequentially prepared. The silver solution was then added dropwise to the sodium borohydride solution under a vigorous stirring. A dark cloud appeared and turned to yellowish brown within a few seconds. When all reactants were completely added, the solution turned dark brown. The solution appeared golden yellow when diluted with distilled water under the concentration lower than 10 ppm.

2.2. Membrane preparation and EMF measurements

The Ag-ISE was prepared according to the procedure developed by us [15]. For this purpose, the ionophore **CU1** (10 $mmol\ kg^{-1}$), KTPCIPB (5 $mmol\ kg^{-1}$), 33 wt.% PVC and 66 wt.% *o*-NPOE were dissolved in 2.5 mL of THF. The cocktail solution was then poured into a glass ring (30 mm i.d.) fixed on a glass plate. The solvent was allowed to evaporate overnight at room temperature to give a transparent membrane (thickness ~ 0.2 mm). The membrane was punched into small sizes (7.5 mm i.d.) and glued with a PVC/THF

slurry on the top of PVC tube and connected to a micro-pipette tip as an electrode body. The polymeric membrane electrodes were conditioned overnight in 0.01 M $AgNO_3$ identical to the filling solution. Potentiometric measurements were carried out with a 16-channel electrode monitor (Lawson Labs Inc., Malvern, PA 19355, USA). A Ag/AgCl was used as reference electrode with 1 M LiOAc as salt bridge electrolyte. Membrane potentials were measured in a stirring solution at ambient temperature in a galvanic cell:



2.3. Determination of the releasing Ag^+ from oxidized AgNPs using H_2O_2

AgNPs (1000 ppm, 100 μL) were added into 10 mL of a buffer solution. Then, 0, 10, 30 and 100 μL of 0.092 M H_2O_2 was added separately in each solution. After stirring for 30 min, solutions were directly measured by the Ag-ISE to determine the activity of free silver ions. The experiment was repeated by increasing H_2O_2 concentration from 0.092 to 9.2 M and 10,000 ppm AgNPs was employed.

2.4. General EMF measurements

A buffer solution (10 mL) of 10 mM magnesium acetate was used as enzyme assay solution. The solution was adjusted to an appropriate pH by dilute acetic acid. Glucose was first diluted in a buffered solution, and the EMF was then measured. Subsequently, AgNPs was added into the solution of glucose. After the EMF was stable GOx (308 U mL^{-1}) was added and the EMF increased consecutively. The experiments were repeated three times for each point. The initial slope method described by Hassan et al. [19–22] was used in all measurements. The EMF was continuously monitored every 3 s (defined as an interval time). Plots of reaction rate were obtained from the differentiation of the change of EMF per interval time under assumption that the rate of potential change ($dEMF/dt$) is directly related to the change in $[H_2O_2]$. The maximum rate of potential change ($dEMF/dt$) was graphically determined by using the rate portion of the curve.

2.5. Studies of interferences

The Ag-ISE was immersed in the buffer solution (25 mL) containing glucose oxidase, and the base line EMF was then recorded. Subsequently, 50 μL of AgNPs (1000 ppm) was added. The EMF immediately jumped to higher base line because of the residual Ag^+ in AgNPs. After the EMF was stable, urea (8.5 mM), glycine (0.5 mM), fructose (10 mM) and sucrose (10 mM) were added after one another. The EMF was recorded after each addition.

2.6. Real sample measurements

A carbonated beverage was diluted by 10 mM magnesium acetate buffer, and pH was adjusted to pH 6. AgNPs (1000 ppm, 20 μL) and GOx (308 U mL^{-1}) were added into the sample solution. The EMF was then recorded. For a glucose-spiked sample, a known amount of glucose was added into the carbonated beverage. AgNPs and GOx were then added in the same manner as described previously. The experiment was carried out in triplicate. The amount of glucose in the sample and the glucose-spiked sample were determined from the maximum rate of the enzyme–substrate reaction.

322

W. Ngontae et al. / Sensors and Actuators B 137 (2009) 320–326

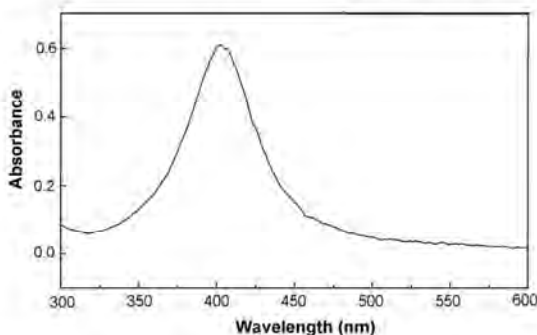


Fig. 1. The plasmon absorption band of diluted 100–1000 from high concentration of the synthesized AgNPs (10,000 ppm) ($\lambda_{\text{max}} = 403$ nm).

3. Results and discussion

3.1. Preparation of AgNPs

AgNPs were synthesized via the chemical reduction process of AgNO_3 using NaBH_4 as adapted from previous reports [15–17]. The plasmon extinction of the synthesized silver nanoparticles measured by a portable UV/vis spectrophotometer (Ocean Optics USB 4000 UV/Vis spectrophotometer) shown in Fig. 1 has a maxima at 403 nm with a narrow full width at half height (FWHM ~ 50 nm). This indicates that the synthesized nanoparticles have a narrow size distribution. The size and shape of the synthesized silver nanoparticles have been further observed by transmission electron microscope (JEOL JEM-2010). The TEM images indicate that AgNPs are spherical and have an average particle size of 14 nm as shown in Fig. 2.

3.2. The fabricated Ag-ISE

The Ag-ISE employed in this article was fabricated using the methodology reported previously [15]. The calix[4]arene containing benzothiazole groups, **CU1**, was used as a neutral ionophore and mixed in PVC plasticized with NPOE. Nernstian's slope can be

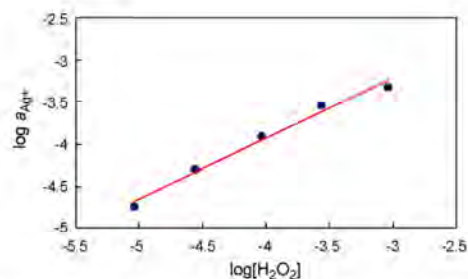


Fig. 3. The relationship between the concentration of H_2O_2 and the activity of free Ag^+ releasing from AgNPs.

observed with the detection limit in micro-molar range and with 4 orders of magnitude working linear range from the non-optimized inner filling solution (10^{-2} M AgNO_3). However, in optimized inner filling solution using the procedure described by Pretsch and co-workers [23], the Ag-ISE fabricated from the synthesized **CU1** exhibits the lower detection limit around 10^{-8} M. The response time of the fabricated Ag-ISE is very fast and the measured potentials are very stable. Principally, a Ag-ISE responds to Ag^+ exclusively; this, therefore, allows us to use the Ag-ISE in the speciation analysis of AgNPs. Both residual Ag^+ and the total Ag content in AgNPs (after oxidizing with H_2O_2) can be determined with good accuracy and precision.

3.3. Relationship between the concentration of H_2O_2 and the releasing of Ag^+ from AgNPs

The relationship between the concentration of H_2O_2 and the concentration of the free Ag^+ generated from AgNPs is investigated by using the different concentration of the mixture of H_2O_2 and AgNPs solution. The concentrations of Ag^+ in each H_2O_2 concentration are determined by direct potentiometry using our fabricated Ag-ISE. According to our previous report [15], AgNPs always contain residual free Ag^+ in the solution. Therefore, the free Ag^+ from AgNPs is first measured and then it is subtracted from the concentration of the mixture. The response EMF is then converted to activity of Ag^+ . It is found that the logarithmic of the concentration

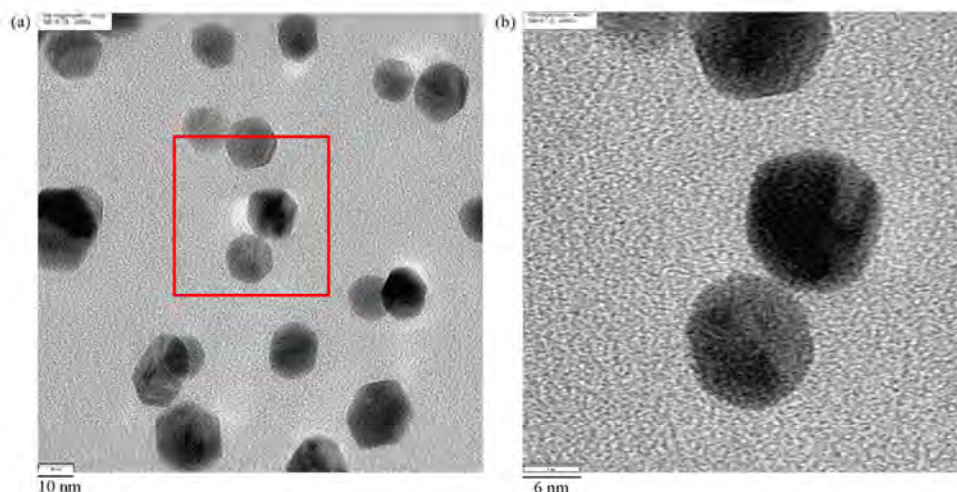


Fig. 2. TEM images of the synthesized AgNPs (a) TEM magnification, 150,000, (b) TEM magnification, 400,000.

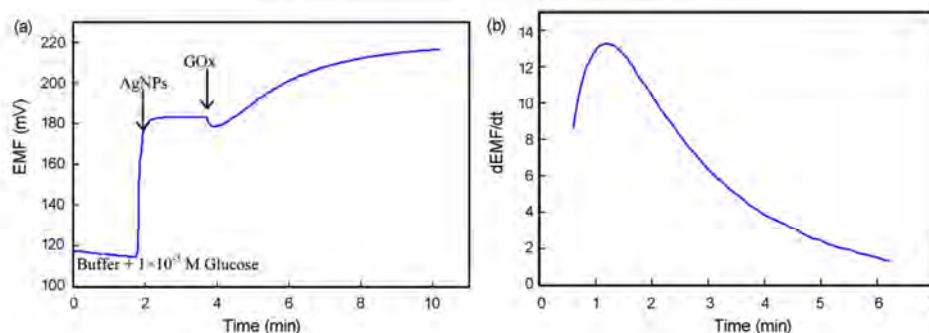


Fig. 4. (a) Continuous time trace line of the EMF change with time. (b) Change of the reaction rate with time after adding GOx.

of H_2O_2 and activity of Ag^+ possesses a linear relationship as illustrated in Fig. 3. This experiment signifies that the change of H_2O_2 concentration corresponds very well to the generation of Ag^+ from oxidized AgNPs. Therefore, free Ag^+ released from AgNPs can be used to determine glucose concentration.

3.4. Measurement of Ag^+ releasing from oxidized AgNPs in reactions of glucose and GOx

Fig. 4a illustrates the resulting EMF versus time of the general experimental procedure. The Ag-ISE is first immersed in the buffer solution of glucose. After the addition of AgNPs, the EMF increases due to the present of residual Ag^+ in AgNPs. GOx is added after the potential stabilizes. The addition of GOx dilutes the sample solution, which causes the sudden drop in EMF. As time proceeds, the GOx converts glucose to gluconic acid and H_2O_2 . The generated H_2O_2 oxidizes AgNPs to free Ag^+ resulting in the gradual increase of the EMF. The increasing EMF is continuously monitored and recorded with respect to an interval sampling time. The derivative of EMF with respect to time is considered as the reaction rate of the enzyme–substrate reaction as presented in Fig. 4b. This value corresponds very well to the glucose concentration, and the maximum rate is used here as a monitoring signal. This approach is quite remarkable because the absolute EMF is not required; only the differences in EMF are needed. Therefore, the accuracy of the reference electrode is rather unimportant.

3.5. Effect of the solution pH

Our Ag-ISE fabricated from **CU1** works well at wide pH range (pH 2–8) without significant EMF change [15]. This characteristic provides many advantages because it does not require a crucial pH adjustment. However, enzyme activity is always affected by several parameters. Solution pH is one of the important factors to the enzyme activity. Therefore, pH of the working assay must be adjusted to a suitable value. To avoid precipitation of Ag^+ , 10 mM magnesium acetate is chosen as a working buffer. The solution pH is varied in the range of 4.5–7 by adjusting with acetic acid as shown in Fig. 5. It is found that at the pH range 6–7, there is a slight change in the reaction rate. Therefore, pH 6 is chosen as a working pH.

3.6. Effect of glucose oxidase (GOx) concentration

The effect of enzyme concentration is studied by fixing glucose concentration at 1.0 mM. The concentration of GOx is varied from 0.38 to 15.4 U mL^{-1} . The results in Fig. 6 show that where the concentration of the enzyme is less than 7.6 U mL^{-1} , the reaction rate is depended on the enzyme concentration. This phenomenon always

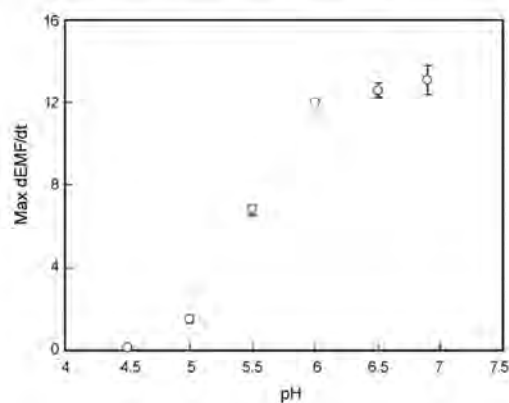


Fig. 5. Effect of the solution pH to the maximum reaction rate.

occurs when the concentration of the enzyme is lower than the substrate. In addition, when the concentration of enzyme is increased from 7.6 to 11.5 U mL^{-1} the reaction rate shows insignificant difference. This signifies that the reaction rate depends on the substrate concentration. However, when the concentration of GOx is higher than 7.6 U mL^{-1} , the precision of the reaction rate is aggravated. Therefore, 7.6 U mL^{-1} is chosen as the working enzyme concentration for the given concentration range (mM range).

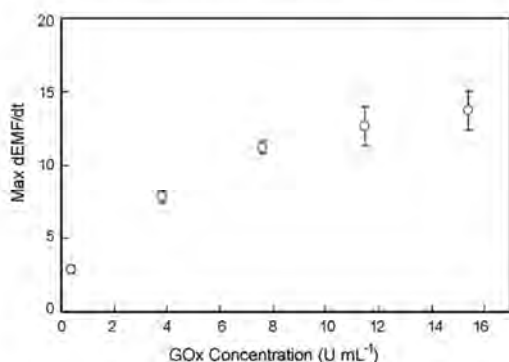


Fig. 6. Effect of the GOx concentration to the maximum reaction rate of 1 mM glucose at pH 6 in 10 mM magnesium acetate buffer.

324

W. Ngeonsae et al. / Sensors and Actuators B 137 (2009) 320–326

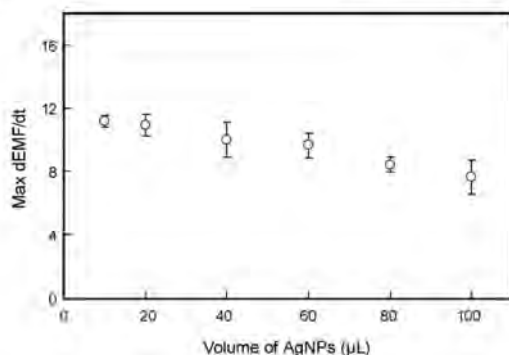


Fig. 7. Effect of the volume of AgNPs solution used in the assay.

3.7. Effect of the quantity of AgNPs

Volumes of AgNPs used in the assay can affect the reaction rate. If the increasing amount of AgNPs causes of the increasing of the reaction rate, it implies that AgNPs involves in a rate-determining step. The relation between the amount of AgNPs and the reaction rate is illustrated in Fig. 7. The results show that the reaction between AgNPs and H_2O_2 is faster than the reaction between the enzyme and the substrate. Therefore, AgNPs do not involve in the rate-determining step. However, when the amount of AgNPs is increased, the reaction rates seem to decrease slightly. Higher volume of AgNPs added results in higher concentration of free Ag^+ that can inhibit enzyme activity. However, residual Ag^+ in 10–20 μL of AgNPs shows no significant inhibition to the enzyme. Therefore, 20 μL of 1000 ppm AgNPs were used in further experiments.

3.8. Glucose calibration curve

All optimized parameters mentioned previously are applied in order to make a glucose calibration curve. Glucose concentrations are varied from 3×10^{-5} to 3×10^{-2} M and the reaction rate is monitored at different concentration change. Fig. 8a shows that the rate of the EMF change (reaction rate) depends on the glucose concentration. The glucose calibration curve is illustrated in Fig. 8b. When the concentration of glucose changes, the reaction rate also changes significantly; a linear correlation between the reaction rate and logarithmic concentration of glucose is obtained (maximum $[dEMF/dt] = 8.62 \times \log[\text{glucose}] + 38.19$). The working linear range is found to be 1×10^{-4} to 3×10^{-3} M and can cover the glucose

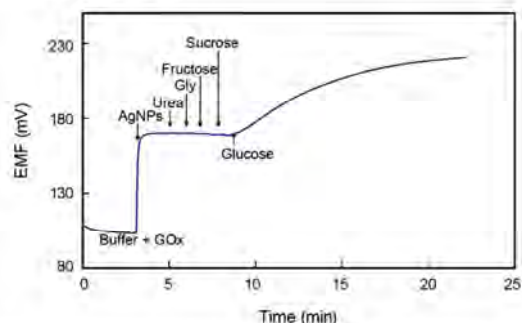


Fig. 9. The time trace line of the EMF change with time after adding interferences.

concentration in many detecting environments especially in diabetic serum. In addition, the lower detection limit of this sensor, obtained from the lowest glucose concentration that can give the EMF change after reacting with GOx, is 1.0×10^{-5} M.

3.9. Study of interferences

The selectivity of a glucose biosensor depends on two major factors: the enzyme–substrate reaction and selective measurements. The enzyme–substrate reaction is very specific due to the nature of enzyme functionality. Glucose oxidase can only react with β -D-glucose without interfering from other types of sugars. Possible interferences in glucose determination such as urea (a protein metabolite), glycine, fructose and sucrose are tested in our measuring system. The results are shown in Fig. 9. The EMF does not significantly change upon addition of interferences. Therefore, the tested chemicals cannot meddle the measuring system. Furthermore after glucose is added, the EMF increases with the same behavior when compared to the system with no interferences.

However, our new method may have some drawback in the presence of possible interferences such as a reducing agent, for example ascorbic acid that can convert Ag^+ to Ag^0 . Moreover, chelating agents that possibly present in the real sample can also reduce the activity of free Ag^+ .

3.10. Repeatability, sensor-to-sensor reproducibility and analysis of real samples

Our approach deals with the enzyme–substrate reaction of GOx and glucose which the rate of reaction depends on oxygen. Therefore, the fluctuation of oxygen in the sample will definitely affect

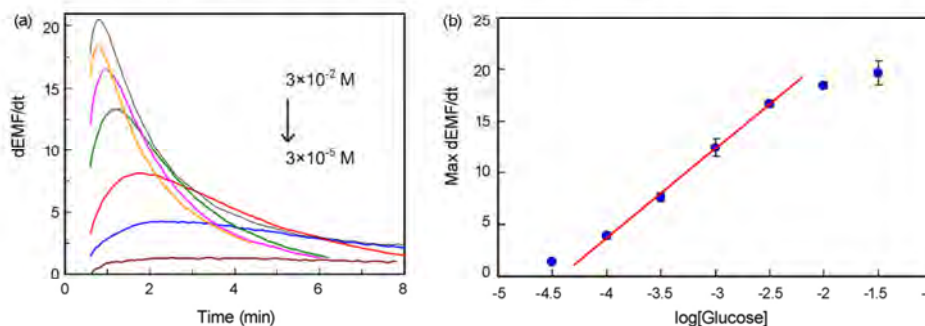


Fig. 8. (a) The derivative of the EMF change with time at different glucose concentration. (b) Calibration curve of the glucose, plotting the maximum reaction rate against logarithmic of glucose concentration.

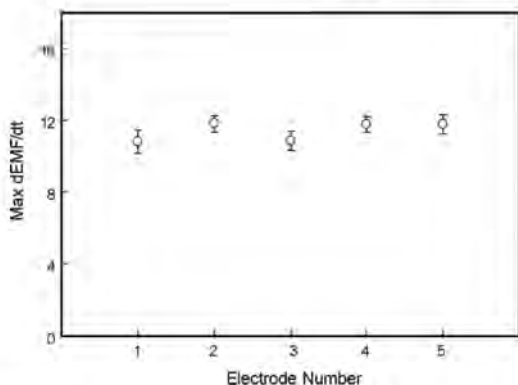


Fig. 10. The sensor-to-sensor reproducibility of 5 Ag-ISEs (1 mM of glucose).

Table 1

Analysis of glucose concentration in beverages.

Sample no.	Glucose added (μmol)	Glucose found (μmol^a)	Recovery (%)	R.S.D. (%)
1	0	1.05 ± 0.09	–	–
	3	4.01 ± 0.19	98	6
2	0	1.56 ± 0.17	–	–
	3	4.46 ± 0.26	97	9
3	0	2.99 ± 0.14	–	–
	10	12.5 ± 0.80	96	8

^a in 10 mL solution.

the reproducibility of the method. The repeatability of our proposed method can be evaluated by measuring the reaction rate of 1 mM glucose repeatedly with the same electrode. Reaction rates of each measuring experiments have showed that the Ag-ISE can be used several times with the relative standard deviation (R.S.D.) less than 7%. Moreover, we also evaluate sensor-to-sensor reproducibility by measuring three replicates of 1 mM glucose by using five different electrodes. The results in Fig. 10 show that the maximum of reaction rates obtained from different electrodes are not significantly different. Therefore, the proposed method in detecting glucose is reliable.

Glucose concentration in beverages is then measured by the proposed method, and results are shown in Table 1. The recovery of the spike samples is higher than 96% with good precision (R.S.D. < 10%). Our concept thus gives good analytical characteristics of glucose detection and can be used for development of future glucose biosensors.

4. Concluding remarks

We have demonstrated the use of silver nanoparticles as metal marker in our Ag-ISE glucose biosensor. The fabricated Ag-ISE remarkably combines two specificities in glucose detection: the enzyme–substrate reaction of GOx and glucose and the selective detection of Ag^+ . The optimum solution pH was 6.0 in 10 mM magnesium acetate buffer. The suitable enzyme concentration used was 7.6 U mL^{-1} and the appropriate volume of Ag nanoparticle redox marker was $20 \mu\text{L}$. The lower detection limit was $1.0 \times 10^{-5} \text{ M}$. The proposed method can be used for determination of glucose concentration range of 0.1–3 mM with good selectivity, accuracy, repeatability and reproducibility. We optimistically think that this method can be further applied for other oxidase enzyme system.

Acknowledgments

This research was financially supported by the Thailand Research Fund (RTA5080006 and IUG5080025). W.J. is a

Ph.D. student supported by Commission on Higher Education.

References

- [1] J. Wang, Electrochemical glucose biosensors, *Chem. Rev.* 108 (2008) 814.
- [2] J. Wang, M. Musameh, Carbon nanotube screen-printed electrochemical sensors, *Analyst* 129 (2004) 1.
- [3] S. Hrapovic, Y.L. Liu, K.B. Male, J.H.T. Luong, Electrochemical biosensing platforms using platinum nanoparticles and carbon nanotubes, *Anal. Chem.* 76 (2004) 1083.
- [4] Y. Xiao, F. Patolsky, E. Katz, J.F. Hainfeld, I. Willner, "Plugging into enzymes": nanowiring of redox enzymes by a gold nanoparticle, *Science* 299 (2003) 1877.
- [5] F. Patolsky, Y. Weizmann, I. Willner, Long-range electrical contacting of redox enzymes by SWCNT connectors, *Angew. Chem. Int. Ed. Engl.* 43 (2004) 2113.
- [6] R. Polsky, R. Gill, L. Kaganovsky, I. Willner, Nucleic acid-functionalized Pt nanoparticles: catalytic labels for the amplified electrochemical detection of biomolecules, *Anal. Chem.* 78 (2006) 2268.
- [7] J.Q. Liu, A. Chou, W. Rahmat, M.N. Paddon-Row, J.J. Gooding, Achieving direct electrical connection to glucose oxidase using aligned single walled carbon nanotube arrays, *Electroanalysis* 17 (2004) 38.
- [8] Y. Huang, W. Zhang, H. Xiao, G. Li, An electrochemical investigation of glucose oxidase at a CdS nanoparticles modified electrode, *Biosens. Bioelectron.* 21 (2005) 817.
- [9] L. Górski, D. Klimaszewska, M. Pietrzak, E. Malinowska, Enzymatic detection of glucose using fluoride-selective electrodes with polymeric membranes, *Anal. Bioanal. Chem.* 289 (2007) 533.
- [10] H.S.M. Abd-Rabboh, M.E. Meyerhoff, Determination of glucose using a coupled-enzymatic reaction with new fluoride selective optical sensing polymeric film coated in microtiter plate wells, *Talanta* 72 (2007) 1129.
- [11] Ş. Kalayci, G. Somer, G. Ekmekci, Preparation and application of a new glucose sensor based on iodide ion selective electrode, *Talanta* 65 (2005) 87.
- [12] G.D. Liu, Y.H. Lin, Nanomaterial labels in electrochemical immunosensors and immunoassays, *Talanta* 74 (2007) 308.
- [13] R. Koncki, Recent developments in potentiometric biosensors for biomedical analysis, *Anal. Chim. Acta* 599 (2007) 7.
- [14] J. Wang, Nanoparticle-based electrochemical bioassays of proteins, *Electroanalysis* 19 (2007) 769.
- [15] W. Ngeontae, W. Janrungratsakul, N. Morakot, W. Aeungmaitrepirom, T. Tuntulani, New silver selective electrode fabricated from benzothiazole calix[4]arene: speciation analysis of silver nanoparticles, *Sens. Actuators B: Chem.* 134 (2008) 377.
- [16] D.L.V. Hynning, C.F. Zukoski, Formation mechanisms and aggregation behavior of borohydride reduced silver particles, *Langmuir* 14 (1998) 7034.
- [17] N. Shirtcliffe, U. Nickel, S. Schneider, Reproducible preparation of silver sols with small particle size using borohydride reduction: for use as nuclei for preparation of larger particles, *J. Colloid Interf. Sci.* 211 (1999) 122.
- [18] Z.Q. Zhang, R.C. Patel, R. Kothari, C.P. Jolinson, S.E. Friberg, Stable silver clusters and nanoparticles prepared in polyacrylate and inverse micellar solutions, *J. Phys. Chem. B* 104 (2000) 1176.
- [19] S.S.M. Hassan, A.F. El-Baz, H.S.M. Abd-Rabboh, A novel potentiometric biosensor for selective L-cysteine determination using L-cysteine-desulhydrase producing *Trichosporon jirovecii* yeast cells coupled with sulfide electrode, *Anal. Chim. Acta* 602 (2007) 108.
- [20] S.S.M. Hassan, G.A. Rechnitz, Determination of glutathione and glutathione reductase with a silver sulfide membrane electrode, *Anal. Chem.* 54 (1982) 1972.
- [21] S.S.M. Hassan, S.A.M. Marzouk, M.M. Abdel Fattah, G.M.S.M. Shoukry, Potentiometric determination of arylsulfatase activity using a novel nitrocatechol sulfate PVC membrane sensor, *Anal. Chem.* 67 (1995) 1887.
- [22] S.S.M. Hassan, R.M. El-Bahnasawy, N.M. Risk, Potentiometric determination of salicylhydroxamic acid (urinary struvite stone inhibitor) based on the inhibition of urease activity, *Anal. Chim. Acta* 351 (1997) 91.
- [23] A. Ceresa, A. Radu, S. Peper, E. Bakker, E. Pretsch, Rational design of potentiometric trace level ion sensors. A Ag^+ -selective electrode with a 100 ppt detection limit, *Anal. Chem.* 74 (2002) 4027.

Biographies



Wittaya Ngeontae is currently a lecturer in the Department of Chemistry, Khon Kaen University, Khon Kaen, Thailand. He earned his Ph.D. in analytical chemistry with Assistant Prof. Wanlapa Aeungmaitrepirom and Associate Prof. Thawatchai Tuntulani at Chulalongkorn University under the Development and Promotion of Science and Technology Talent project (DPST). In 2006, he was a visiting scholar with Professor Eric Bakker. His research interests include synthesis of new ionophores based on the calixarene platform. Moreover, he is interested in the applications of ISEs and optical sensors for bio-molecules and environments.



Wanwisa Jaurungroatsakul received her MS degree in chemistry from Chulalongkorn University under the supervision of Associate Prof. Thawatchai Tuntulani. She is currently a Ph.D. student in chemistry supported by the Commission on Higher Education. Her research interest is concerning ISEs and their applications in sensing biomolecules.



Pattwat Maneewattanapinyo is currently a Ph.D. student in physical chemistry, Faculty of Science, Chulalongkorn University, Thailand. He got his Bachelor Degree in Chemistry in 1998 and Master Degree in Petrochemistry and Polymer Science in 2002 from Faculty of Science, Chulalongkorn University, Thailand. His research interests include synthesis of highly concentrated silver nanoparticles for industrial applications.



Sanong Ekgasit is currently an associate professor at the Department of chemistry, Faculty of Science, Chulalongkorn University, Thailand. He got his Bachelor Degree in Chemistry in 1989, Master Degree in Polymer Technology in 1992 from Chulalongkorn University, and Ph.D. in Polymer Science and Engineering in 1996 from Case Western Reserve University, USA. His research interests include molecular-spectroscopy, surface plasmon resonance spectroscopy, and synthesis and applications of metal nanoparticles for optical sensors.



Wanlapa Aeungmaitrepirom is currently an assistant professor in the Department of Chemistry at Chulalongkorn University, Thailand. She earned her Ph.D. in Analytical Chemistry at Université Louis Pasteur, France after obtaining B.Sc. and M.Sc. in Chemistry from Chulalongkorn University. Her research interests include fabrications of new ion selective electrodes and development of new extractants for environmental concerns.



Thawatchai Tuntulani is currently an associate professor in the Department of Chemistry at Chulalongkorn University, Thailand. He earned his PhD in Chemistry with Prof. Marcetta Y. Darensbourg at Texas A&M University, USA after obtaining a Bachelor Degree of Engineering from Chiang Mai University, Thailand. He did his post-doctoral studies with Prof. Jean-Marie Lehn before joining Chulalongkorn University in 1995. His research interests include syntheses of derivatives of calix[4]arene and other macrocyclic compounds and development of electrochemical and optical sensing materials for ions and biomolecules.

VITAE

Name: Mr. Pattwat Maneewattanapinyo

Date of Birth: October 30, 1977 **Birth Place:** Bangkok, Thailand

Address: 98/48, Phetkasem road, Phasicharoen, Bangkok 10160, Thailand,
E-mail address: fuktongg@hotmail.com

Education:

2009 Doctor of Philosophy in Chemistry
Chulalongkorn University, Thailand

2002 Master of Science in Chemistry
Chulalongkorn University, Thailand

1998 Bachelor of Science in Chemistry
Chulalongkorn University, Thailand

Conferences:

December 12-14, 2007 International Graduates Congress 2007 (3rd
MPSGC), MALAYSIA

September 1-3, 2009 ChinaNANO2009, China

Research Publications:

1. A. Sereemaspun, P. Hongpiticharoen, R. Rojanathanes, **P. Maneewattanapinyo**, S. Ekgasit, and W. Warisnoicharoen, Inhibition of Human Cytochrome P450 Enzymes by Metallic Nanoparticles: A Preliminary to Nanogenomics, *Int. J. of Pharmacol.* 4(6) (2008) 492.
2. W. Ngeontae, W. Janrungroatsakul, **P. Maneewattanapinyo**, S. Ekgasit, W. Aeungmaitrepirom, and T.Tuntulani, Novel potentiometric approach in glucose biosensor using silver nanoparticles as redox marker, *Sens. Actuators B: Chem.* 137 (2009) 320.